

NOTE TO USERS

**Page(s) missing in number only; text follows.
Microfilmed as received.**

1-3

This reproduction is the best copy available.

UMI

THE UNIVERSITY OF CALGARY

**SCC INITIATION STUDY OF X-52 PIPELINE STEEL AND ITS VARIOUS
MICROSTRUCTURES IN NEAR NEUTRAL pH BICARBONATE SOLUTION**

by

VLADIMIR E. SIZOV

A THESIS

**SUBMITTED TO THE FACULTY OF GRADUATE STUDIES
IN PARTIAL FULFILMENT OF THE REQUIREMENTS FOR THE
DEGREE OF MASTER OF SCIENCE IN MECHANICAL ENGINEERING**

DEPARTMENT OF MECHANICAL AND MANUFACTURING ENGINEERING

CALGARY, ALBERTA

JUNE, 1999

© VLADIMIR E. SIZOV 1999



National Library
of Canada

Acquisitions and
Bibliographic Services

395 Wellington Street
Ottawa ON K1A 0N4
Canada

Bibliothèque nationale
du Canada

Acquisitions et
services bibliographiques

395, rue Wellington
Ottawa ON K1A 0N4
Canada

Your file Votre référence

Our file Notre référence

The author has granted a non-exclusive licence allowing the National Library of Canada to reproduce, loan, distribute or sell copies of this thesis in microform, paper or electronic formats.

The author retains ownership of the copyright in this thesis. Neither the thesis nor substantial extracts from it may be printed or otherwise reproduced without the author's permission.

L'auteur a accordé une licence non exclusive permettant à la Bibliothèque nationale du Canada de reproduire, prêter, distribuer ou vendre des copies de cette thèse sous la forme de microfiche/film, de reproduction sur papier ou sur format électronique.

L'auteur conserve la propriété du droit d'auteur qui protège cette thèse. Ni la thèse ni des extraits substantiels de celle-ci ne doivent être imprimés ou autrement reproduits sans son autorisation.

0-612-48369-X

Canada

ABSTRACT

Initiation of Stress Corrosion Cracking (SCC) in Near-Neutral-pH Bicarbonate solution on X-52 pipeline steel has been investigated by Slow Strain Rate Test. To determine the most susceptible conditions of Near-Neutral-pH SCC initiation, a number of experiments were conducted with various electro-potentials, slow strain rates, pH values of the solution.

The initiation of Near-Neutral-pH SCC was found in the potential range from $-800\text{mV}_{\text{SCE}}$ to $-1100\text{mV}_{\text{SCE}}$. The most susceptible potential is around $-900\text{mV}_{\text{SCE}}$. The most susceptible strain rate is around $2.5 \times 10^{-7} \text{1/s}$. The crack growth rate was calculated for different potentials.

The influence of residual stresses on Near-Neutral-pH SCC initiation was examined. It was found that as the temperature of stress relief increases the susceptibility of the steel decreases.

Several heat treatments were performed and susceptibility investigation was conducted on obtained microstructures. All microstructures were susceptible to Near-Neutral-pH SCC. The critical stresses and crack growth rates were calculated.

ACKNOWLEDGEMENTS

The Author wishes to express his sincere gratitude to his supervisor, Dr. X. Mao for his guidance, assistance and support throughout the entire research and preparation of this thesis. He is also thankful to PhD student B. Gu and research assistant L. Yang for fruitful discussions and help in conducting the experiments.

The Author wishes to express his sincere appreciation to his wife Marina for her continuous love, support and encouragement.

TABLE OF CONTENTS

Approval Page	II
Abstract	III
Acknowledgements	IV
Table of Contents	V
List of Tables	VIII
List of Figures	IX
Abbreviations	XIV
Chapter 1 Problem Overview and Objectives	4
Chapter 2 Literature Review	6
2.1 Introduction	6
2.2 The History of First SCC Encounters	7
2.3 Stress Corrosion Cracking of Pipelines	10
2.4 Classification of SCC Mechanisms	11
2.4.1 SCC Mechanisms on Anodic Dissolution	11
2.4.1.1 Mechano-Electrochemical	13
2.4.1.2 Film Rupture	14
2.4.1.3 Stress Adsorption	16
2.4.1.4 Dissolution Mechanism	17
2.4.1.5 Atomic Surface Mobility	19
2.4.1.6 Film-induced Cleavage	20
2.4.1.7 Localized Surface Plasticity	21

2.4.2 Mechanisms of Hydrogen Related Cracking	22
2.4.2.1 Hydrogen-Related Phase-Change Mechanisms	25
2.4.2.2 Hydrogen - Enhanced Local Plasticity Mechanism	26
2.4.2.3 Decohesion Mechanism	28
2.4.3 Near-Neutral-pH SCC vs. High-pH SCC in Pipeline Steel	28
2.4.3.1 High-pH Stress Corrosion Cracking	30
2.4.3.1.1 Environmental Factors	31
2.4.3.1.2 Metallurgical Factors	32
2.4.3.1.3 Mechanical Factors	33
2.4.3.2 Near-Neutral-pH Stress Corrosion Cracking	34
2.4.3.2.1 Environmental Factors	34
2.4.3.2.2 Metallurgical Factors	35
2.4.3.2.3 Mechanical Factors	36
Chapter 3 Experiment Methodology	37
Chapter 4 Investigation of Susceptibility to Near-Neutral-pH SCC of X-52 Pipeline Steel	46
4.1 Determination of the Most Susceptible Environments	48
4.2 Critical Stress of Near-Neutral-pH SCC Initiation	53
4.3 Strain Rate Effect on SCC Initiation	65
4.4 Effect of pH Value of the Solution	73
4.5 Growth Rate Calculation of Near-Neutral-pH SCC	78

Chapter 5 The Effect of Residual Stresses and Microstructure Change of Near-Neutral-pH SCC	81
5.1 Microstructure of Heat-Treated Samples and Its Influence on SCC Initiation	85
5.1.1 Microstructure of Heat-Treated Samples	85
5.1.2 Effect of Microstructure on SCC Initiation	91
5.1.3 Influence of Microstructure Differences on SCC Growth Rate	102
5.2 Residual Stresses and Their Influence on Near-Neutral-pH SCC Initiation and Propagation	105
Chapter 6 Observations and Conclusions	123
References	127

LIST OF TABLES

1. Table 3.1. Chemical Composition of X-52 Pipeline Steel	37
2. Table 3.2. Mechanical Characteristics of X-52 Pipeline Steel	37
3. Table 3.3. The Chemical Composition of NS-4	42
4. Table 3.4 Heat Treatment Parameters	45
5. Table 5.1 Material Properties of Heat-Treated Samples	91
6. Table 5.2.1 Macro-Residual Stresses Measured by X-ray Diffraction Method	106
7. Table 5.2.2 Material Properties of Stress Relieved Samples	106

LIST OF FIGURES

1. Fig 3.1	Stress –Strain Curve at Different Potentials	38
2. Fig 3.2(a)	Standard Straight Flat Sample	40
3. Fig 3.2(b)	Flat Conical Sample	41
4. Fig 3.3	The Schematic Diagram of Environmental Chamber for Slow Strain Rate Test	43
5. Fig 4.1.1	The Surface of the Sample at 15% of Strain	
	(a) Potential $E_{SCE}=-712mV$	50
	(b) Potential $E_{SCE}=-750mV$	50
6. Fig 4.1.2	The Surface of the Sample at 15% of Strain	
	(a) Potential $E_{SCE}=-800mV$	51
	(b) Potential $E_{SCE}=-900mV$	51
7. Fig 4.1.3	The Surface of the Sample at 15% of Strain	
	(a) Potential $E_{SCE}=-1000mV$	52
	(b) Potential $E_{SCE}=-1100mV$	52
	(c) Potential $E_{SCE}=-1200mV$	52
8. Fig 4.2.1	Surface of the Sample at Different Strain Level	
	(a) 3%	54
	(b) 5%	54
	(c) 7.5%	54
	(d) 15%	54
9. Fig 4.2.2	Conical Sample, Stress Calculation at Different Cross-Sectional Areas	56

10. Fig 4.2.3	Surface of Sample at Different Stress Levels ($E_{SCE}=-800mV$)	57
11. Fig 4.2.4	Surface of Sample at Different Stress Levels ($E_{SCE}=-900mV$)	58
12. Fig 4.2.5	Surface of Sample at Different Stress Levels ($E_{SCE}=-1000mV$)	59
13. Fig 4.2.6	Surface of Sample at Different Stress Levels ($E_{SCE}=-1100mV$)	60
14. Fig 4.2.7	Surface of Sample at Different Stress Levels ($E_{SCE}=-1200mV$)	61
15. Fig 4.2.8	Normalised Initiation Stress vs. Potential	63
16. Fig 4.2.9	Effect of the Potential on Crack Initiation	64
17. Fig 4.3.1	Sample Surface at Different Stress Levels ($SR = 2.5 \times 10^{-7} 1/s$, $E_{SCE}=-900mV$)	67
18. Fig 4.3.2	Sample Surface at Different Stress Levels ($SR = 1 \times 10^{-7} 1/s$, $E_{SCE}=-900mV$)	68
19. Fig 4.3.3	Sample Surface at Different Stress Levels (Static Load, $E_{SCE}=-900mV$)	69
20. Fig 4.3.4	Sample Surface at Different Stress Levels ($SR=1 \times 10^{-6} 1/s$, $E_{SCE}=-900mV$)	70
21. Fig 4.3.5	Normalised Critical Stress of Initiation vs. Strain Rate	71
22. Fig 4.3.6	Crack Density vs. Strain Rate for Different Stress Levels	72
23. Fig 4.4.1	Crack Density vs. Stress for Different pH	75
24. Fig 4.4.2	Sample Surface at Different Stress Levels ($SR=5 \times 10^{-6} 1/s$, $E_{SCE}=-900mV$, Purging Gas – Pure Nitrogen (N_2), Solution pH=8.5)	76

25. Fig 4.4.3 Sample Surface at Different Stress Levels	
(SR=5x10⁻⁶1/s, E_{SCE}=-712mV (OCP), Purging Gas - 5% CO₂	
Balanced with N₂, Solution pH=4)	77
26. Fig 4.4.1 Crack Growth Rate vs. Potential	80
27. Fig 5.1 (a) Spherical Inclusion	83
(b) Slightly Elongated Inclusion	83
28. Fig 5.2 Initiation of SCC at the Inclusions and Specific	
Crystallographic Planes	84
29. Fig 5.1.1.1 Microstructure of As-Received Sample	
(a) Transverse Direction of Pipe	86
(b) Longitudinal Direction of Pipe	86
30. Fig 5.1.1.2 Microstructure of 950°C Furnace Heated/1 hr + Water	
Cooled and Tempered	
(a) 475°C/2hrs Tempered	87
(b) 650°C/2hrs Tempered	87
31. Fig 5.1.1.3 Microstructure of	
(a) 950°C/10 min/WC	89
(b) 950°C/10 min/WC + Tempered at 250°C/2 hrs	89
(c) 950°C/10 min/WC + Tempered at 450°C/2 hrs	90
(d) 950°C/10 min/WC + Tempered at 650°C/2 hrs	90
32. Fig 5.1.2.1 Sample Surface at Different Stress Levels (950°C/10 min/WC)	93
33. Fig 5.1.2.2 Sample Surface at Different Stress Levels	
(950°C/10min/WC+250°C/2hrs)	94

34. Fig 5.1.2.3 Sample Surface at Different Stress Levels	
(950°C/10min/WC+450°C/2hrs)	95
35. Fig 5.1.2.4 Sample Surface at Different Stress Levels	
(950°C/10min/WC+650°C/2hrs)	96
36. Fig 5.1.2.5 Sample Surface at Different Stress Levels	
(950°C/1Hr/WC+650°C/2hrs)	97
37. Fig 5.1.2.6 Critical Stress of Different Microstructures	100
38. Fig 5.1.2.7 Crack Density vs. Stress	101
39. Fig 5.1.3.1 Crack Growth Rate for Different Heat Treatments	104
40. Fig 5.2.1 (a) Stress Relieved Sample at 250°C/2hrs	107
(b) Stress Relieved Sample at 450°C/2hrs	107
(c) Stress Relieved Sample at 550°C/2hrs	108
(d) Stress Relieved Sample at 650°C/2hrs	108
41. Fig 5.2.2 Critical Stress of SCC Initiation for Stress Relieved Steel	110
42. Fig 5.2.3 Sample Surface at Different Stress Levels	
(Stress Relieved at 250°C for 2 Hours)	111
43. Fig 5.2.4 Sample Surface at Different Stress Levels	
(Stress Relieved at 450°C for 2 Hours)	112
44. Fig 5.2.5 Sample Surface at Different Stress Levels	
(Stress Relieved at 550°C for 2 Hours)	113

45. Fig 5.2.6	(a) SEM Image of Slip Bands within Grains on Etched Surface of the Sample	115
	(b) SEM Image of Slip Bands within Grains on Etched Surface of the Sample under Higher Magnification	116
46. Fig 5.2.7	(a) SEM Image of Cracks within the Grain on Etched Surface of the Sample	117
	(b) SEM Image of Cracks Propagating Through Several Grains on Etched Surface of the Sample	118
47. Fig 5.2.8	Crack Density vs. Stress	121
48. Fig 5.2.9	Crack Growth Rate for Stress Relieved Samples	122

Abbreviations

1/s – 1/seconds

AC – Air Cooled

BCT – Body Central Tetrahedral

CE – Counter Electrode

Cm – Centimeter

CV – Crack Velocity

d – Material density

D – Pipe Diameter

EDS - Energy Disperse Spectrometry

EDX – Energy Disperse X-ray

F – Faraday's constant

FC – Furnace Cooled

FIC – Film Induced Cleavage

HELP – Hydrogen-Enhanced Local Plasticity

Hr(s) – Hour(s)

HRB – Hardness Rockwell scale B

i_a – anodic current

K_{IC} – Fracture Toughness for Mode I crack

km – kilometers

LSP – Localized Surface Plasticity

M – Atomic Weight of Metal

mg – Milligrams

Min – Minutes

MPa – Mega Pascal

NRC – National Research Center

NS-4 – Nova Solution 4

OCP – Open Circuitry Potential

P – Operating Pressure

P – Operating Pressure

Q_f – Charge density

RE – Reference Electrode

SCC – Stress Corrosion Cracking

SCE – Saturated Calomel Electrode

SEM – Scanning Electron Microscope

SMYS – Specified Minimum Yield Stress

SR – Strain Rate

SR@250 – Stress Relieved at 250°C

SSRT – Slow Strain Rate Test

t – Thickness

TCPL – Trans Canada Pipeline

WC – Water Cooled

WE – Working Electrode

Z – Valence

ϵ – Strain

μm – micron (micro meters)

σ_{cr} – Critical Stress

σ_{y} – Yield Stress

σ – Stress

NOTE TO USERS

**Page(s) missing in number only; text follows.
Microfilmed as received.**

1-3

This reproduction is the best copy available.

UMI

Chapter 1

Problem Overview and Objectives

Stress Corrosion Cracking is a preferential attack on areas under stress in a corrosive environment, where such an environment alone would not have caused corrosion. Currently two forms of Stress Corrosion Cracking are known.

The first form is Classical SCC [8,9]. It is known that this cracking is intergranular and can occur in highly concentrated carbonate – bicarbonate solution ($\text{HCO}_3^- - \text{CO}_3^{2-}$). The aqueous solution in this case has pH value from 9 to 10. This form of cracking was found first in 1965 [10]. The extensive research has been done and it was determined that Classical SCC occurs in a very restricted range of electro-chemical potential: $-550 \div -650 \text{ mV}_{\text{SCE}}$, and dominated by film rupture and dissolution.

Much later a different form of SCC was found in Canada. In contrary to the first form, this one was transgranular and was associated with low pH environments (pH around 7.0). So called Non-classical or Near-Neutral-pH SCC is fairly new phenomena and not everything is clear in the mechanism of initiation and propagation of it in pipeline steel. In the past few years research work has been concentrated on reproducing Non-classical SCC [29 – 32], defining controlling parameters [33 - 35] and measuring crack growth rates for pipeline steel because of their implications for pipe life prediction estimates [36 - 40]. Nevertheless, the considerable scatter in data and the limited research is not enough to explain the nature of Non-classical SCC. The mechanism, major contributors, and critical stresses of Near-Neutral-pH SCC are still unknown. There is no extensive research on the initiation processes.

As a result the following objectives were set for this investigation of Near-Neutral-pH Stress Corrosion Cracking.

Using slow strain rate test (SSRT) and SEM fractographic examination, investigate SCC initiation and propagation conditions for X-52 pipeline steel in Near-Neutral-pH bicarbonate solution.

1. Find the most susceptible environments for Near-Neutral-pH SCC by performing several tests at different potentials and different strain rates of loading.
2. Determine the Critical Stress of Near-Neutral-pH SCC initiation for as received steel, using specially designed for this purpose – tapered sample.
3. Investigate strain rate effect on Near-Neutral-pH SCC initiation, by changing the strain rate of loading and looking at variation of critical stress and crack density on the surface of the sample.
4. Investigate the influence of hydrogen on Near-Neutral-pH Stress Corrosion Cracking, by deliberately changing pH value of the solution and purging it with a different gasses (5%CO₂ balanced with N₂ and pure N₂).
5. Calculate Near-Neutral-pH SCC growth rate for as-received, stress relieved and various microstructure samples.
6. Investigate the susceptibility of different types of microstructure of X-52 steel to Near-Neutral-pH SCC. Define variation of critical stresses and crack density for different microstructure.
7. Determine the influence of residuals stresses in the steel on Near-Neutral-pH SCC initiation, by looking at variation of critical stresses and crack density.

Chapter 2

Literature Review

2.1 Introduction

Stress Corrosion Cracking – a cracking process that requires the simultaneous action of a corrodent and sustained tensile stress (This excludes corrosion-reduced sections, which fail by fast fracture. It also excludes intercrystalline or transcrystalline corrosion, which can disintegrate an alloy without either applied or residual stress [1].)

Research of Classical (High-pH) SCC has been undergoing for more than 30 years. For today the mechanism of this phenomenon and factors which influence the initiation and propagation of this kind of cracking are well understood. At the same time the Non-classical (Near-Neutral-pH) SCC is relatively new phenomenon, it was discovered only about 10 – 15 years ago. Although extensive research has been done to investigate this type of cracking, the mechanism and the major factors, influencing initiation and propagation of Near-Neutral-pH SCC are still not understood.

In this chapter a general characteristics and various mechanisms of Stress Corrosion Cracking will be reviewed. Both High-pH SCC and Near-Neutral-pH SCC of pipeline steel will be compared, based on the existing research published in different scientific journals. This will set up a background for planning and implementing experimental investigation of Near-Neutral-pH SCC.

2.2 The History of First SCC Encounters

The earliest incidents, which can be related to Stress Corrosion Cracking (SCC), go back in the history of British Empire presence in India in 1880s. In the military troops strange phenomena was noticed – brass (70%Cu/30%Zn) cartridge cases started cracking for no particular reason. Apparently ammunition stocks were too close to horses' stables and cartridge cases were exposed to humid ammoniac atmospheres. The problem was traced to residual stresses and solved by stress-relief annealing. The same problem with application of brass appeared in rapidly growing electric power generation industry. Professor Roberts-Austen made two important contributions to the problem: he showed that the phenomenon was not restricted to brass or even to base alloys. And in analyzing the stresses in the wire he placed emphasis for the first time on the necessary role of tensile stress in SCC.

As a result, the earliest literature on SCC can be associated with the beginning of this century. As time went on, there was an increase of interest in SCC. This can be resulted by two factors: 1) The problem with general corrosion has been overcome by more thorough control of environment and use of more corrosion-resistant materials, which resulted in increase of localized corrosion; 2) Industry moved to higher operational stresses, accompanied by more extensive and effective use of welding, which resulted in higher residual stresses in structures.

By the end of the 19th century “caustic cracking” of riveted boiler steel could also be found as an example of SCC and as another indication that the problem might occur in

might occur in a number of alloy systems, given the wrong conditions. The wrong conditions in caustic cracking are a combination of local high concentration of free alkali and elevated temperature. During various investigations of SCC it was concluded that this type of failure could be overcome by influencing on three of the following elements: mechanics, metallurgy and chemistry of the environment.

Andrew [2] was one of the firsts to the possible explanation of intergranular cracking of boiler steel. He proposed that the embrittlement to be caused by hydrogen penetration onto ferric materials. The mechanism of oxide film rupture was suggested in Straub and Parr [3] papers. In these first papers the caustic cracking of boilers was referred to the stress remaining in the boilers seams after riveting in addition to operational stresses and it was considered to be high enough to exceed the fracture strength of steel. The possibility of fatigue mechanism as a cause of caustic cracking of boilers was suggested by Wolff [4] and McAdam [5], which brought up a question in difference between Stress Corrosion and Corrosion Fatigue. In 1921 Fletcher [6] suggested explanation that corrosion is concentrated in the regions, which suffered the most of cold work (under stress the grain boundary will have higher energy and therefore suffer enhance corrosion).

The characteristics of SCC may be summarized as follows:

1. Tensile stress is required. This stress may be supplied by service loads, cold work, residual stresses, heat treatment, and by the wedging action of corrosion products.
2. Only alloys are susceptible, not pure metals, though there may be a few exceptions to this rule.

3. Generally only a few chemical species in the environment are effective in causing SCC of a given alloy.

4. The species responsible for SCC in general need not be present either in large quantities or in high concentrations.

5. With some alloy/corrosive combination, such as titanium and crystalline sodium chloride, or austenitic stainless steel and chloride solutions, temperatures substantially above room temperature may be required to activate some process essential to SCC.

6. An alloy is usually almost inert to the environment, which causes SCC.

7. Stress Corrosion Cracking is always macroscopically brittle in appearance, even in alloys, which are very tough in purely mechanical fracture tests. (Shear lips may occur in conjunction with stress corrosion cracks, but these shear lips are not part of the stress corrosion process. As a corollary, there does not appear to be a stress corrosion fracture analog to the full shear slant fracture of purely mechanical origin.)

8. Microscopically the fracture mode in SCC is usually different from the fracture mode in plane strain fractures of the same alloy.

9. There appears to be a threshold stress below which SCC does not occur, at least in some systems.

2.3 Stress Corrosion Cracking of Pipelines

The first incident of external stress corrosion cracking (SCC) on natural gas pipelines was reported in the mid-1960s [10] in the United States. After several failures the extensive investigation of Stress Corrosion Cracking began. As a result of this investigation a theory of so called Classical Stress Corrosion Cracking was developed. This type of cracking is also called High-pH SCC.

The awareness of SCC on the Canadian pipelines began in 1985. TransCanada Pipe Line had three failures on the Northern Ontario portion of its pipelines between March 1985 and March 1986. They were considered to be the first evidence of SCC, although it was determined later that SCC had occurred on other pipelines in the 1970s. The type of SCC, which was detected on these failures, was different from the High-pH SCC, which has been found on other pipes in the world. At the time, this new form was called "Low pH SCC", more recently it was referred to as Near-Neutral-pH SCC [7].

Stress Corrosion Cracking is not a problem unique to Canadian pipelines. SCC has been recognized as a cause of pipeline failures in countries around the world. Pipelines in Australia, Iran, Iraq, Italy, Pakistan, Saudi Arabia, the former Soviet Union and the United States have also been affected by SCC.

For SCC to occur on an engineering structure, three conditions must be met simultaneously: a specific crack promoting environment must be present, metallurgy of the material must be susceptible to SCC, and tensile stresses above some threshold value must be present.

2.4 Classification of SCC Mechanisms

Prior to discussing classifications of pipeline SCC, I would like to mention different known mechanisms of Stress Corrosion Cracking. All of these mechanisms can be divided into those mechanisms that involve embrittlement of the metal as a consequence of corrosive reactions or those in which the cracks grow by extremely localized dissolution processes. For a given SCC system, whether anodic dissolution or hydrogen induced cracking dominates the cracking process should be analyzed depending on chemical, mechanical, electrical and metallurgical variables.

2.4.1 SCC Mechanisms on Anodic Dissolution

In the anodic dissolution mechanism, the applied stress causes plastic deformation and rupture of films on the metal surface. The rupture of the film exposes bare metal to the environment that undergoes rapid anodic dissolution. The crack propagates by dissolution, but the passive film prevents corrosion of the crack walls so a crack geometry is maintained. If the film formation rate is slow or creep rate is high, crack will blunt. On the other hand – high passivation rate and/or low creep rate – the passive film maintain coverage of the metal surface, preventing crack advance. So, where creep rates are high and repassivation rates are low, there will be continues process. Where creep rates are low and repassivation rates are high, there will be more discontinuous process.

Interganular SCC failures are frequently attributed to this mechanism since impurities at the grain boundaries have effects on repassivation and creep behavior.

Anodic dissolution most commonly associated with High-pH SCC since it has intergranular fracture surface. In alloy – environment systems such as carbon steel and low alloy steels in caustic, nitrates, phosphates and in concentrated carbonate-bicarbonate, cracking is intergranular and the steel exhibit active-passive behavior. At the same time line pipe steel in the Near-Neutral-pH environments do not exhibit passivation.

The crack velocity of anodic dissolution mechanism can be estimated using Faraday's law:

$$\frac{da}{dt} = \frac{i_a M}{ZFd} \quad (1)$$

Where da/dt is crack velocity, i_a – the anodic current density, M – atomic weight, Z – the oxidation state of the solvated species, d – density, F is Faraday's constant.

The results of recent cyclic load and interrupted constant displacement rate tests, performed by TCPL, have shown that Near-Neutral-pH SCC propagation does not occur under constant load or constant displacement condition. In contrast, alloy-environment system where the anodic dissolution mechanism is thought to operate all exhibit crack growth under constant load or constant displacement conditions.

The mechanisms on anodic dissolution can be divided into the following categories: 1) Mechano-Electrochemical, 2) Film Rupture, 3) Stress Adsorption, 4) Dissolution Mechanism, 5) Atomic Surface Mobility, 6) Film-Induced Cleavage, 7) Localized Surface Plasticity.

2.4.1.1 Mechano-Electrochemical

This category includes the high strain rate at the tip of the growing crack causing continuous depolarization of the anodic area so that cracking by electrochemical dissolution can continue. There is a great role of strain in causing the rupturing of islands of material resistant to electrochemical dissolution that has previously produced all the fracture area except the resistant islands.

Dix (1940), with Mears and Brown (1945) were apparently the first to propose that galvanic cells are set up between continuous intermetallic precipitates and adjacent metal at grain boundaries or through paths within the grains, the ensuing corrosion acting under stress to open up a crack. The applied stress was considered helpful in rupturing surface films, thereby exposing fresh metal at the tip of the crack, allowing the reaction to continue.

Engell and Baumel (1959) expressed doubt that the electro-chemical theory could be applied to mild steel because stressed steel wires exposed to nitrate solutions underwent discontinuous extension, the rapid portions of which they interpreted as intermittent cracking. The resultant calculated rate of cracking, i.e., 0.02 cm/second, is equivalent to a current density of 540 amp/cm² at the tip of the crack, which value is so high as to cast doubt, they stated, on the electrochemical model. In later papers (Baumel and Engell, 1961), however, they implied that the discontinuous extension they observed was caused by discontinuous creep which occurred regardless of damaging or non-damaging environments.

The weakness of the electrochemical theory was uncovered through observations that some metals crack only in specific electrolytes whereas electrochemical action would in fact be expected in a variety of related chemical media of comparable electrical conductivity. Furthermore there appears to be no reasonable electrochemical explanation why additions of extraneous anions to damaging environments should act as inhibitors for SCC, e.g. chlorides and acetates for carbon steels in boiling nitrate solutions. Simple galvanic effects between tip and walls of the crack, in other words, are not alone sufficient to explain the cause of fracture.

A modification of the electrochemical-mechanical model was suggested by Pickering and Swann (1963) based on thin-film electron microscopy. They proposed that an observed network of tubular corrosion pits forming along preferred paths such as active slip planes could account for cracking by ductile fracture of the tenuous walls of numerous adjacent pits.

2.4.1.2 Film Rupture

This model envisions the cyclic formation and rupture of films of corrosion product. Film rupture or slip-step dissolution was first mentioned by Dix, was modified and extended by Logan (1952) for various metals including aluminum and magnesium alloys, and by Forty and Humble (1963) for a brass. The common point of view is that a film of brittle surface corrosion product ruptures under stress, allowing progressive exposure of metal underneath to further chemical attack. The film -covered side of the

crack may, in some instances, act as cathode. Support of this mechanism was derived from potential measurements or from visible or microscopic examination of metals that had undergone SCC. Such a mechanism, however, if applicable at all, is probably not general because (1) SCC in α -brass is observed in absence of visible or suspected films, e.g., in alkaline NH_4OH , (2) pure metals on which brittle or cathodic corrosion products form quite readily are immune, and (3) tarnished metals in air on which equally brittle films exist do not fail. Farmery and Evans (1955-6) doubted that oxide film rupture could enter the cause of SCC in 7% Mg-Al alloy because cracks, the growth of which was stopped by cathodic polarization, did not necessarily reactivate when the applied current was discontinued. Also both chloride ions which supposedly break down oxide films, and nitrate ions which supposedly favor oxide films, can act as inhibitors for stress corrosion cracking of mild steel and of austenitic stainless steels respectively. Obviously some factor other than rupture of an oxide or other type brittle film is responsible for SCC in most observed instances of metal fracture.

As one of the first proposed stress corrosion cracking (SCC) mechanisms, film rupture theory still receives considerable support. Tensile stress is assumed to produce sufficient strain to rupture the surface film at an emerging slip band, and a crack then grows by anodic dissolution of the unfiled surface at the rupture site. Most investigators now agree that film rupture is essential to initiate cracking, but considerable controversy persists as to how a stress corrosion crack grows thereafter.

2.4.1.3 Stress Absorption

Stress Absorption model presents the reduction of energy to form a new surface by adsorption of specific species. The mechanism of cracking by this name proceeds not by chemical or electrochemical dissolution of metal at the tip of a crack, but instead by weakening of already strained metal atom bonds through adsorption of the environment or its constituents. The surface energy of the metal is reduced, encouraging the metal to part under tensile stress. This mechanism is related to the simplified Griffith criterion of crack formation that equates strain energy in the metal to the surface energy of the incipient crack area.

Since stress corrosion cracks propagate in an apparently brittle manner, although at low velocities, the fracture stress (σ_c) to cause the spread of an elliptical crack, Length $2(c)$, is given by

$$\sigma_c = \left(\frac{2E\gamma_s}{\pi c} \right)^{\frac{1}{2}} \quad (2)$$

Where E is Yong's modulus and γ_s is the surface energy. Clearly, any process that lowers γ_s will reduce the stress for brittle fracture and γ_s may be lowered by the absorption of appropriate species at the fracture surface.

Uhlig originally proposed that specific aggressive dissolved species adsorb at "mobile defect sites", weakening the cohesive bonds between adjacent atoms at the crack tip. Adsorption in this mechanism is assumed to be potential dependent, to account for cathodic suppression of stress corrosion cracking below a "critical potential". Effects of

inhibitor species are explained by assuming competitive adsorption between aggressive and inhibiting anions.

An explanation of metallurgical effects on SCC requires the assumption of adsorption at mobile defect sites. The nature and character of such defects have not been specified. Pure metals are thought to be resistant because the defect sites move in and out of the surface areas at the root of a notch too rapidly for adsorption to succeed.

Where plastic deformation is involved in fracture, Oraowan suggests that the surface energy term in equation (2) needs to be modified to take into account the work done in plastic deformation. so that to γ_S should be added γ_P , the work for plastic strain. Now γ_P is greater than γ_S by a few orders of magnitude, and therefore any reduction in the latter by absorption will have a negligible effect on the fracture stress. Moreover, in some instances mechanism involving enhanced local plasticity caused by the presence of hydrogen has become apparent in recent years and, for those cases at least, the mechanism of crack growth is hardly consistent with an approach based on Equation (2).

2.4.1.4 Dissolution Mechanism

Early theories of stress corrosion cracking were concerned with a two-stage mechanism: 1) the electrochemical reaction produces a pit and from this, 2) a crack runs a short distance from this pit and the electrochemical reaction then occurs again.

Crack grows due to a dissolution-controlled process and the crack-tip strain rate is such that filming of the crack tip is prevented. Thus, writing Faraday's second law as a penetration rate, the crack velocity (CV) can be given by

$$\frac{da}{dt} = \frac{i_a M}{ZFd} \quad (3)$$

Where i_a - anodic current density, M - atomic weight of the metal, Z - valence of the solvated species, and F - Farady's constant.

Equation (3) represents an upper-bound crack velocity by continuous dissolution, requiring strain rates, and stresses or stress intensity factors that probably do not exist in many service situations until the later stages of stress corrosion crack growth. The earlier stages of growth may involve lower crack velocities, than those given by Equation (3). Once a crack tip has become filmed, growth will cease, until the film is ruptured and dissolution can restart until film growth prevents it again, the frequency of such events depending upon the crack-tip strain rate and the dissolution and film growth rate. Integration of the current transients over an appropriate time interval will provide the relevant anodic charge (or charge density) passed (Q_f), which can then be incorporated into Equation (3) to reflect the fact that the crack is not propagating continuously at the upper bound, i.e.,

$$CV = \frac{Q_f}{\epsilon_f} \epsilon_{cr} \times \frac{M}{ZFd} \quad (4)$$

Where ϵ_f - strain to rupture the film and ϵ_{cr} - crack tip strain rate.

2.4.1.5 Atomic Surface Mobility

Galvele has suggested that many forms of environmentally induced cracking grow by the capture of surface vacancies at the crack tip and counter-current surface diffusion of atoms away from the crack tip. The mechanism predicts that stress corrosion cracking should be prevalent at temperatures below 50% of the metal's melting point, T_m , and in the presence of low melting surface compounds, when surface mobility is maximized in preference to bulk diffusion in the metal crystal. The effect of critical environments to cause stress corrosion cracking (SCC) is explained by low melting compounds that enhance surface mobility.

According to this model compounds with higher melting points are protective. This appears to raise a difficulty in explanation of iron-base alloys cracking, while predicting that nitrates would promote cracking because the melting point of iron nitrate is very low, it would predict that Fe_3O_4 is a protective compound, since its melting point is $1597^\circ C$. It has already been mentioned that in many instances of SCC in steels, the potential range for cracking is associated with Fe_3O_4 formation. Galvele surmounts this problem by invoking arguments relating to the breakdown the film, chemically or electrochemically, so that active-passive transitions and potential dependence, for example, are expected to be involved in SCC. In that sense, the surface-mobility model is not essentially different from some considered earlier.

2.4.1.6 Film-Induced Cleavage

The film-induced cleavage (FIC) mechanism has been proposed to explain discontinuous transgranular crack growth and high transgranular crack growth rates. FIC suggests the presence of brittle surface films, to include dealloyed films on certain alloys and oxides on pure metals and other alloys. A crack growing in the film may propagate further into the underlying metal if it reaches sufficient velocity at the film/metal interface. Anodic dissolution and corrosion are not necessary to propagate cracks but only to form the required brittle surface film. Thus, relatively low anodic dissolution rate forms a brittle surface film and a fast-growing crack in the film may penetrate for some distance into the ductile substrate metal before its growth is arrested. The surface film must develop again at the crack tip surface before a new burst of brittle crack growth is possible. Thus, a low anodic current at a strained surface can lead to rapid, discontinuous, brittle cracking, according to the FIC mechanism.

Unfortunately, there is no a priori reason to expect that surface films or layers are sufficiently brittle to support a brittle crack or that such a crack will be sustained after crossing the interface into the underlying ductile matrix. Most passive films are very thin and hydrated. While they can be ruptured, it seems unlikely that they would be sufficiently brittle to support the FIC. Dealloyed layers are unlikely to have sufficient adhesion to the substrate or inherent brittleness to sustain cracking.

The characteristics of Near-Neutral-pH SCC also do not appear to be consistent with Film-Induced Cleavage mechanism. It requires the presence of a brittle coherent

oxide film, de-alloyed layer, or some other brittle film or layer. There is no evidence that a film or layer with the required properties is present.

2.4.1.7 Localized Surface Plasticity

Metallurgical effects on SCC are not easily explained by models that contain only reactions on the surface, but not the effects of the corrosive environment on the properties of the underlying metal. Mechanical creep precedes the initiation of SCC, and is accelerated by anodic currents. Such anodic currents can originate, of course, from the usual anodic corrosion reactions. Creep accelerated by anodic current implies softening by a surface defect structure that attenuates the normal strain hardening that accompanies primary creep. Corrosion induced relief of strain hardening may be one symptom of a critical corrosion effect on metallurgical properties during SCC. That is, SCC may result from a defect structure ahead of the crack tip, as proposed in the mechanism, localized surface plasticity (LSP).

In the LSP mechanism, film rupture supposedly initiates large anodic currents at the rupture site by galvanic coupling of the exposed active surface to surrounding noble passive surfaces. The passive film must be in a weakened state to prevent rapid passivation which would suppress crack growth. These weakened states usually occur at critical potentials near the boundaries of the passive potential region and are probably influenced by the presence of critical anions such as Cl^- . These galvanic anodic currents produce a softened defect structure locally at the rupture site, which coincides with the crack tip for

a growing crack. The softened structure, which would normally deform plastically, can do so to only a limited extent in the microscopic volume ahead of the crack, when constrained by the surrounding material of full strength and hardness. Microstrain within the softened, yet constrained, crack-tip volume produces a triaxial stress state (plane-strain condition), which suppresses plastic slip. Continued strain can only propagate a brittle crack.

A vacancy-saturated defect structure is one that may be responsible for stress corrosion. Others may be possible as well, and the LSP mechanism is not restricted to any specific defect structure type. However, it is notable that vacancies have been credited with causing increased creep by anodic reaction and by cyclic loading.

The LSP mechanism seems to explain several metallurgical related effects in SCC. Resistance of pure metals is explained by the lower degree of strain hardening in pure metals, as compared to alloys. Thus, extensive deformation and ductility in pure metals are permissible before relief of strain hardening is sufficient to initiate cracks. Highly strain hardenable alloys, even of low yield strength (e.g., stainless steels and brasses), are often highly susceptible.

2.4.2 Mechanisms of Hydrogen Related Cracking

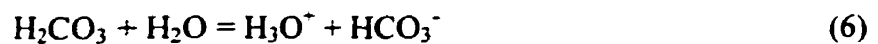
The most plausible mechanism for crack propagation in the Near-Neutral-pH environment is a hydrogen-related mechanism. It is well established that hydrogen can cause several types of damages to steels including H₂S cracking, delayed hydrogen

embrittlement of high strength steels, and hydrogen effect on plasticity of low strength steels [23]. The mechanism of all these different forms of hydrogen embrittlement all involve the entry of hydrogen into the lattice, the formation of unstable brittle hydrides, the formation of strain induced martensite, the pinning of dislocations and hydrogen enhanced localized plasticity.

The most likely source of hydrogen in Near-Neutral-pH SCC is carbonic acid, formed by the dissolution of carbon dioxide in the groundwater [24].



The carbonic acid can further react with water to produce a hydronium ion and a bicarbonate ion.



The hydronium ion is then reduced to generate hydrogen at the metal surface.

The carbonic acid can also be dissociated in two steps: [25]



Then hydrogen ions are reduced into hydrogen atoms:



It was also found that in the pH from 4 to 6, in addition to the H^+ reduction as shown above, another cathodic reaction was favored to directly reduce carbonic acid into a hydrogen atom and bicarbonate ion:



This additional cathodic reaction causes the H_2CO_3 to be more corrosive than a completely dissociated acid at the same pH.

Some alloys fail under stress in corrosive conditions because of the entry of hydrogen atoms into the alloy lattice. This phenomenon is called Hydrogen Induced Cracking.

Various investigators have suggested that the brittle nature of SCC can only be accounted for by a mechanism controlled by hydrogen induced cracking, which has brittle cleavage-like features very similar to those of SCC. It is generally assumed that hydrogen acts to weaken interatomic bonds in the plane strain region at the crack tip. The result is a singular crack with little branching.

The process of hydrogen induced cracking involves hydrogen evolution, absorption, diffusion and embrittlement. Hydrogen may be present from reduction of water or acid by



or



in neutral and acidic solutions, respectively.

Stress corrosion cracking (High-pH SCC), which relies on an anodic dissolution for at least a part of the propagation process, can be avoided by cathodic protection. Hydrogen induced cracking, in contrary, is induced by cathodic polarization since this promotes hydrogen development.

Unfortunately, such a simplified definition does not always make a clear distinction. In some instances, extensive cathodic formation of hydrogen and subsequent measured entry into the metal lattice has stopped growing stress corrosion cracks. Proponents have suggested that in some way hydrogen may enter the lattice at the crack

tip, despite contrary surface potentials. Nevertheless, very deep, growing stress corrosion cracks have been stopped effectively in low-strength ductile alloys by cathodic polarization with accompanying hydrogen evolution. Hence, hydrogen is not generally accepted as the cause of stress corrosion cracking in most low strength ductile alloys. However, hydrogen induced cracking (HIC) has generally been accepted as the controlling mechanism of failure for the less ductile high strength iron, titanium, and some aluminum alloys. Following are three main possible hydrogen induced cracking mechanisms.

2.4.2.1 Hydrogen-Related Phase-Change Mechanisms

A number of metallic systems have demonstrated hydrogen embrittlement resulting from stress-induced formation of hydrides or other relatively brittle phases and the subsequent brittle fracture of these phases. Several types of phases may take part in this failure mechanism, e.g. hydrides, martensitic phases, etc. the basic requirements are that these phases be stabilized by the presence of hydrogen and the crack-tip stress field, and that the phase that forms be brittle. The typical system that exhibits failure by this mechanism - forms stable hydrides in the absence of stress and these hydrides are thermodynamically more stable under the stress conditions at the crack tip. In some cases, hydrides can be shown to result from this stress stabilization even when they are not formed in the absence of the stress.

The embrittlement mechanism may be qualitatively described as follows. Under

the applied stress, the chemical potential of the solute hydrogen and the hydride are reduced at tensile stress concentrations, such as crack tips. Diffusion of hydrogen to these elastic singularities and precipitation of hydrides at the crack tips then occur. The phase change is accompanied by a decrease in the critical stress intensity for crack propagation because the hydrides are generally brittle phase. The crack may propagate into the hydride, the formation of which is accompanied by a high, compressive stress field. The greatly decreased K_{IC} allows rapid crack propagation when the applied stress is only moderately increased, and the crack propagates by cleavage until the hydride-solid solution boundary is reached. At this point, the crack enters ductile phase with a high K_{IC} and the crack stops until more hydride is formed. The process repeats itself, resulting in discontinuous crack growth through the stress-induced hydride phase and with hydride formation along the flanks of the cracks.

2.4.2.2 Hydrogen - Enhanced Local Plasticity Mechanism

In many cases, the definition of hydrogen-related fracture as a brittle fracture is based on loss of macroscopic ductility and/or relatively low-resolution studies of the fracture surface. Beachem first suggested, on the basis of careful fractographic examination, that hydrogen embrittlement of steels was in fact associated with locally enhanced plasticity at crack tip. While the concept of enhanced plasticity appears to be at variance with embrittlement, there is no contradiction when it is recalled that the distribution of hydrogen can be highly nonuniform under an applied stress. Thus, locally

the flow stress can be reduced, resulting in localized deformation that leads to highly localized failure by ductile processes, while the total macroscopic deformation remains small. Strain-to-failure measurements made over a macroscopic gauge length will be greatly reduced despite the high degree of local plasticity. Examination of the fracture surfaces at low resolution will induce a conclusion of a brittle fracture surface because of the highly localized nature of the ductile failure.

The HELP mechanism is operative for hydrogen in solid solution and for gaseous hydrogen environments. In both cases, the application of a stress results in a nonuniform distribution of hydrogen with a high concentration in front of an elastic singularity such as a crack or a precipitate. The high local stress field at the tip of a crack reduces the chemical potential of solute hydrogen, and as a result of diffusion, the concentration is locally increased. The tip of the crack is also the most likely place for hydrogen entry from a gaseous atmosphere since it is the place where plastic deformation first occurs, and hence any surface barriers to entry are minimized. The resistance of dislocation motion, and thus the flow stress, is decreased by the presence of hydrogen. Thus, in the regions of high hydrogen concentration, the flow stress is decreased and slip occurs at stress below those required for plastic deformation in other parts of the specimen; i.e., slip localization occurs in the vicinity of the crack tip.

2.4.2.3 Decohesion Mechanism

One of the oldest mechanisms of hydrogen embrittlement is decohesion. It is associated hydrogen embrittlement with a decrease in the atomic bond strength resulting from the local concentration of hydrogen. Thus, the fracture is cleavage, which occurs when the applied stress exceeds the cohesive stress. This cleavage fracture is generally accompanied by plastic deformation, which greatly increases the total energy of fracture and hence the macroscopic K_{IC} . In the systems in which fracture occurs transgranularly, it is expected to be along the cleavage planes and to exhibit the fractography of cleavage, while intergranular fracture should occur directly along the grain-boundary surfaces. In intergranular fracture, the cohesive energy and cohesive force of the grain boundary decreases due to the presence of hydrogen.

Evidence for a hydrogen-related decrease in the cohesive energy may be sought in the elastic constants, atomic force constants derived from phonon dispersion curves, surface-energy measurements, fracture surface energies, and theory.

2.4.3 Near-Neutral-pH SCC vs. High-pH SCC in Pipeline Steel

Most of the early failures were intergranular in nature, whereas, many of the recent failures that have occurred in Canada are transgranular. It is now recognized that there are at least two forms of external SCC on underground pipelines. The intergranular form is referred to as high-pH or classical SCC while the transgranular form is referred to

as low-pH, non-classical, or Near-Neutral-pH SCC. In the following table a comparison of these two forms of cracking is given:

Table 2.1. Comparison of High-pH and Near-Neutral-pH SCC.

Characteristic	Near-Neutral-pH SCC	HIGH-pH SCC
Electrolyte pH	6.5 to 7.5	9 to 10
Fracture Mode	Transgranular	Intergranular
Cracking Orientation	Longitudinal	Longitudinal
Numerous Surface Cracks	Yes	Yes
Linking of Cracks	Yes	Yes
Patches of Cracks	Yes	Yes
Corrosion of Crack Faces	Yes	No
Corrosion of Pipe	Sometimes	Usually Not
Association with Iron Carbonate and Magnetite Films	Yes	Yes
P/S Potential, CCS	Native Potential	-722mV
Width of Potential Range	Probably > 100mV	Narrow (<100mV)
Temperature Dependence	Not established	Arrhenius Behavior

These data shows that both Stress Corrosion Cracking occur in patches with hundreds of cracks on the pipe surface that are generally longitudinal in direction, and localized to a small area of pipe on a joint. This is known as a tent effect. The “tent” (gap

where liquid can be trapped) is formed between the seam which goes straight along the pipe or in a spiral and a coating tape. These cracks link up to form long shallow flaws that can lead to rupture. In both cases, the fracture faces are usually covered with black magnetite (Fe_3O_4) or iron carbonate films. However there are number of differences in the two forms of cracking. The cracks associated with Near-Neutral-pH SCC are generally wide and transgranular in nature with evidence of corrosion on the crack walls. High-pH stress corrosion cracks are generally intergranular and are usually sharp with little evidence of corrosion of the crack walls. In many cases, the near-neutral-pH cracking is associated with the long seams, where tenting of the tape coating has led to a build-up of iron carbonate paste on the pipe surface. On the other hand, high-pH stress corrosion cracks are usually found in the body of the pipe. Pitting corrosion and CO_2 attacks also are occasionally associated with Near-Neutral-pH SCC sites while high-pH stress corrosion cracks usually are not associated with significant corrosion.

2.4.3.1 High-pH Stress Corrosion Cracking

High-pH SCC typically found within 20km downstream of compressor. It is generally located on the bottom of the pipe or in the lower quadrants it is rarely associated with corrosion.

2.4.3.1.1 Environmental Factors

When SCC was first observed on natural gas pipeline, nitrates, phosphates, and caustic were considered as possible causative agents. But neither electrolyte nor ground water samples, taken from beneath coatings at failure sites didn't prove this assumption. In the beginning of 70's it was found that a concentrated carbonate-bicarbonate solution could also cause SCC of pipeline steel [9]. The evidence for concentrations of carbonates at the pipe surface was found in a limited number of cases [10]. And was concluded that concentrated carbonate-bicarbonate solution was responsible and mechanism for the development of the environment was developed by Wenk. Essentially, the cathodic protection (CP) system causes a pH increase at the pipe surface. Carbon dioxide, which is present in the soil, is rapidly absorbed by high-pH solution to generate the concentrated carbonate-bicarbonate ($\text{CO}_3\text{-HCO}_3$) environment. In labs it is simulated using 1N NaHCO_3 – 1N Na_2CO_3 .

High-pH SCC of pipeline steel occurs over a very limited potential range that is about 100mV wide and is centered around -722mV Cu/CuSO_4 (this is associated with active-passive transition in potentiodynamic polarization curve¹¹)[11] at 75°C and moves in the positive (noble) direction with decreasing temperature [12]. From the field experience it is found that gas discharge temperature usually exceeds 35°C . Which supports the temperature dependant influence.

High-pH SCC also occurs over a limited pH range, centered around 9. At pH above 10, the solution is primary composed of carbonate and the passive film characteristics and electrochemistry is not conducive to SCC. At pH below 8, the

solution is dominated by the bicarbonate iron and cracking does not occur unless cations such as NH_4^+ are present.

The limited potential and pH range over which SCC occurs in the high-pH environment explains the infrequent occurrence High-pH SCC on most pipeline systems. In order for the concentrated high-pH environment to develop, significant current flow to the pipe is required, generated high-pH environment absorbs carbon dioxide (CO_2) from the ground. On the other hand, the potential range for SCC lies between the native potential of most pipelines, and adequate protection, -850mV (Cu/CuSO_4). This paradox can be resolve if it is assumed that the environment and potential vary on a seasonal basis, with SCC occurring during periods of the year when adequate CP is not achieved.

2.4.3.1.2 Metallurgical Factors

The attempts to correlate the occurrence of SCC with metallurgical parameters did not bring success. SCC was found to occur on pipelines having a variety of diameters, wall thickness, pipe grades, compositions, manufacturers, and joining techniques. It was found that major alloy additions, $>1\%$, of some elements could increase SCC resistance, but such additions were too expensive. Differences in the SCC susceptibility of different pipeline steels, measured by differences in the threshold stress for crack initiation, were found in the studies, but cause of differences was not identified.

2.4.3.1.3 Mechanical Factors

In order for stress corrosion cracks to initiate and propagate tensile stress must be present at the crack tip. The cracking usually initiates at flaws on the surface where stress concentration exists. Below some value of the tensile stress (threshold stress) crack initiation does not occur.

In many cases longitudinal SCC have occurred in the body of the pipe where the primary stress in the hoop stress generated by internal pressure. (Barlow's formula):

$$\sigma = \frac{PD}{2t} \quad (13)$$

(Where P-operating pressure; D- the pipe diameter; t – wall thickness)

It is supported by the fact that SCC occurs much less frequently on heavy wall pipe, where hoop stresses are lower.

It has been found that threshold stress for machined surfaces approaches the yield stress on most materials, but is significantly reduced for an actual pipe surface by the presence of mill scale and pits on the surface [13]. For mill scaled surfaces, threshold stress measured in the laboratory are typically between 60% and 70% of specified minimum yield strength (SMYS) in the high pH environment [14].

Cyclic stress also affects SCC – the small pressure fluctuations associated with operation of natural gas pipeline tend to exacerbate SCC [15]. This effect has been attributed to the occurrence of cyclic creep at the crack tips, which facilitates the rupture of passive film.

2.4.3.2 Near-Neutral-pH Stress Corrosion Cracking

It was thought that aspects of SCC were reasonably well understood until one pipeline company started experiencing SCC on their polyethylene tape and asphalt coated pipelines in the 1980's. An extensive field investigation program showed that the occurrence of SCC correlated with near neutral pH ($\text{pH} < 8$) dilute CO_2 containing electrolytes and that cracking was not observed where high-pH electrolytes were detected [16].

Near Neutral pH SCC can be found anywhere, although 65% found in the first valve section. It can be found associated with welds, with corrosion or other stress risers.

2.4.3.2.1 Environmental Factors

Electro-chemical study of line pipe steel clearly demonstrated that the Near-Neutral-pH SCC environments do not promote passivation and do not exhibit active-passive transition, which are commonly observed with High-pH SCC environment [17]. Parkins [18] reported that environmentally induced cracks could be initiated on the surfaces of line pipe steels in the Near-Neutral-pH environment under cyclic loading conditions. The crack initiate most readily on natural, corroded, mill scaled surfaces. Harle [19] produced transgranular crack propagation in Near-Neutral-pH environment using precracked compact type specimens of line pipe steels.

The results of these studies and field observations all indicate that the environment responsible for Near-Neutral-pH SCC are: 1) The potential is around free corrosion potential -760 to -800mV (Cu/CuSO_4); 2) There is no correlation of occurrence of Near-Neutral-pH SCC with the temperature; 3) dilute groundwater containing dissolved CO_2 . As in the case for High-pH SCC, the source of the CO_2 is decay of organic matter in the soil. So in case of Near-Neutral-pH SCC, cathodic protection current cannot flow to the pipe either because of shielding of the current by coating such as tapes, high resistance soils, or a poor cathodic protection system design, which leads to generation of Near-Neutral-pH.

2.4.3.2.2 Metallurgical Factors

Near Neutral pH SCC has been observed on a number of pipelines having different grades and yield strength. They do all appear to be carbon-manganese steels with a ferrite/pearlite microstructure. There are no laboratory or field data indicating that one particular microstructure or grade of steel is significantly more resistant to Near-Neutral-pH SCC. Results of constant displacement rate tests by Harle [20] demonstrated that coarse grain heat affected zone microstructure adjacent to the weld is significantly more susceptible to cracking than the base material in Near-Neutral-pH. High velocities also have been observed at the bond line of the electric resistance weld than in the base metal in X-52 line pipe steel.

2.4.3.2.3 Mechanical Factors

The mechanical conditions for Near-Neutral-pH SCC appear to be more restrictive than those for High-pH SCC. In SSR tests, cracking is generally only observed within the necked region of the specimen where plastic deformation and true stresses are very high. In constant displacement rate testing [21], cracking is only observed where dynamic loading conditions are present. No evidence of crack growth has been found under constant load or constant displacement conditions.

A threshold stress for crack initiation in the Near-Neutral-pH environment has not been established.

Chapter 3

Experiment Methodology

The material, which was selected for experiment was provided by Prudential Steel Ltd. in form of 2 foot pipe segment of commercial grade X-52 (grade 359), Category II, Sour Service [26] steel line pipe. Outside Diameter 323.9mm, thickness is equal to 5.6mm. The chemical composition and mechanical characteristics of this steel is shown in the following tables:

Table 3.1. Chemical Composition of X-52 Pipeline Steel

C	Mn	P	S	Si	Cu	Ni	Cr
0.0742	0.841	0.01	0.0072	0.205	0.026	0.0383	0.0416
Sn	Mo	Al	Nb	V	Ti	Ca	B
0.0083	0.0078	0.0427	0.0153	0.0027	0.0017	0.0029	0.0001

Table 3.2. Mechanical Characteristics of X-52 Pipeline Steel

Steel	Yield Strength (Min), Mpa	Ultimate Tensile Strength (Min), MPa	Ultimate Tensile Strength (Max), MPa
X-52	359	455	-

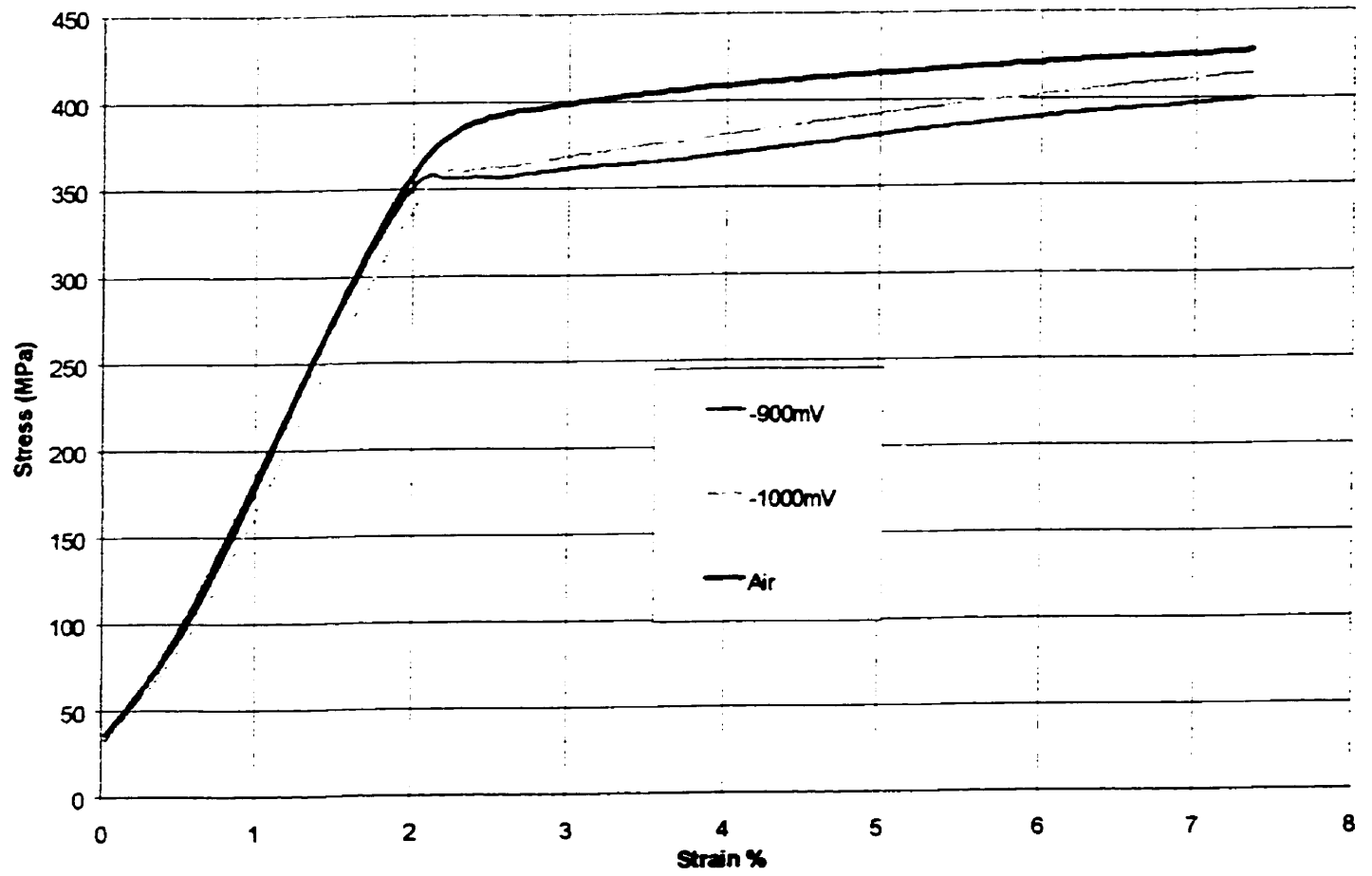


Fig 3.1 Stress - Strain Curve at Different Potentials

The selection of this particular type of pipe was made due to extensive application of it in oil and gas transmission systems. The samples for the test were cut along the longitudinal direction of pipe. Stress vs. Strain charts in the air and solutions at several potentials presented on Fig 3.1. During the course of the experiment two different types of samples were used. The first type is a standard flat straight sample commonly used for the tensile test (Fig 3.2(a)). The second type is a conical sample it was used to determine critical stress of Stress Corrosion Cracking initiation (Fig 3.2(b)). All the samples were chosen to be flat to facilitate surface preparation and observation of samples after the test. Prior to the test all samples were polished to $3\mu\text{m}$., cleaned by methanol and dried with compressed air. Several tests were performed without prior polishing: with original surface of the pipe, sand blasted surface and electro-polished surface. The observation of crack initiations on these samples in Scanning Electron Microscope was extremely difficult, since the surface roughness was much higher than initial size of cracks.

In order to perform the experiments in aqueous solution the environmental cell was designed and fabricated.

The solution used for the experiment is a standard NS-4 (Nova Solution 4). This Near-Neutral-pH Bicarbonate solution is used for simulating the trapped liquid between pipe and its coating, found on Near-neutral SCC sites. The initial pH of NS4 prior to the tests was around 7.4. The chemical composition of it is given in Table 3.3

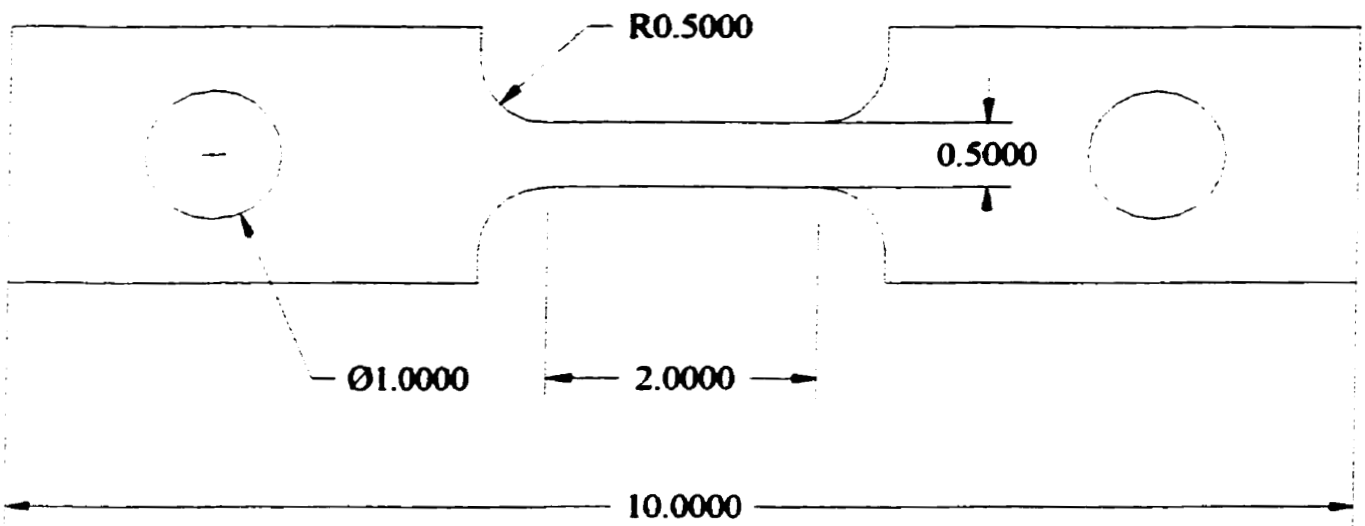


Fig 3.2 (a) Standard Straight Flat Sample

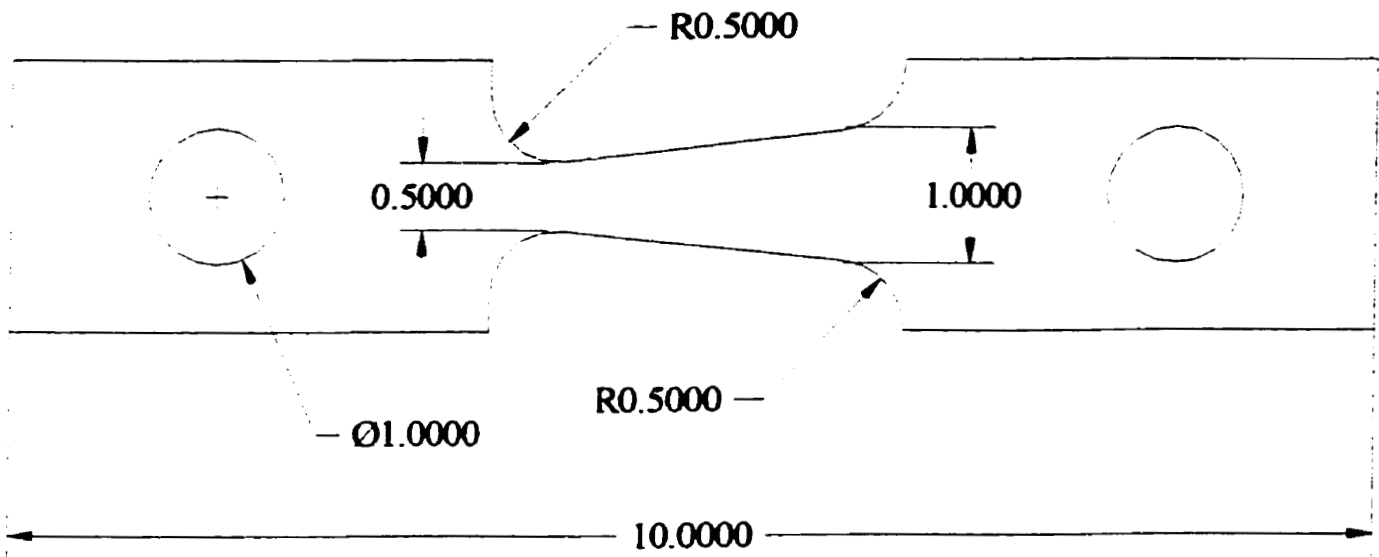


Fig 3.2 (b) Flat Conical Sample

Table 3.3. The Chemical Composition of NS-4

Chemicals	mg/L
NaHCO ₃	483
KCl	122
CaCl ₂ ·2H ₂ O	137
MgSO ₄ ·7H ₂ O	131

The schematic diagram of testing set-up for the slow strain rate tests (SSRT) is shown on (Fig 3.3). On this diagram environmental cell is shown with a specimen inside under tensile load. The potential is applied from the potentiostat to the specimen, which is acting as cathode and platinum (Pt) spiral wire acts as anode. The Standard Calomel Electrode (SCE) is used as a reference electrode for measurement of potential applied to the specimen. The gas (CO₂ 5% balance with N₂ or just pure N₂) is flowing from the gas tank through the flow meter, which regulates gas supply, to environmental chamber. The excess gas is leaving the environmental chamber through exhaust gas tube.

Before every test the solution was preconditioned by bubbling it with 5% CO₂ (carbon dioxide) balanced with N₂ (nitrogen) for at least 12 hours. After this preconditioning period pH of the solution decreased from 7.4 (initial pH) to the level of 6.8. The same gas was bubbled through the solution during the entire period of the tests.

During several tests the gas used for bubbling through the cell was N₂ (nitrogen). This was done to avoid penetration of O₂ (oxygen) into the cell. By the end of the test the pH level of the solution increased to the level of 8.5.

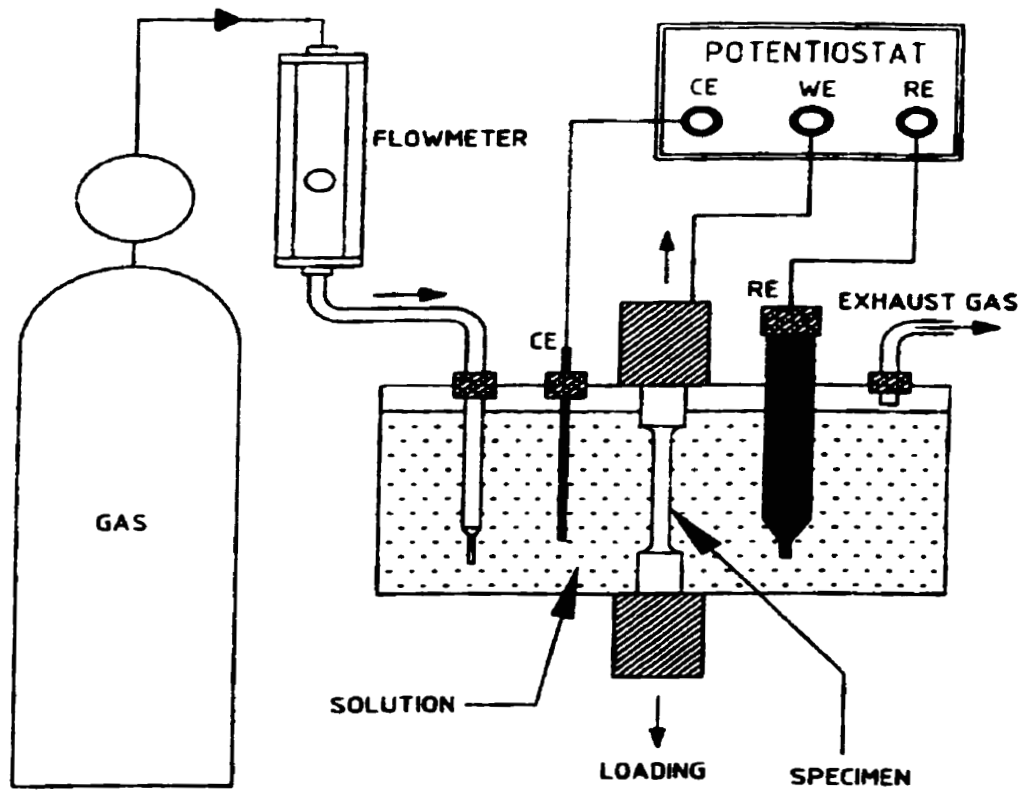


Fig 3.3 The Schematic Diagram of Environmental Chamber for Slow Strain Rate Test.

For the sake of analysis a number of tests were done in NS4 solution when pH was deliberately decreased to 3.7 by adding sulfuric acid. During this test 5% CO₂ (carbon dioxide) balanced with N₂ (nitrogen) was used for bubbling through environmental cell. These tests were done to determine the influence of hydrogen on crack initiation and propagation.

After each test the samples were cleaned with acetone, AC-tape and dried using compressed air. All of the samples were examined using Scanning Electron Microscope (SEM) as well as optical microscope.

First the influence of the potential on SCC initiation was investigated, strain rate of 5×10^7 1/sec was used to perform the tests at different potentials. Then a number of slow strain rate tests (SSRT) were performed at different strain rates 1×10^7 1/sec, 2.5×10^7 1/sec, 5×10^7 1/sec and 10^6 1/sec with fixed potential of $-900 \text{mV}_{\text{SCE}}$.

During the investigation of pH influence on SCC initiation strain rate 5×10^7 1/sec and potential $-900 \text{mV}_{\text{SCE}}$ were used.

Chapter 5 discusses the influence of residual stresses and microstructure change on Near-Neutral-pH SCC initiation and propagation. In order to conduct the experiments to get this type of data, various heat treatments were performed to stress relieve or change microstructure of pipeline steel. Table 3.4 shows different heat treatment performed during experiment. To investigate microstructure all the samples were polished to $3 \mu\text{m}$ and etched with 3% Nital Etchant (3% HNO₃ + methanol). The observation of microstructure was done through optical microscope.

Table 3.4 Heat Treatment Parameters

Quenched & Tempered Conditions	Stress Relieving Conditions
950°C/10min + WC	250°C/2hrs + FC
950°C/10min + WC + 250°C/2hrs + AC	450°C/2hrs + FC
950°C/10min + WC + 450°C/2hrs + AC	550°C/2hrs + FC
950°C/10min + WC + 650°C/2hrs + AC	650°C/2hrs + FC
950°C/1 hr + WC + 650°C/2hrs + AC	

WC – Water Cooled; AC – Air Cooled; FC – Furnace Cooled

Chapter 4

Investigation of Susceptibility to Near-Neutral-pH SCC of X-52 Pipeline Steel

Within last several years not very many investigation of Near-Neutral-pH SCC initiation has been done. At the same time it is vital for the industry to know the parameters when pipeline steel is the most susceptible in Near-Neutral-pH environment, growth conditions and mechanism of crack initiation and propagation. One of the most contributing papers in this field was by CANMET presented at the International Pipeline Conference in 1998 in Calgary. In their investigation they found that the early crack initiation can be correlated with corrosion pits and inclusions. The second, later stage of initiation they found is not related to any surface irregularities and can be referred to specific crystallographic planes. These are very important results, but at the same time several questions remain open. First is restricted loading conditions used during experiment: the stress ratio R (minimum stress/maximum stress) and loading frequency f were $R = 0.4$ and 0.6 and $f = 1\text{Hz}$ and 0.1Hz . This restricted loading might lead to a question if the developed cracks had more mechanical (in this case it would be fatigue) than environmental reason for initiation and propagation. The second question is the potential applied to the sample during the experiment. In case of CANMET investigation - Free Corrosion Potential was used. This is not the case if one tries to imitate the "holiday" (the center of the damaged coating on the pipe) the potential of this particular place sometimes is not at Free Corrosion Potential. On the other hand Free Corrosion Potential can be used to imitate the environment which is created at site of coating

debonding without rupture or environment at the surface of the pipe in a distance from the “holiday” where the coating creates a shielding effect on cathodic protection.

Having all this information in mind, the objectives of the susceptibility investigation are following:

1. First of all the most susceptible environments for Near-Neutral-pH SCC have to be determined. This will be done by performing several tests at different potentials and different strain rate of loading.
2. Second the critical stress of Near-Neutral-pH SCC initiation for as-received steel has to be determined, using specially designed for this purpose – conical sample.
3. Strain rate effect on Near-Neutral-pH SCC initiation has to be investigated.
4. The influence of hydrogen on Near-Neutral-pH Stress Corrosion Cracking initiation has to be examined. This will be done by deliberately changing pH of the solution and purging it with a different gasses (5%CO₂ balanced with N₂ and pure N₂).
5. Near-Neutral-pH SCC growth rate has to be calculated.
6. The susceptibility of different types of microstructure of X-52 steel to Near-Neutral-pH SCC have to be investigated and critical stresses for different microstructure have to be found.
7. To determined the influence of residuals stresses in the steel on Near-Neutral-pH SCC initiation.

4.1 Determination of the Most Susceptible Environments

A number of Slow Strain Rate Tests were conducted using standard straight samples in environmental chamber, each of the tests was done at a different potential. The potential was changed from Free Corrosion Potential (-712mV) to -1200mV vs. SCE. At this stage of experiment all the samples were taken to 15% of strain. Strain rate was kept at a constant level of $5 \times 10^{-7} 1/s$, the gas used for purging through the environmental chamber was 5% carbon dioxide CO_2 balanced with nitrogen N_2 . On the Fig 4.1.1 (a, b) we can see the images of the surfaces for two different samples taken to 15% of strain at constant value of potential: a) Free Corrosion Potential $E_{SCE} = -712mV$ and b) $E_{SCE} = -750mV$. As it can be seen on both of these pictures no SCC developed. At the same time high degree of surface dissolution can be observed. Electro-chemical processes, which are going on in the environmental chamber, can be expressed in the follow way:

- 1) 5% carbon dioxide gas reacts with water in Near Neutral aqueous NS4 Solution:



- 2) At this point there are two ways for Near Neutral solution in which Electro-chemical reaction can flow:

- a) carbonic acid react further with water and produce hydronium ion and bicarbonate ion:



Then hydronium ion dissociate even further into water and hydrogen ion [28]:



b) carbonic acid dissociate into ion of hydrogen and ion of bicarbonate:



3) The last set of reaction basically explains the reason of uniform dissolution, which we observed, on the surface of the sample. They are reduction of hydrogen and oxidation of iron:



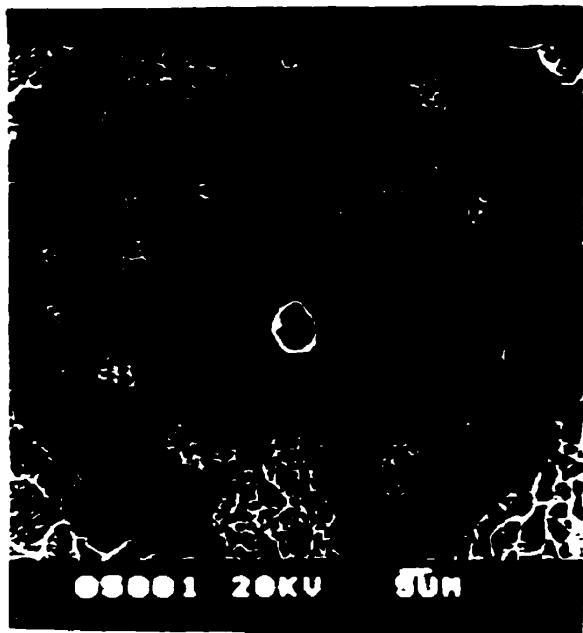
The last reaction is happening due to lack of electrons supplied by impressed current, in case of -750mV , or no electron at all supplied by impressed current, in case of Free Corrosion Potential. So electrons have to be taken Electro-chemically from iron, which leads to its dissolution.

It is noticed that iron grains are undergone much lower dissolution rate, than grain boundary, where content of iron is lower, what is quite reasonable for general corrosion. This may be associated with dissolution of metallic iron into ferrous ion Fe^{2+} , which is in the form of $\text{Fe}(\text{OH})_2$ and/or FeCO_3 , depending on the pH value and HCO_3^- concentration in the solution. These reactions can be express as:

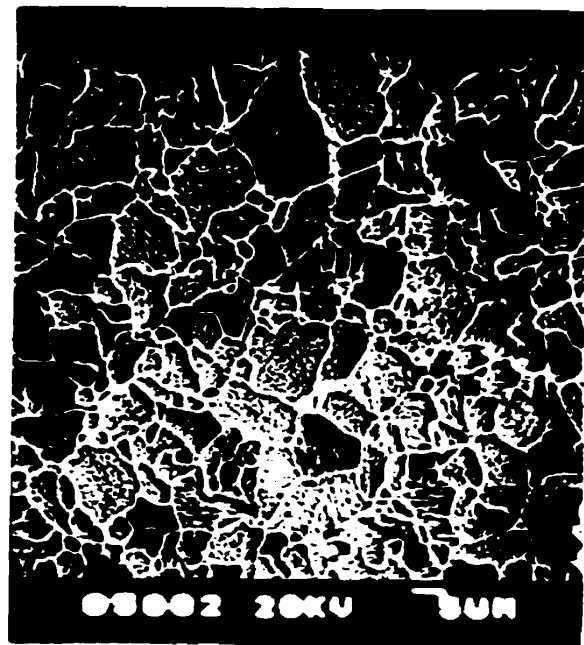


or





(a) Potential $E_{SCE} = -712\text{mV}$



(b) Potential $E_{SCE} = -750\text{mV}$

Fig 4.1.1 The Surface of the Sample at 15% of Strain

The next set of pictures on Fig 4.1.2 shows the surface of the samples tested at potential $E_{SCE} = -800\text{mV}$ and $E_{SCE} = -900\text{mV}$. On these pictures Stress Corrosion Cracks development is clearly seen. It should be mentioned that at this two potentials cracks look kind of different: at $E_{SCE} = -900\text{mV}$ cracks are very obvious, wide open and at the potential $E_{SCE} = -800\text{mV}$ cracks are much thinner, but longer. This can be explained by higher presence of atomic hydrogen at the lower potential and possible influence of it on the width of cracks. Due to higher supply of electrons the dissolution rate ($\text{Fe} \rightarrow \text{Fe}^{+2} + 2\text{e}^-$) is greatly decreased, at the same time rate of hydrogen reduction ($\text{H}^+ + \text{e}^- \rightarrow \text{H}$) is still the same.



(a) Potential $E_{SCE} = -800\text{mV}$



(b) Potential $E_{SCE} = -900\text{mV}$

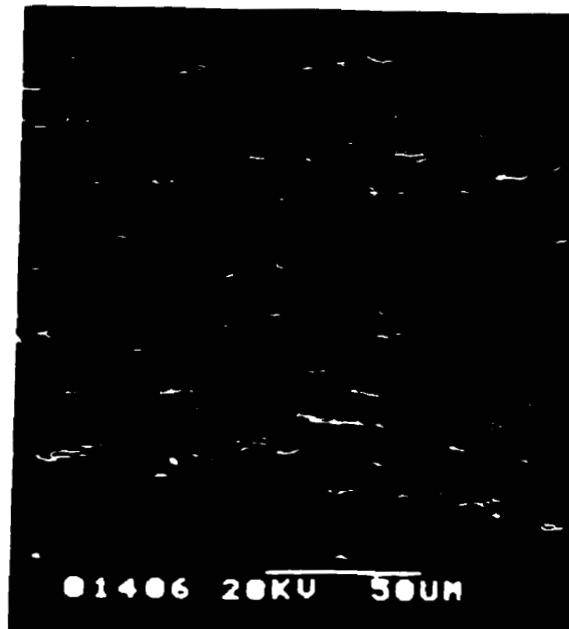
Fig 4.1.2 The Surface of the Sample at 15% of Strain

On the Fig 4.1.3 we can see the next set of pictures showing the surface of the sample at the potentials $E_{SCE} = -1000\text{mV}$, -1100mV and -1200mV . From this pictures it can be seen that Stress Corrosion Cracks continue appearing on the surface of the steel, although it should be mentioned that with the further decrease of potential the crack density decrease as well. This can be explain by better cathodic protection of the sample, which reaches more and more sites of highly localized dissolution at lower potentials. (Highly localized dissolution is assumed to be involved in crack initiation.)

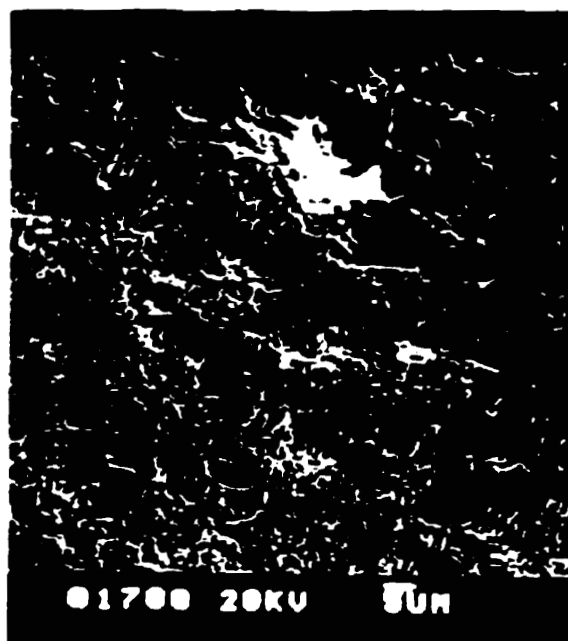
One of the features, which was noticed at lower potentials (starting from potential $E_{SCE} = -1100\text{mV}$) was appearance of white deposit on the surface of the sample.



(a) Potential $E_{SCE} = -1000\text{mV}$



(b) Potential $E_{SCE} = -1100\text{mV}$



(c) Potential $E_{SCE} = -1200\text{mV}$

Fig 4.1.3 The Surface of the Sample at 15% of Strain

The cracks could still be found under this deposit, which means that it was penetrable for electro-chemical reactions, which were happening during the experiment.

One of the possibilities is that cracks could develop prior to the appearance of this deposit and then stopped or at least slowed down its development due to the protective deposit on the surface of the steel. But this is probably not the case, because there is no passivation region on the polarization curve for this steel in this environmental setting. The chemical composition of white deposit was investigated using EDX. It was found that it contains calcium (Ca). Unfortunately the equipment which was used does not detect light elements and it was not possible to determine exact chemical composition, but based on other researches results and chemistry of the solution, the assumption can be made that it is calcium-carbonate (CaCO_3): $\text{Ca}^{+2} + 2\text{HCO}_3^- \rightarrow \text{CaCO}_3 + 2\text{H}^+$.

So based on all of the above results the conclusion can be made that the Near-Neutral-pH SCC occurs only in the potential range from $E_{\text{SCE}} = -800\text{mV}$ to $E_{\text{SCE}} = -1200\text{mV}$.

4.2 Critical Stress of Near-Neutral-pH SCC Initiation

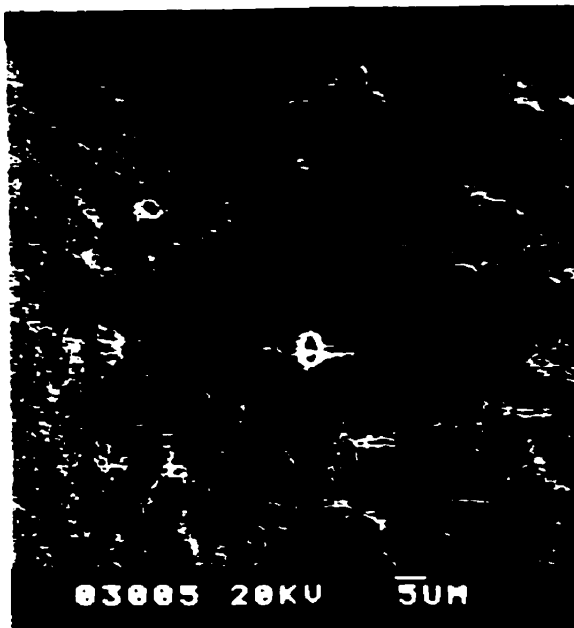
The next step of the investigation was to determine the critical stress of Stress Corrosion Cracking initiation. For this purpose in the beginning only straight standard samples were used. The samples were loaded with the same strain rate of $5 \times 10^{-7} \text{1/s}$. It was already known that at 15% of strain there are a lot of mature cracks on the sample Fig 4.2 (d), so it was decided to load the sample to one half of this strain (7.5%). Still a lot of cracks were found on the sample Fig 4.2 (c).



(a) 3%



(b) 5%



(c) 7.5%

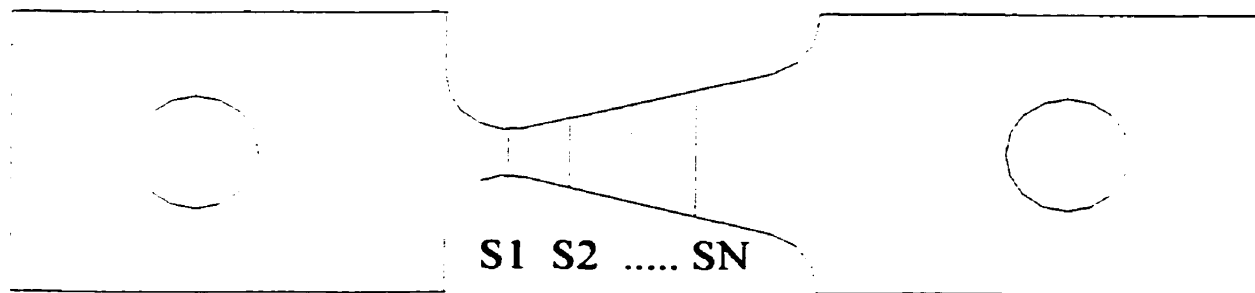


(d) 15%

Fig 4.2.1 Surface of the Sample at Different Strain Level

They were considerably smaller compared to the sample loaded to 15% of strain but the number of cracks or better to say crack density was about the same. So the next sample was loaded to 5% strain. The crack initiation on the surface irregularities and polishing marks were found only Fig 4.2 (b). This by the way supports the idea that the primary crack initiation sites are inclusions and surface irregularities of all kind. So next sample was loaded to 3% of strain. This time no cracks were found on the surface of the sample, only corrosion pits from dissolve inclusions were visible Fig 4.2 (a).

So having in mind all of this, a different design of tested sample was introduced. The purpose of this sample was to find the critical stress of Stress Corrosion Cracking initiation. Although from previous results, when straight sample was used, we had an idea of what the critical stress should be, we wanted to have different stages of SCC development on the same sample and determined the level of the critical stress for different conditions of test settings and microstructure of the steel. The idea behind the design was very simple: if the sample has different cross sectional areas the stress level for different cross sections would be different $\sigma_1 = P/S_i$. So the new sample had a conical shape with two times difference in cross sectional areas at the ends of the sample gage. See Fig 4.2.2. During the experiment with this type of samples all the samples were taken to the level of ultimate stress and then unloaded to prevent necking. If necking happens the result might be not very reliable due to localized plasticity, continues development of cracks in the necking area, and decrease of the stress level throughout the sample where there are still elastic deformations. On the following pictures the development of cracks at different stress levels on the conical samples for different applied potentials are shown.



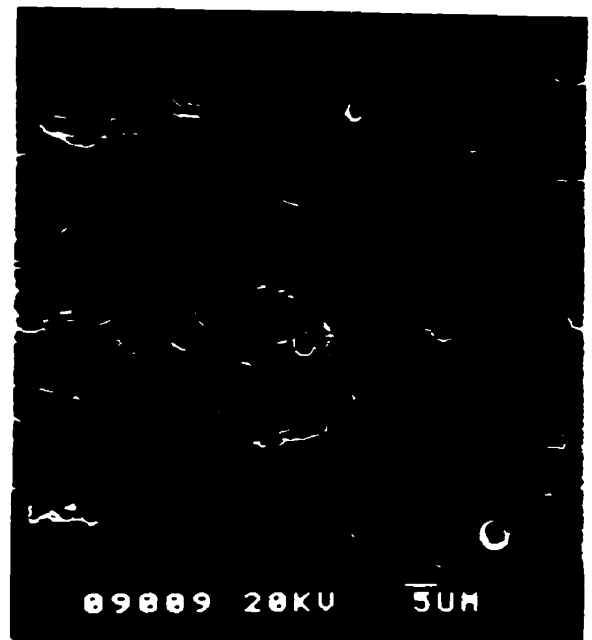
$$\sigma_N = P/S_N$$

Fig 4.2.2 Conical Sample. Stress Calculation at Different Cross-Sectional Areas.

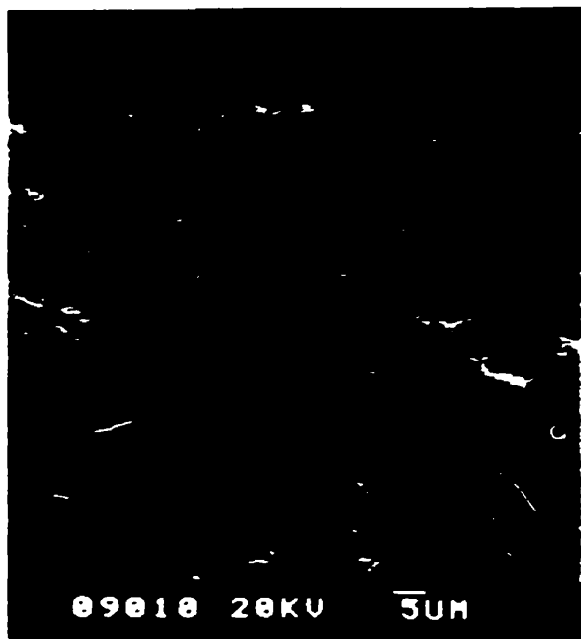
(P – applied load, S_N – cross- sectional area, σ_N – Stress at N- cross sectional area)



(a) $\sigma = 464$ MPa



(b) $\sigma = 438$ MPa

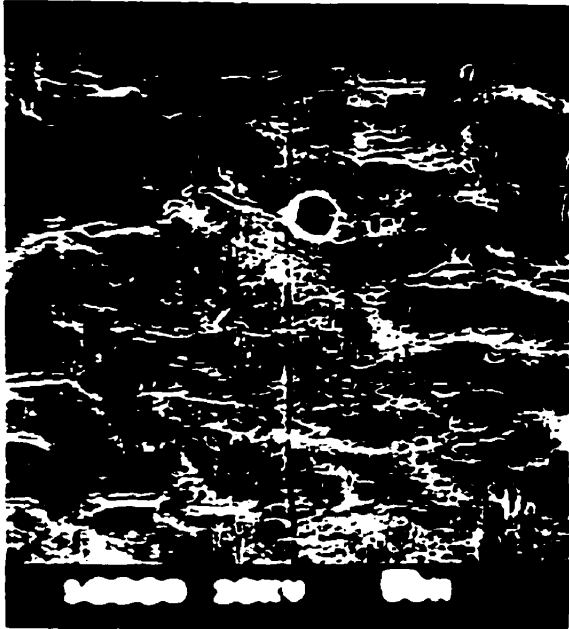


(c) $\sigma = 414$ MPa



(d) $\sigma = 391$ MPa

Fig 4.2.3 Surface of Sample at Different Stress Levels ($E_{SCE} = -800$ mV)



(a) $\sigma = 445$ MPa



(b) $\sigma = 423$ MPa

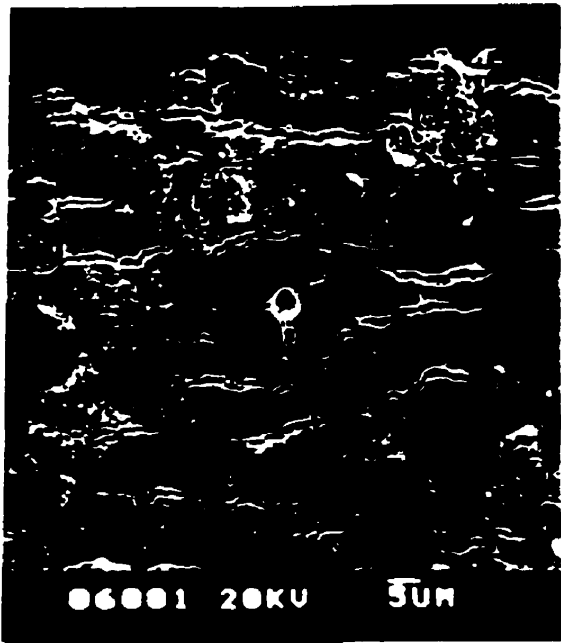


(c) $\sigma = 410$ MPa



(d) $\sigma = 396$ MPa

Fig 4.2.4 Surface of Sample at Different Stress Levels ($E_{SCE} = -900$ mV)



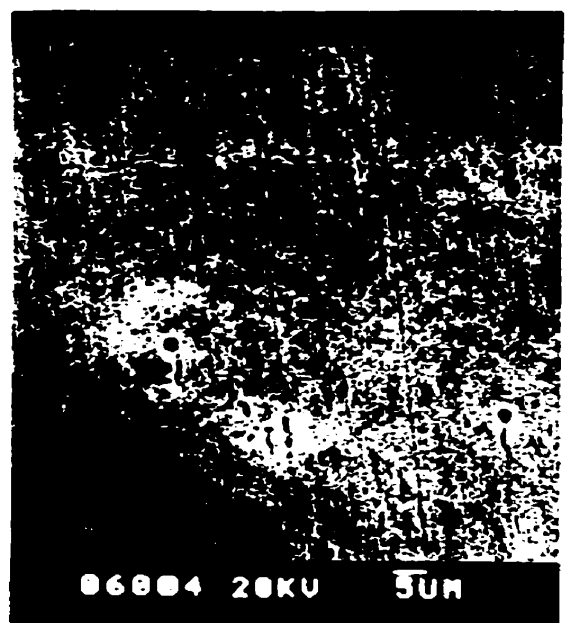
(a) $\sigma = 449$ MPa



(b) $\sigma = 421$ MPa



(c) $\sigma = 397$ MPa



(d) $\sigma = 380$ MPa

Fig 4.2.5 Surface of Sample at Different Stress Levels ($E_{SCE} = -1000$ mV)



(a) $\sigma = 478$ MPa



(b) $\sigma = 449$ MPa



(c) $\sigma = 429$ MPa



(d) $\sigma = 410$ MPa

Fig 4.2.6 Surface of Sample at Different Stress Levels ($E_{SCE} = -1100$ mV)



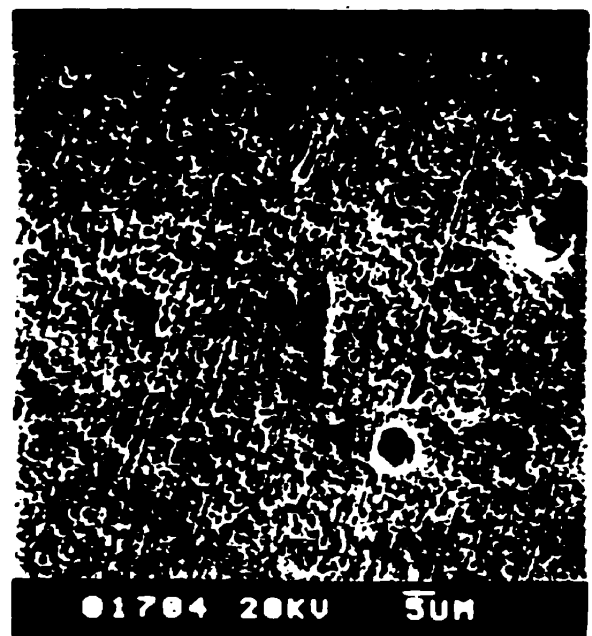
(a) $\sigma = 479$ MPa



(b) $\sigma = 449$ MPa



(c) $\sigma = 429$ MPa



(d) $\sigma = 355$ MPa

Fig 4.2.7 Surface of Sample at Different Stress Levels ($E_{SCE} = -1200$ mV)

During examination of the samples it was noticed that the maximum density of the cracks on all of the samples is in the middle area of particular section of the sample. From the pictures above several observations can be made:

1. As in CANMET report, two categories of crack locations were found. Primary locations of crack initiation are all kind of surface irregularities such as inclusions, corrosion pits, polishing marks, cavities developed due to dissolution of inclusions. But as it can be seen from the pictures above these are not the only locations for SCC initiation. Much higher number of cracks appears on the surface, which does not have any visible surface irregularities. One of the possibilities is that this type of crack initiation site may be explained by the existence of residual stresses, that built-up along specific crystallographical planes. This will be discussed in more details later.
2. The Critical Stress of SCC initiation can be found. For this purpose the stress at which the very initiation of cracks were observed on the surface of conical sample was calculated. It was found that critical stress is not exactly the same for different potentials applied to the samples. Fig 4.2.8 shows the level of critical stresses for different potentials. From this chart it is obvious that the lower the potential the higher the critical stress. This is quite reasonable result considering that lower potential gives better cathodic protection, reducing highly localized dissolution on one hand, and higher amount of content of hydrogen on the surface of the samples, results in loss of steel ductility on the other hand. It also should be mentioned that all critical stresses are just above the level of Yield Stress.

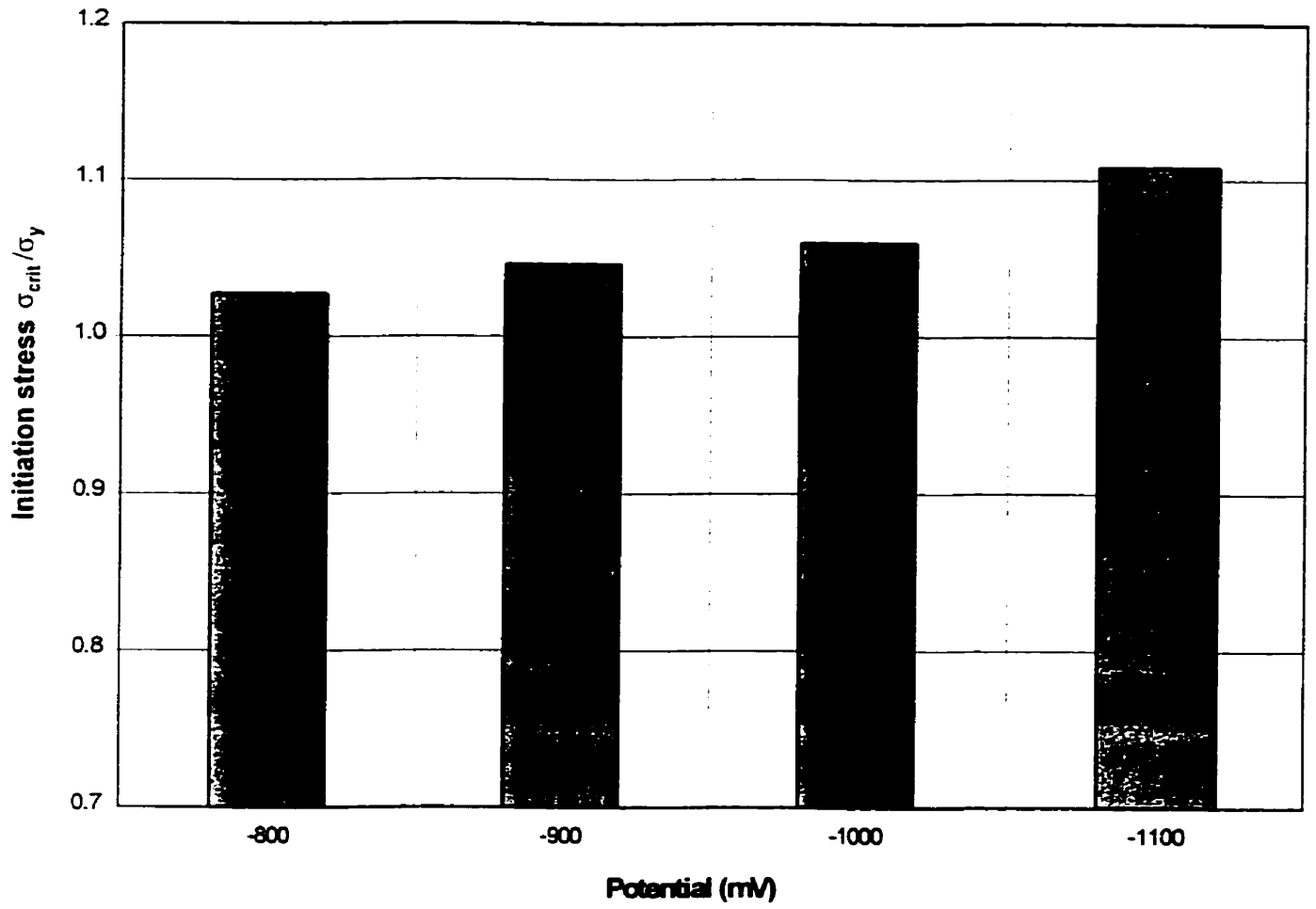


Fig 4.2.8 Normalised Initiation Stress vs. Potential

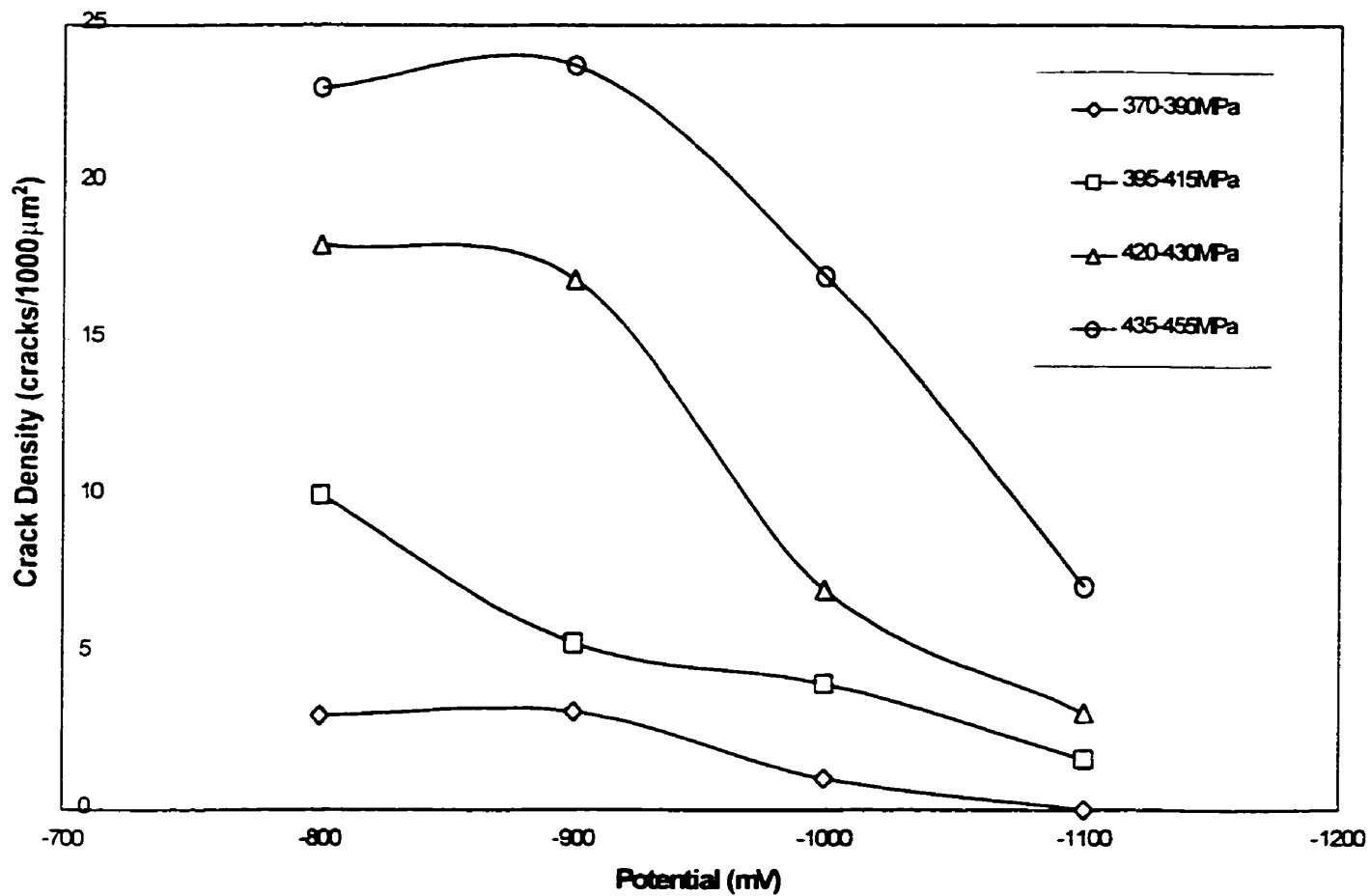


Fig 4.29 Effect of the Potential on Crack Initiation

3. Based on the charts above the crack evolution for different potentials at different stress levels can be observed.

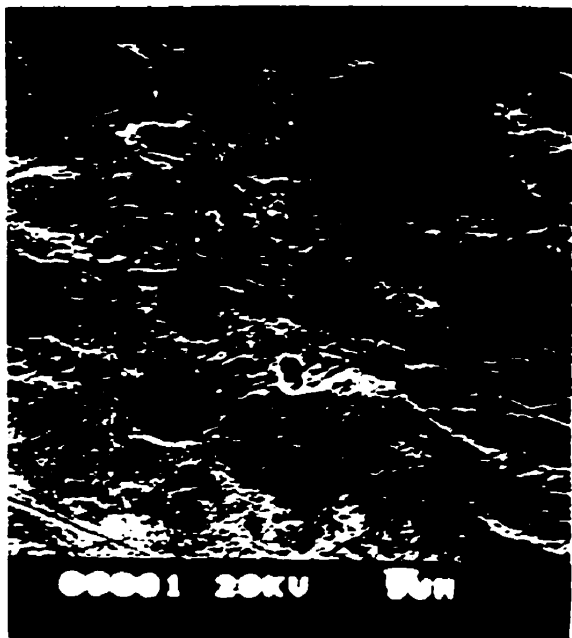
From the Fig 4.2.9 conclusion can be made that applied potential $E_{SCE}=-900\text{mV}$ is the most favorable for crack initiation and propagation. It has the highest crack density for various stress levels. At the same time the lower the potential is, the less favorable conditions for SCC initiation and propagation exists. At the potential of $E_{SCE}=-1200\text{mV}$ SCC was not found. These results indicate that SCC initiation is not determined only by the amount of hydrogen entering steel surface, but also related to preferential highly localized dissolution and some chemical reactions, happening on the steel surfaces. It also should be mentioned that at the lower potentials the cracks look wider, this can be related to hydrogen influence on the crack development.

4.3 Strain Rate Effect on SCC Initiation

Throughout the entire experiment Slow Strain Rate Test was used. As a result one of the important parameters for SCC development is a strain rate. In case of SCC dominated by anodic dissolution (High-pH SCC), cracking only occur within certain strain rate range. Below and above this range SCC initiation decreases. If the strain rate is too low it is unable to rapture a passive film at the crack (film grows faster than it is raptured), whereas when the strain rate is too high the crack blunts, allowing a very large region surrounding the crack tip to actively corrode. On the other hand in case of hydrogen induced cracking we see different tendency. Hydrogen has more time to enter

the metal lattice at lower strain rates; as a result the susceptibility to hydrogen induced cracking is always higher at lower strain rates.

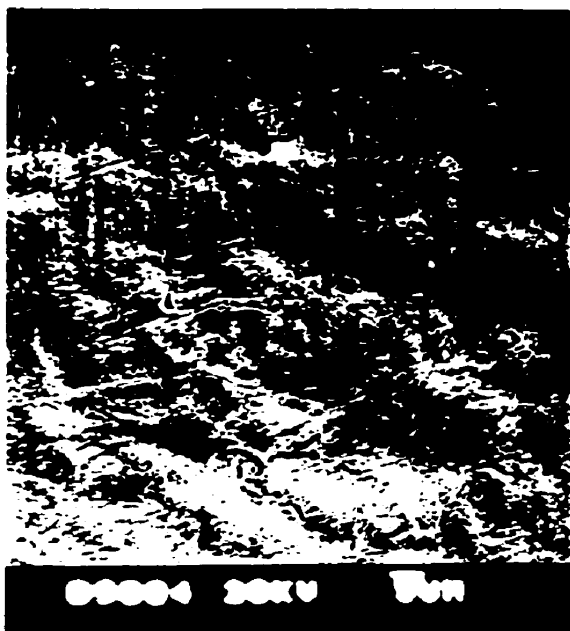
So the next logical step was to determine the influence of strain rate on the Near-Neutral-pH SCC initiation. A number of tests were conducted at the different strain rates. All the initial tests had a strain rate equal to $5 \times 10^{-7} 1/s$, so it was decided to reduce the strain rate twice to the level of $2.5 \times 10^{-7} 1/s$. When the critical stress for this strain rate was calculated, it decreased to level of 360 MPa (or 97% of the Yield Stress). In other words the susceptibility became higher. Fig 4.3.1 shows cracks on the surface of the sample at different stress levels. So the next step was to reduce the strain rate even lower to $1 \times 10^{-7} 1/s$. In contrary to the previous result, this time the critical stress jumped up to 405 MPa (or 109% of the Yield Stress). Fig 4.3.2 shows the pictures of steel surfaces at different stress levels. When the strain rate was decayed to zero, which means static load, the cracks were not found at all. Fig 4.3.3 shows pictures of different samples, which were tested for a various periods of time (84, 120, 140 hours). This suggested again that Near-Neutral-pH SCC is controlled not only by hydrogen but also by other factors which give a substantial contribution into initiation process. Following all of these, the strain rate was increased to $1 \times 10^{-6} 1/s$ in order to investigate the influence of it at higher levels. Fig 4.3.4 shows pictures of steel surfaces at different stress levels. This time the critical stress of initiation went up, not as dramatically as in case with strain level of $1 \times 10^{-7} 1/s$, but still it shows the trend of susceptibility decrease to SCC. It is quite possible that kinetics of some corrosion reaction is associated with Near-Neutral-pH SCC initiation process, and this corrosion kinetics is not able to keep up the pace with the mechanical deformation at higher strain rates.



(a) $\sigma = 432$ MPa



(b) $\sigma = 411$ MPa



(c) $\sigma = 392$ MPa



(d) $\sigma = 364$ MPa

Fig 4.3.1 Sample Surface at Different Stress Levels ($SR = 2.5 \times 10^{-7}$ 1/s, $E_{SCE} = -900$ mV)



(a) $\sigma = 451$ MPa



(b) $\sigma = 423$ MPa



(c) $\sigma = 405$ MPa



(d) $\sigma = 382$ MPa

Fig 4.3.2 Sample Surface at Different Stress Levels ($SR = 1 \times 10^{-7} 1/s$, $E_{SCE} = -900mV$)



(a) $\sigma = 405$ MPa 84h(7008)



(b) $\sigma = 405$ MPa 120h(8009)

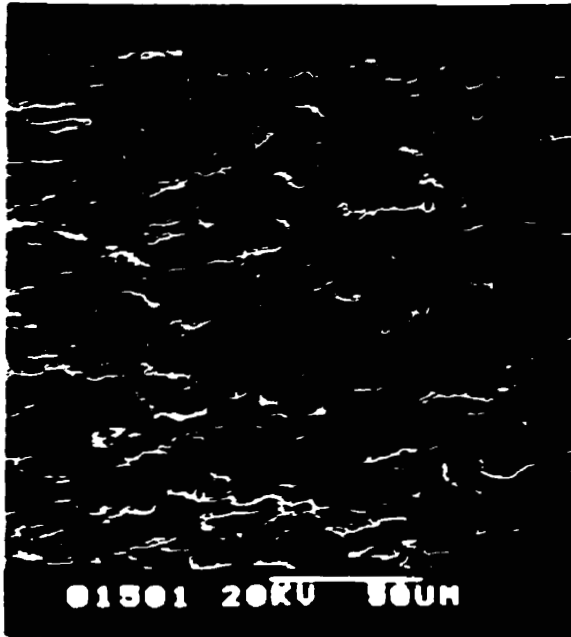


(c) $\sigma = 405$ MPa 140h (1501)



(d) $\sigma = 405$ MPa 140h(1500)

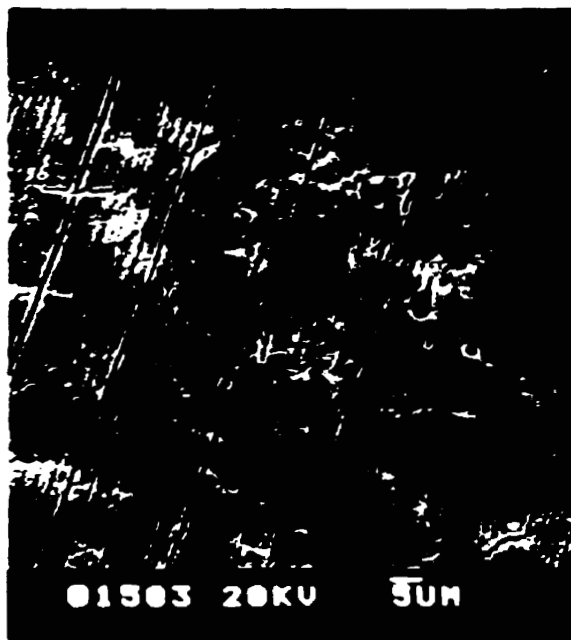
Fig 4.3.3 Sample Surface at Different Stress Levels (Static Load, $E_{SCE} = -900$ mV)



(a) $\sigma = 466$ MPa



(b) $\sigma = 443$ MPa



(c) $\sigma = 410$ MPa



(d) $\sigma = 387$ MPa

Fig 4.3.4 Sample Surface at Different Stress Levels ($SR=1 \times 10^{-6} 1/s$, $E_{SCE}=-900mV$)

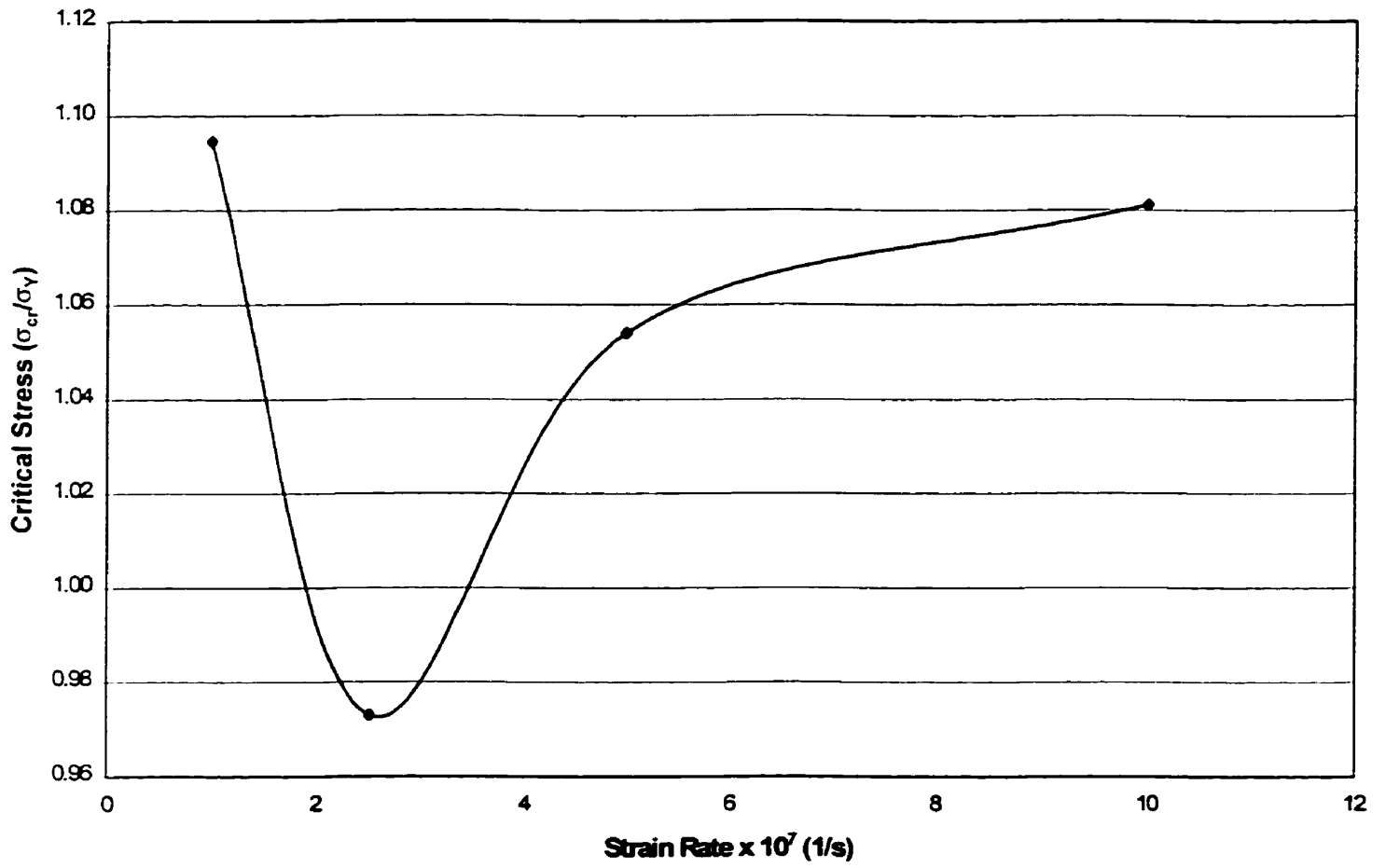


Fig 4.3.5 Normalised Critical Stress of Initiation vs Strain Rate

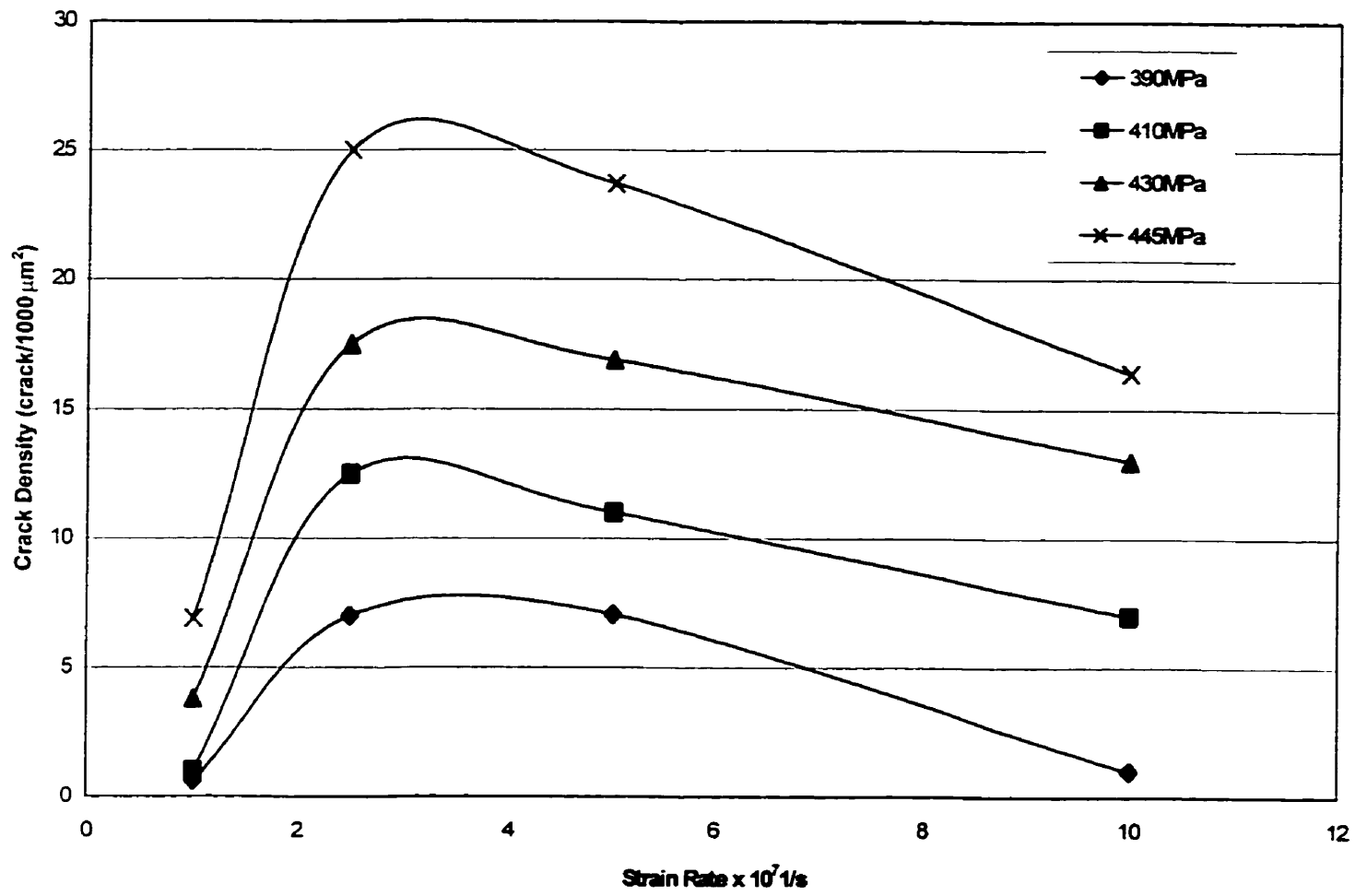


Fig 4.3.6 Crack Density vs. Strain Rate for Different Stress Levels

When the strain rate is reduced below some value, the generation of SCC initiation sites (inclusions, slip bands. etc) is not keeping up with kinetics of corrosion reactions at the tip of the crack. Corrosion blunts the tip of the crack, reducing singularity and SCC does not initiate. So there exists the most susceptible strain rate range, to generate Near-Neutral-pH SCC. On Fig 4.3.5 this range is clearly seen. It is in the range from 1.5×10^{-7} to 6×10^{-7} 1/s. On the next Fig 4.3.6 the crack density vs. strain rate for different stress levels is shown and again this chart is strongly support the existence of most susceptible range of Near-Neutral-pH SCC initiation and propagation.

4.4 Effect of pH Value of the Solution

One of the most critical parameters on Near-Neutral-pH SCC initiation is pH value of the solution used in environmental chamber. As it was stated before the initial pH value of NS-4 solution prior to the experiment was 7.2. Before every test there was a period of preconditioning – the solution was purged with 5% carbon dioxide (CO₂) balanced with nitrogen (N₂) for 12 – 24 hours. After this procedure pH value of the solution would drop to a saturation point of 6.8 due to the following reaction:



Higher content of carbonic acid in the solution decreased its pH. The pH of the solution did not drop any lower, since it was purged with 5% of carbon dioxide balanced with nitrogen, and 6.8 is saturation point. Had we purged it with pure carbon dioxide, pH would have decreased even further.

So all of the crack initiations up to this point were generated at pH value of 6.8.

Hydrogen plays the major role in Near-Neutral-pH SCC initiation and propagation. The amount of hydrogen ions in the solution is directly related to solution's pH value. So the idea was - by different means change pH value of the solution (amount of hydrogen ions in it) and see if the same type of cracks can be generated and what would be initiation parameters.

First the purging gas was changed to pour nitrogen (N₂). By doing this, the author hoped to bring pH value up since the following reaction



will not be happening any longer and there will not be a source of hydrogen ions in Near-Neutral-pH solution in form of carbonic acid, formed by the dissolution of carbon dioxide in the groundwater [27].

At the same time by purging nitrogen through NS-4 solution we can avoid excess oxygen entering into the environmental chamber and as a consequence avoid the oxidation reactions on the steel surfaces. So as a result of purging the solution with pour nitrogen, pH value went up to 8.5. This was due to regular cathodic reaction happening in the environmental chamber:



So the hydroxide ions gave a rise to pH value. The test was conducted with applied potential of $E_{\text{SCE}} = -900\text{mV}$. Since the potential was not very far into the cathodic region pH did not rise any higher. After the test was conducted SCC initiation was found, but the critical stress considerably increased, making steel less susceptible at this pH level. On the other hand, we needed to decrease pH value in order to increase amount of hydrogen ions in the solution and compare the results with regular pH 6.8.

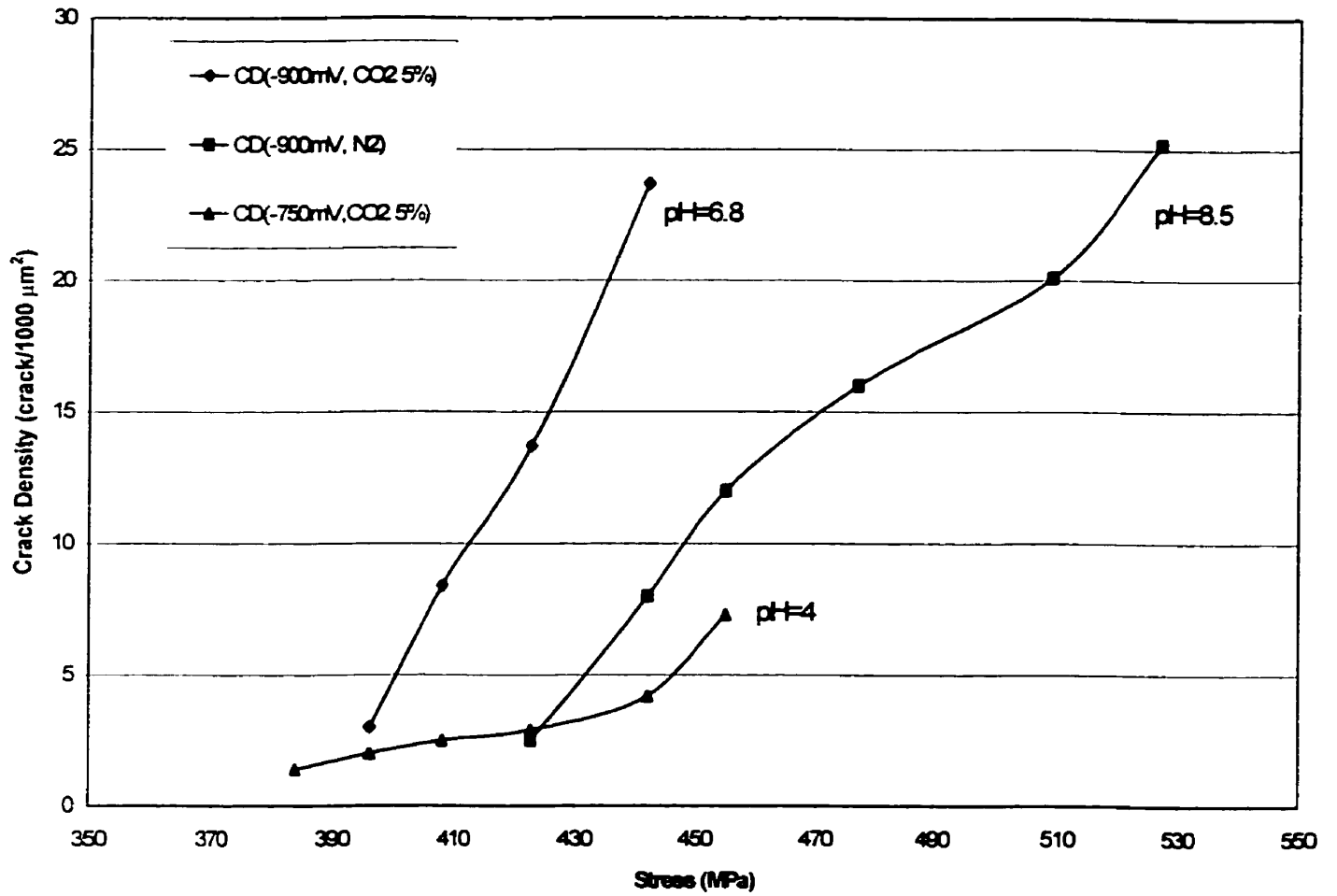
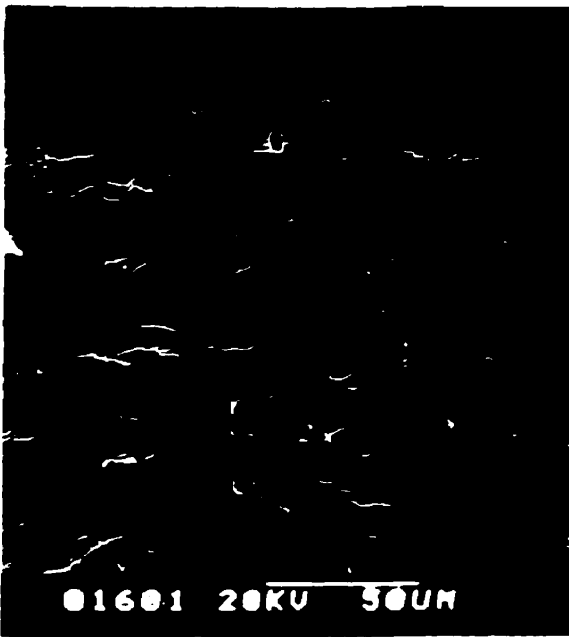
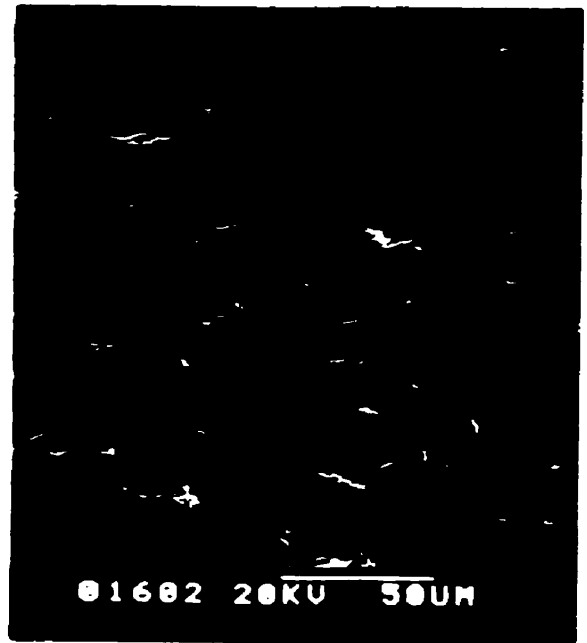


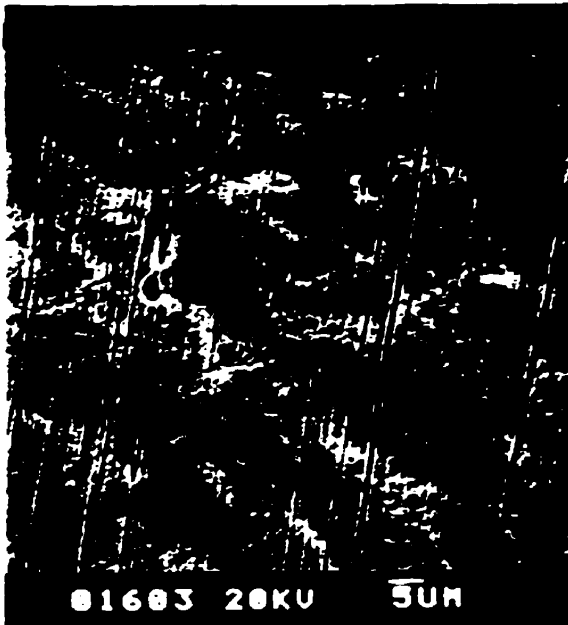
Fig 4.4.1 Crack Density vs Stress for Different pH



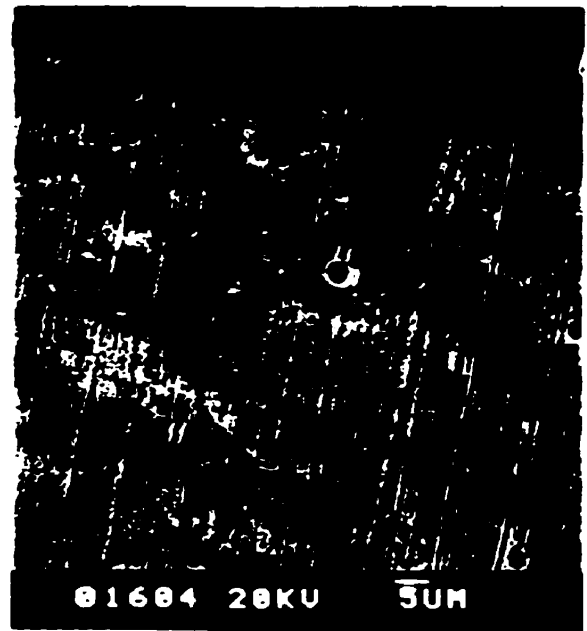
(a) $\sigma = 509$ MPa



(b) $\sigma = 476$ MPa

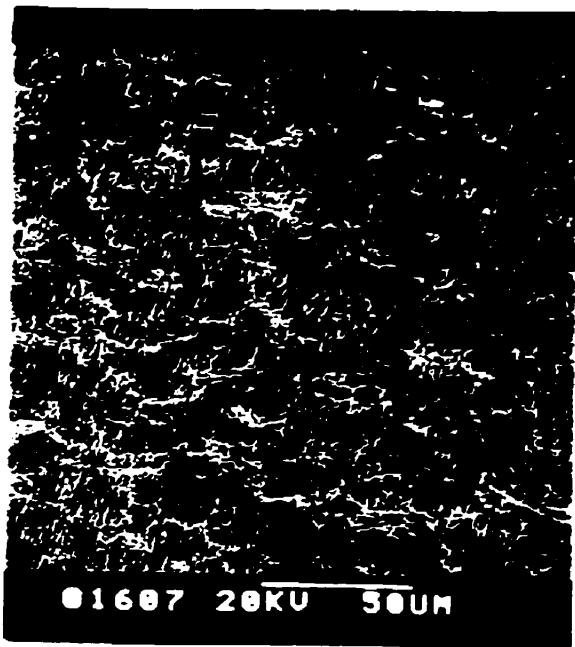


(c) $\sigma = 455$ MPa



(d) $\sigma = 423$ MPa

Fig 4.4.2 Sample Surface at Different Stress Levels ($SR=5 \times 10^{-6} 1/s$, $E_{SCE}=-900mV$,
Purging Gas – Pure Nitrogen (N_2), Solution pH=8.5)



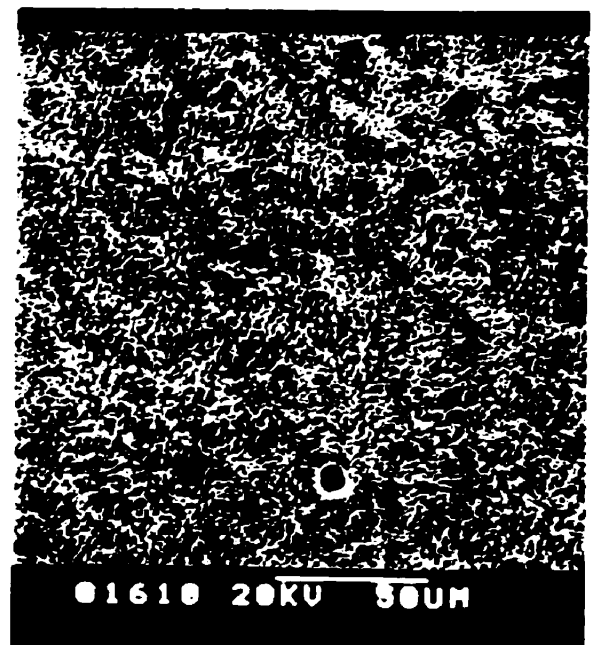
(a) $\sigma = 449$ MPa



(b) $\sigma = 434$ MPa



(c) $\sigma = 407$ MPa



(d) $\sigma = 384$ MPa

Fig 4.4.3 Sample Surface at Different Stress Levels ($SR=5 \times 10^{-6}$ 1/s, $E_{SCE}=-712$ mV (OCP), Purging Gas - 5% CO_2 Balanced with N_2 , Solution pH=4)

The sulfuric acid (H_2SO_4) was added into NS-4 solution, to decrease pH value to the level of 4. This time the test was conducted at Free Corrosion Potential ($E_{SCE}=-712mV$).

It should be recalled that in the beginning of this chapter the results show no SCC initiation at Free Corrosion Potential, when pH was 6.8. This time, when the pH was decreased and the amount of hydrogen ions in the solution increased, SCC initiation was found. More than that the critical stress of initiation decreased, making steel more susceptible to crack initiation.

All of above strongly support the idea of necessity of hydrogen accumulation for initiation of Stress Corrosion Cracking. Fig 4.4.1 shows the results of these experiments. On Fig 4.4.2 the pictures of steel surfaces at different stress levels, when the solution was purged with pure nitrogen. On Fig 4.4.3 the steel surfaces are shown after the sample been tested in the 4 pH solution.

4.5 Growth Rate Calculation of Near-Neutral-pH SCC

One of the parameters, which were calculated during investigation of Near-Neutral-pH SCC, was cracks growth rate. The basic information for calculation was taking from files stored by computer during the experiment. For the calculation of crack length the average of 20 cracks within $1000\mu m^2$ was used. Then this average crack length was divided by the period of time between the crack initiation and stress level at which the length was calculated. This procedure was done for different testing condition including heat-treated samples.

Fig 4.5.1 shows the average SCC growth rates at different potentials. As it can be seen from this chart, crack growth rate increases as the potential decreases. This strongly suggests that Near-Neutral-pH SCC propagation rate is enhanced by hydrogen entering the steel. Which bring us to a conclusion that the propagation of Near-Neutral-pH SCC is dominated by the mechanism of hydrogen induced cracking. That is why it was found that ductility of steel is decreases as the potential decreases.

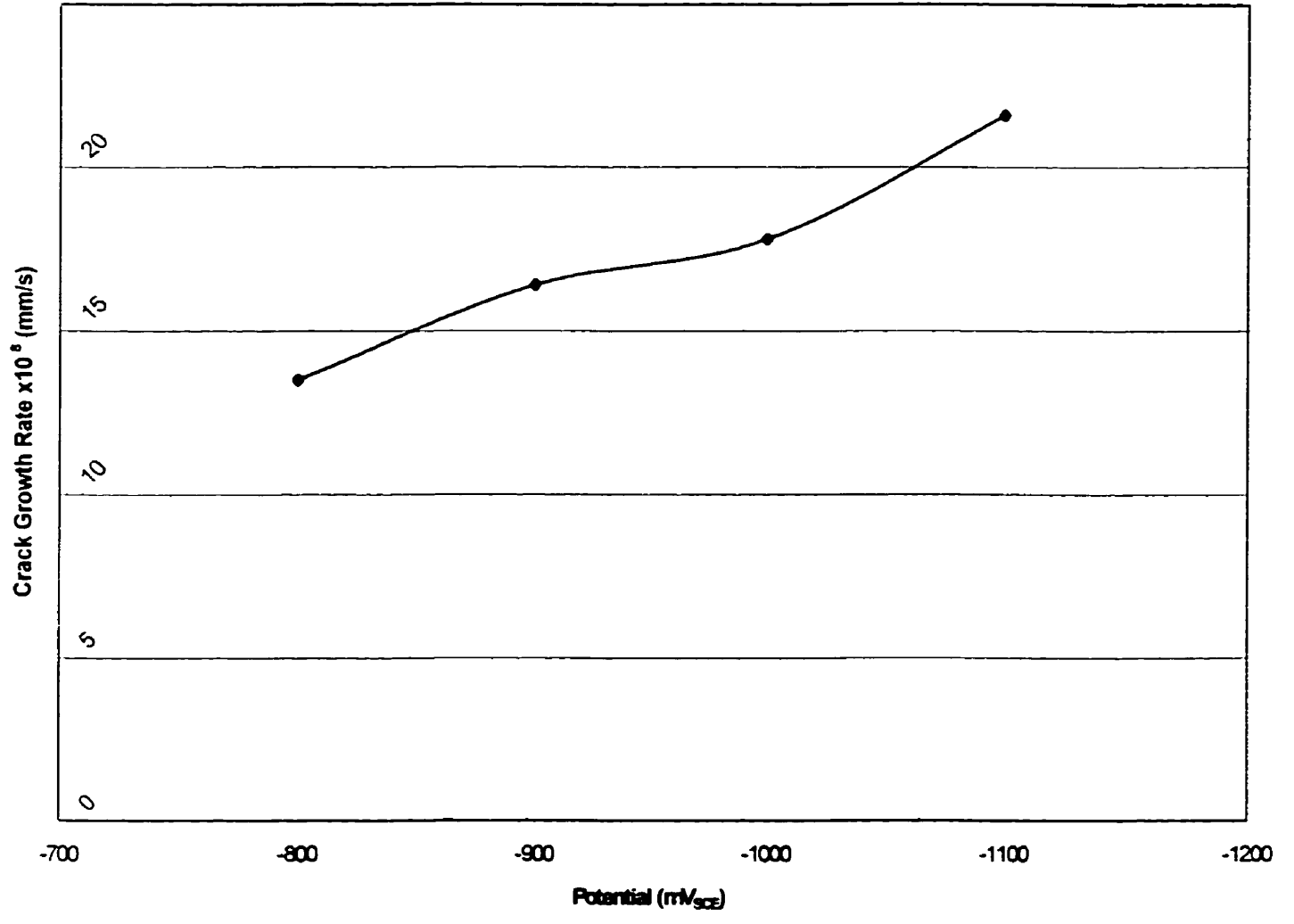


Fig 4.4.1 Crack Growth Rate vs Potential

Chapter 5

The Effect of Residual Stresses and Microstructure Change of Near-Neutral-pH SCC

Some common features typical for pipeline steel are inclusions and residual stresses. Concentrating on investigation of these two factors plus looking on susceptibility of various types of microstructure, one can get a clue on the process of initiation and propagation of Near-Neutral-pH SCC in pipeline steel.

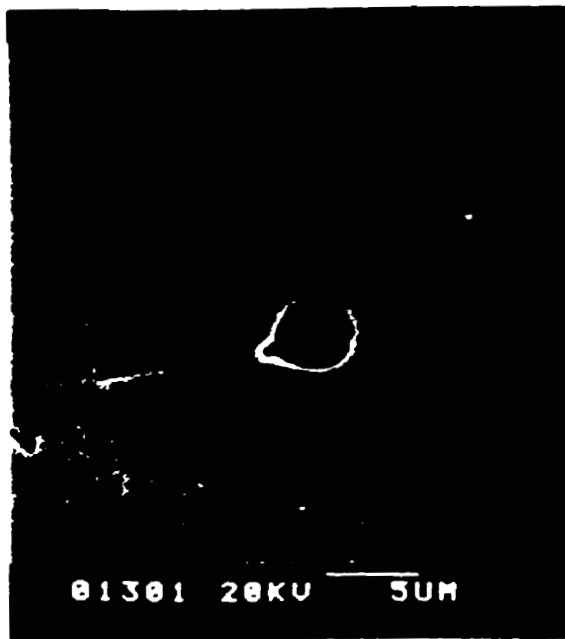
Residual stresses are always present in pipeline steel due to fabricating processes such as rolling, bending, welding and installation during construction. It is quite known that residual stresses can reach up to 25% of specified material yield stress. This can substantially influence SCC initiation and propagation during lifetime of pipe.

Talking about inclusions, it should be mentioned that there was an abandon presence of them in older pipelines, but in recent years with introduction of inclusion control in the industry the number of inclusions was considerably decreased. In our case Sour Service X-52 pipeline steel was investigated. Sour Service pipeline steel is distinguished by low number of inclusions with manganese (Mn) and sulfa (S) content.

During inclusion observations two typical shapes were found on the surface of the steel: spherical and slightly elongated inclusions (Fig 5.1). EDX examination showed that most of the inclusions contain following chemical elements: calcium (Ca), manganese (Mn), and sulfa (S), aluminum (Al) in different proportion. Although some inclusions were found that contain only manganese (Mn) or only aluminum (Al), the majority of inclusions had high content of aluminum or calcium and less of manganese and sulfa.

As a consequence of inclusion presence and due to trapping effect, hydrogen concentration, generated during Electro-chemical processes, is considerably increased at the interface of non-metallic inclusions and matrix. At the same time applied current of cathodic protection may not be able to reach inclusions and surrounding areas due to a difference in the chemical composition with bulk area. This leads to appearance of cathodic (light) and anodic (dark) areas [41], which set up the stage for highly localized dissolution of iron. This makes the site of inclusion preferential for crack initiation and propagation. On Fig 5.2 (a, b) it can be clearly seen that inclusions are preferential and one of the first sites for Near-Neutral-pH SCC to initiate. At the same time inclusions are not the only sites for SCC initiation. From Fig 5.2 (c, d) we can see that on the surface, which does not have inclusions, there are also a lot of crack initiations. This second type of crack initiation may be related to specific crystallographic planes, which have high concentration of residual stresses or may be referred to slip bands. This was partially discussed in the research done by CANMET and presented at International Pipeline Conference in 1998.

The effect of microstructure change on SCC initiation needed to be investigated. It was shown before that fine grain steel is less susceptible to Sulfa Stress Cracking than steel with coarse grain. It was also reported that fine spheroidised carbides uniformly dispersed in ferrite gives the best resistance to hydrogen induced cracking in H₂S environment compared to other types of microstructure. For this reason, it would be interesting to determine the microstructure and grain size, which has the highest SCC resistance.



(a) Spherical Inclusion



(b) Slightly Elongated Inclusion

Fig 5.1

(a)

(b)



(c)

(d)

Fig 5.2 Initiation of SCC at the Inclusions and Specific Crystallographic Planes

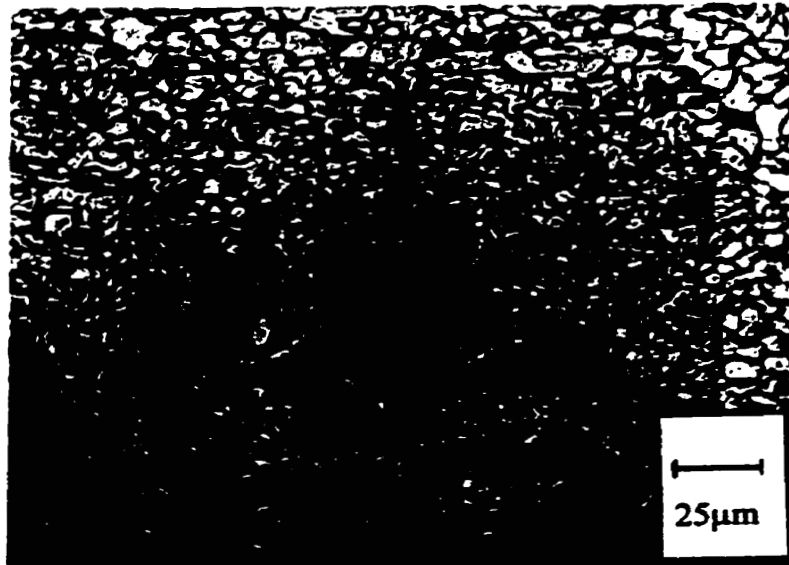
The tested material and different heat treatment used are described in Chapter 3 “Experiment Procedures”. It should be mentioned though, that all of the tests for heat-treated samples were conducted at the strain rate of 5×10^{-7} and applied potential $E_{SCE} = -900\text{mV}$. Unless otherwise noted the following discussion is using microstructure in longitudinal direction.

5.1 Microstructure of Heat-Treated Samples and Its Influence on SCC Initiation

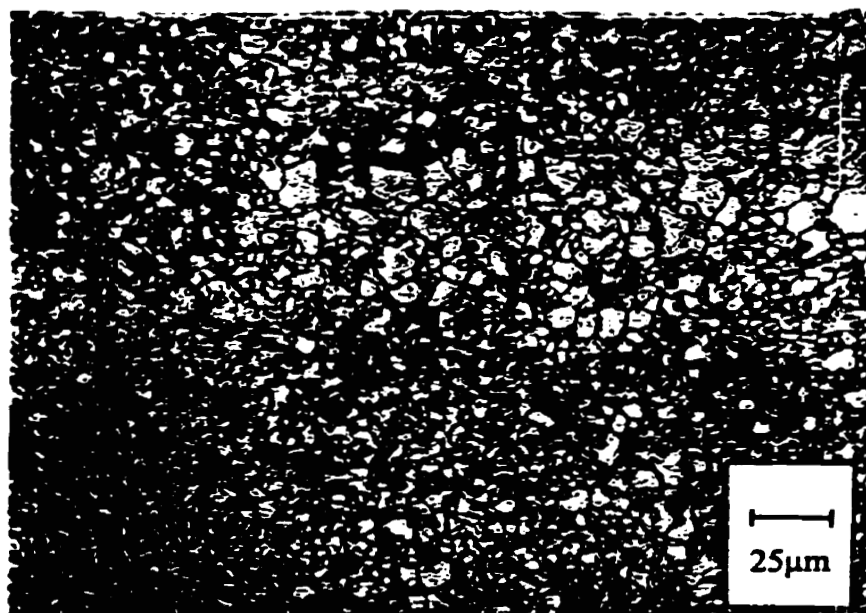
5.1.1 Microstructure of Heat-Treated Samples

The surface of as-received samples was polished, etched and the picture taken in both transverse and longitudinal directions of the pipe. On Fig 5.1.1.1, it can be seen that the microstructure contains slightly elongated fine ferrite and pearlite grains in transverse direction of the pipe. This can be explained due to cold rolling effect during fabrication process. The average grain size is about $8 \mu\text{m}$. The austenitizing temperature for all heat-treated samples was 950°C .

In the beginning the samples were furnace – heated to 950°C and soaked at this temperature for 1 hour. Since the soaking time was quite long, it enhanced the grain growth. Fig 5.1.1.2 (a) shows microstructure of quenched and tempered at 475°C for 2 hours sample with coarse tempered lath martensite with hardness HRB80. Fig 5.1.1.2 (b) shows microstructure of quenched and tempered at 650°C for 2 hours sample with fine spheroidised carbides uniformly dispersed in ferrite, with coarse grains (about $45\mu\text{m}$),

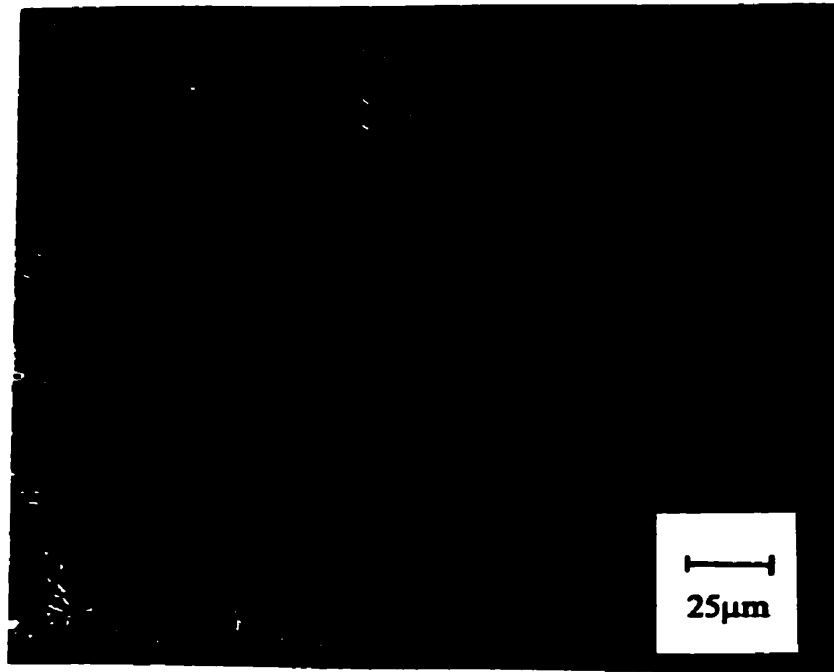


(a) Transverse Direction of Pipe

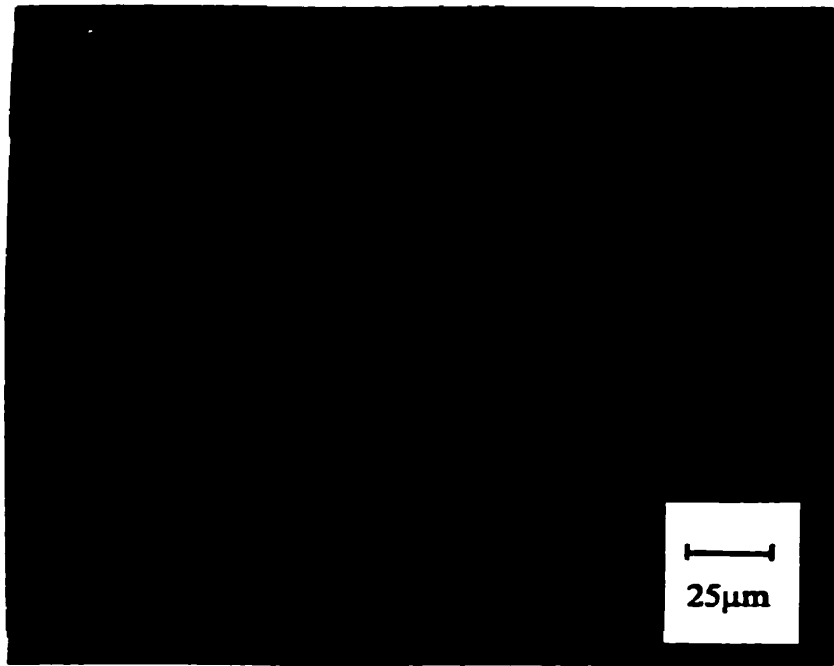


(b) Longitudinal Direction of Pipe

Fig 5.1.1.1 Microstructure of As-Received Sample



(a) 475°C/2hrs Tempered



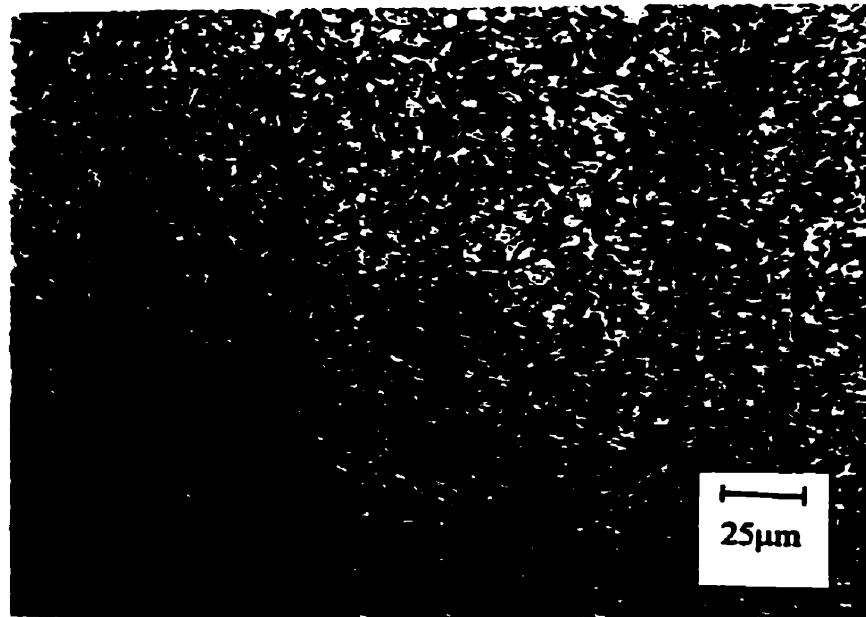
(b) 650°C/2hrs Tempered

Fig 5.1.1.2 Microstructure of 950°C Furnace Heated/1 hr + Water Cooled and Tempered

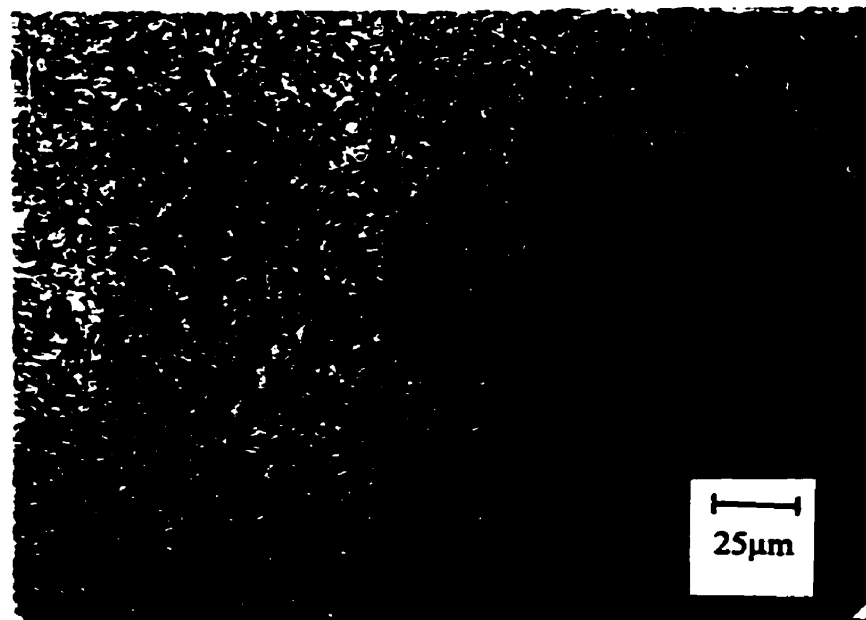
hardness HRB76. Having in mind that the finer grains might be less susceptible to SCC, it was decided to prepare some samples with the same microstructure but finer grains. This time the samples were put in the furnace at the temperature 950°C, but only for 10 minutes. The rest of the procedure was basically the same, except this time, the following three tempering temperatures were used: 250°C, 450°C, and 650°C. (Fig 5.1.1.3)

- a) When the sample was just water cooled, fine lath martensite was obtained. This type of microstructure also called hidden acicular martensite. Hardness is HRB100. Fig 5.1.1.3(a).
- b) At low temperature tempering (250°C) the precipitation of certain amount of carbides started, although microstructure change cannot be visible through optical microscope, it is reflected on the hardness change. Hardness is HRB94. Fig 5.1.1.3(b)
- c) At the tempering temperature of 450°C, more precipitation of carbide took place, although it is still not visible through optical microscope, it can be seen from hardness that the changes are taking place. Hardness is HRB90. Fig 5.1.1.3(c)
- d) At 650°C temperature tempering, the fine carbide spheroids precipitated in ferrite. Ferrite average grain size is 10µm. Again carbides are too fine to see them through optical microscope, but the grain boundaries are sharper than other quenched and tempered samples, this means that hidden acicular structure disappeared. Hardness is HRB75. Fig 5.1.1.3(d)

In the Table 5.1 the mechanical properties for heat-treated samples, selected for investigation, are listed.

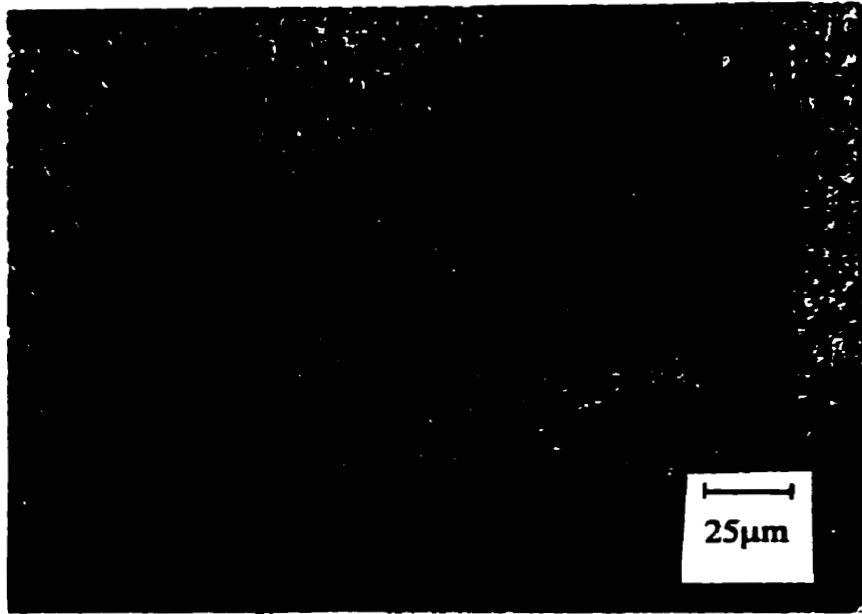


(a) Lath Martensite HRB100

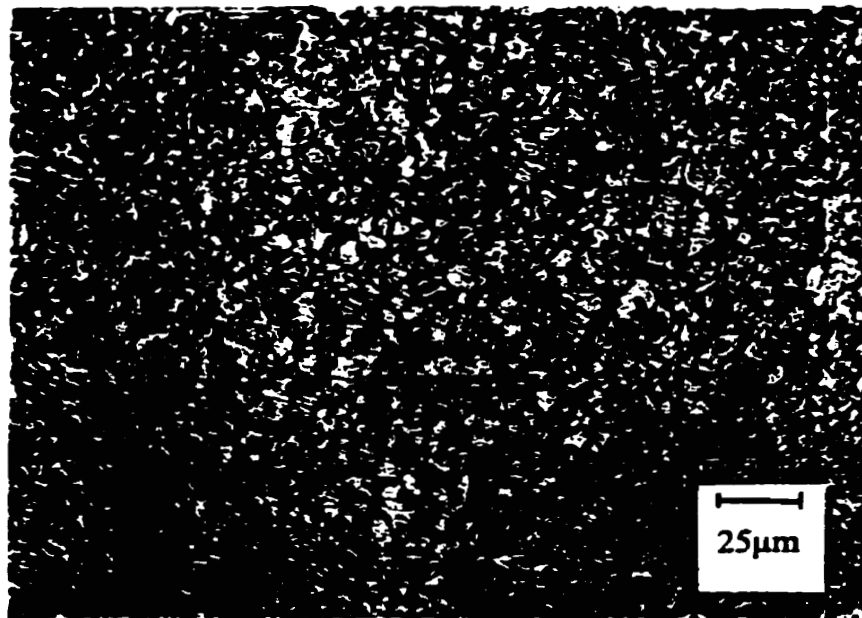


(b) Low Temperature Tempering (250°C) HRB94

Fig 5.1.1.3 Microstructure of (a) 950°C/10 min/WC, (b) 950°C/10 min/WC + Tempered at 250°C/2 hrs.



(c) Tempering Temperature of 450°C (HRB90)



(d) 650°C Temperature Tempering (HRB75)

Fig 5.1.1.3 Microstructure of (c) 950°C/10 min/WC + Tempered at 450°C/2 hrs, (d) 950°C/10 min/WC + Tempered at 650°C/2 hrs

Table 5.1 Material Properties of Heat-Treated Samples

Heat-Treatment	Yield Stress (0.2%) (MPa)	Hardness (HRB)
As-received	370	83
950°C/10 min/WC	730	100
950°C/10min/WC+250°C/2hrs	700	94
950°C/10min/WC+450°C/2 hrs	670	90
950°C/10min/WC+650°C/2 hrs	380	75

5.1.2 Effect of Microstructure on SCC Initiation

Heat-treatment of steel considerably changes its microstructure and mechanical property. As a result, Electro-chemical behavior of the sample tested in NS4 solution under conditions, which were described in Chapter 3, changes too. Straight standard as well as conical samples were tested. The following set of pictures present the surface of the samples at different stress levels, undergone different heat-treatment.

Fig 5.1.2.1 - 950°C/10 min/WC; Fig 5.1.2.2 - 950°C/10min/WC+250°C/2hrs; Fig 5.1.2.3 - 950°C/10min/WC+450°C/2hrs; Fig 5.1.2.4 - 950°C/10min/WC+650°C/2hrs; Fig 5.1.2.5 - 950°C/1hr/WC+650°C/2hrs. Cracks were found on all pictures. This means that all of the presented types of microstructure are susceptible to Near-Neutral-pH SCC. Of course crack development is not the same for different microstructures. For instance, the quenched sample, but not tempered, has very obvious cracks. They are fairly wide

Fig 5.1.2.1 - 950°C/10 min/WC; Fig 5.1.2.2 - 950°C/10min/WC+250°C/2hrs; Fig 5.1.2.3 - 950°C/10min/WC+450°C/2hrs; Fig 5.1.2.4 - 950°C/10min/WC+650°C/2hrs; Fig 5.1.2.5 - 950°C/1hr/WC+650°C/2hrs. From these pictures initiation and propagation of cracks are clearly seen. This means that all of the presented types of microstructure are susceptible to Near-Neutral-pH Stress Corrosion Cracking. Of course crack development is not the same for different microstructures. For instance, the quenched sample, but not tempered, has very obvious cracks. They are fairly wide opened and the initiation observed at the surface irregularities such as pits, inclusions as well as at the surface, which does not have surface irregularities. It should be recalled that martensite has single phase BCT structure, which is supersaturated with carbon. In contrast to as received pearlite-ferite microstructure, strength and hardness properties are attributed to the effectiveness of the interstitial carbon atoms in blocking dislocation motions (effect of solid solution) [42]. There are relatively few slip systems (along which dislocations move) in the BCT structure.

The sample which was tempered at lowest temperature of 250°C, has cracks as well, they are longer and a little wider compared to the next (tempered at 450°C) sample. The cracks on the surface of the sample, which was tempered at 450°C are thin and not so obvious, most of them are on fairly smooth surface, which does not have irregularities, so corrosion pits do not act as preferential initiation sites. The sample, which was tempered at 650°C has probably the lowest SCC resistance. The cracks on this sample are longer and wider than on the rest of the presented microstructure. It should be mentioned, that during tempering process, single-phase BCT martensite, saturated with carbon, transforms to the tempered martensite, composed of stable ferrite and cementite.



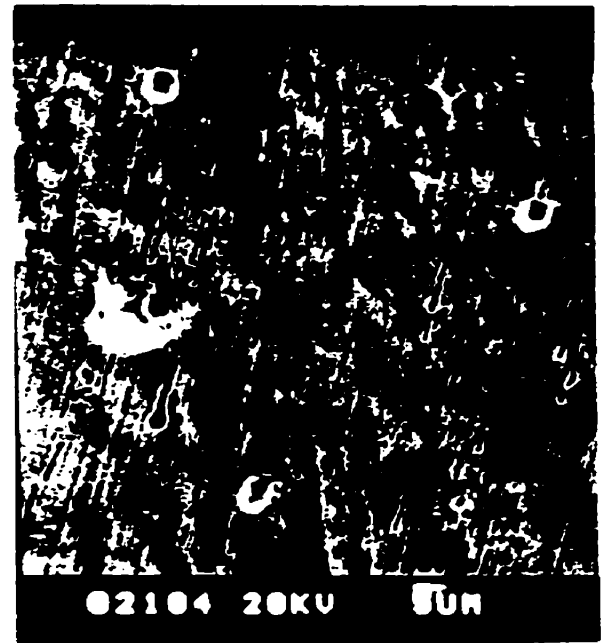
(a) $\sigma = 718$ MPa



(b) $\sigma = 707$ MPa

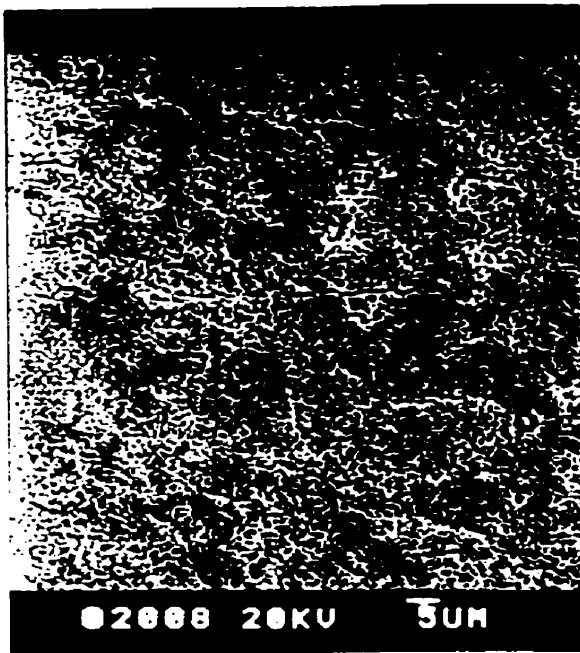


(c) $\sigma = 671$ MPa

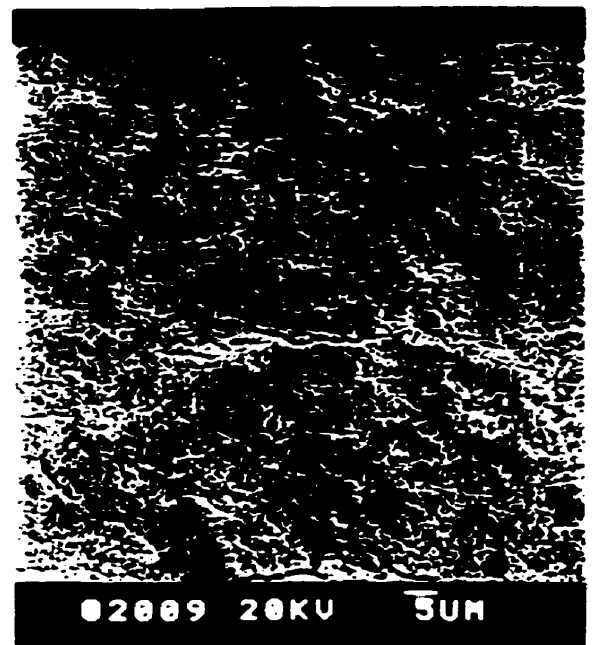


(d) $\sigma = 643$ MPa

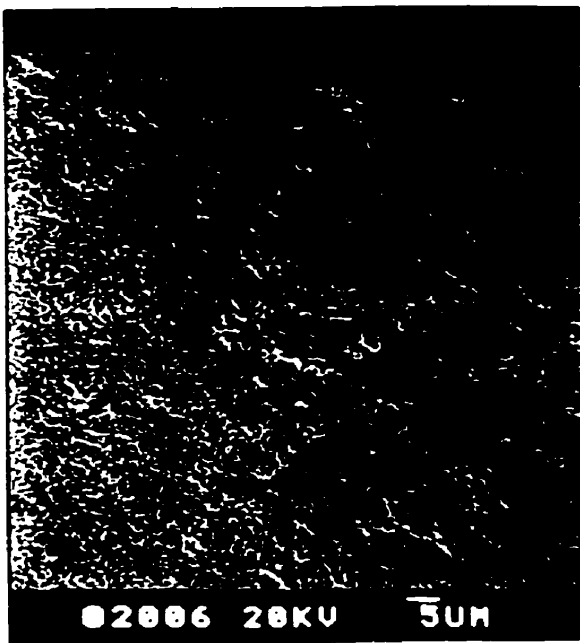
Fig 5.1.2.1 Sample Surface at Different Stress Levels (950°C/10 min/WC)



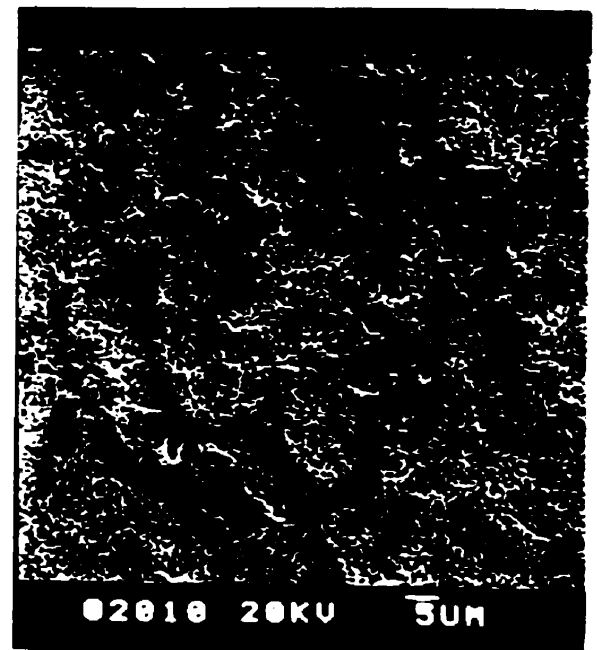
(a) $\sigma = 697$ MPa



(b) $\sigma = 687$ MPa

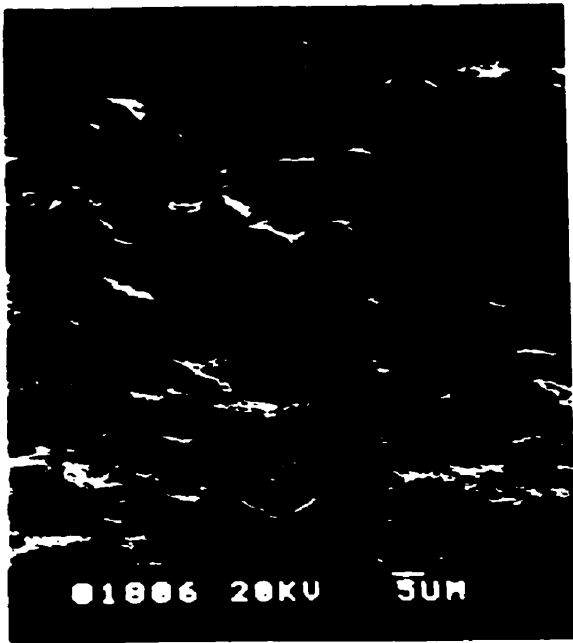


(c) $\sigma = 667$ MPa



(d) $\sigma = 645$ MPa

Fig 5.1.2.2 Sample Surface at Different Stress Levels (950°C/10min/WC+250°C/2hrs)



(a) $\sigma = 645$ MPa



(b) $\sigma = 624$ MPa

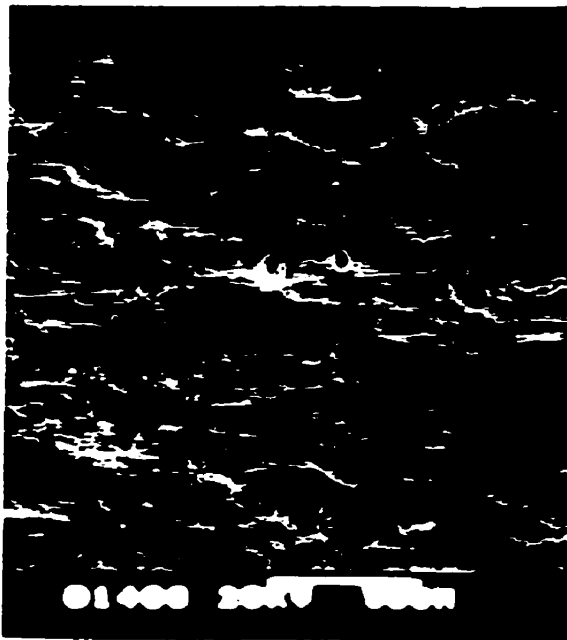


(c) $\sigma = 595$ MPa



(d) $\sigma = 568$ MPa

Fig 5.1.2.3 Sample Surface at Different Stress Levels (950°C/10min/WC+450°C/2hrs)



(a) $\sigma = 406$ MPa



(b) $\sigma = 387$ MPa



(c) $\sigma = 375$ MPa



(d) $\sigma = 353$ MPa

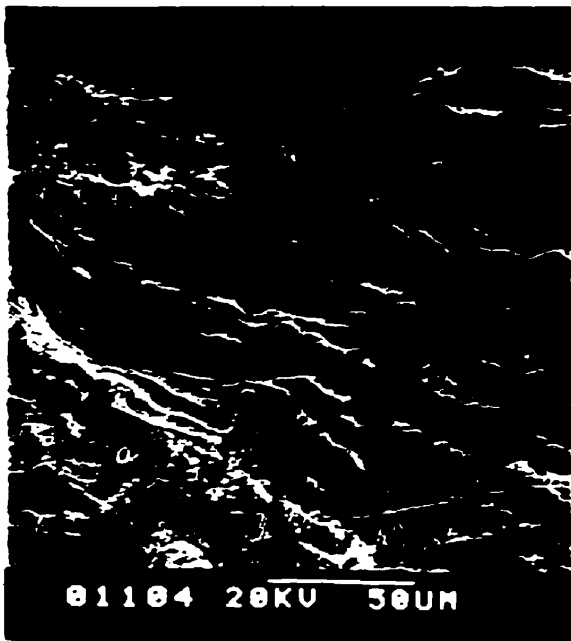
Fig 5.1.2.4 Sample Surface at Different Stress Levels (950°C/10min/WC+650°C/2hrs)



(a) $\sigma = 428$ MPa



(b) $\sigma = 406$ MPa



(c) $\sigma = 379$ MPa



(d) $\sigma = 361$ MPa

Fig 5.1.2.5 Sample Surface at Different Stress Levels (950°C/1Hr/WC+650°C/2hrs)

The hardness and strength of tempered martensite maybe explained by the large ferrite – cementite phase boundary area per unit volume that exists for the very fine and numerous cementite particles. The hard cementite reinforces the ferrite matrix along the boundary, and these boundaries act as barriers to dislocation motion. The size of these cementite particles influences the mechanical behavior [42].

It is interesting to compare the influence of the grain size on Near-Neutral-pH SCC susceptibility. As it was mentioned before in H₂S environments finer grains are more resistant to Sulfa Induced Cracking. Let's see if it is the case for Stress Corrosion Cracking in Near-Neutral-pH environment. Comparing pictures on Fig 5.1.2.4 (950°C/10min/WC+650°C/2hrs) and Fig 5.1.2.5 (950°C/1hr/WC+650°C/2hrs) we can see that in case of coarse grains (Fig 5.1.2.5) cracks are much longer and wider than in case of fine grains (Fig 5.1.2.4). It makes sense, since Near Neutral pH SCC has transgranular morphology, for the crack it is easier to develop within one big grain, than through several small one with consequential penetration through several grain boundaries. So we can make a conclusion that fine grains have higher resistance to Near-Neutral-pH SCC.

The next step in the experiment was to find the Critical Stresses of Near-Neutral-pH SCC initiation for different microstructures and compare them with Critical Stress of as-received sample, to define the most resistant morphology of steel to SCC. In order to have this done the conical samples were used. On the Fig 5.1.2.6 there is a chart showing Critical Stress levels and Yield Stress for different heat-treated samples. From the chart we can notice that all the Critical Stresses are lower than Yield Stresses for different heat-treatment. The Yield Stress used here is obtained from the test conducted in the air. It

also should be noticed that for as received sample the critical stress is above the Yield Stress. It can be seen that quenched sample has the highest Critical Stress, it also has the highest level of Yield Stress. It followed by samples tempered at 250°C, 450°C, as-received and 650°C. This strongly suggests the dependence of Critical Stress on the Yield Stress and Hardness, because from this chart it is obvious that as the Yield Stress and Hardness decrease, the Critical Stress decreases. It also should be noted that only “as received” sample has Critical Stress above its Yield Stress, on the rest of the microstructures crack initiation begins before stress level reaches Yield point. Even though the absolute value of critical stress for these tempered samples higher than “as received” sample, if we relate this to the Yield Stress, “as received” sample is in more advantageous position compared to tempered samples.

If we look at the dependence of Critical stress vs. microstructure it can be noticed that Critical stress increase as dislocation motions are more and more restricted. In case of martensite, the restrictions come from interstitial carbon atoms. They tend to segregate around dislocations in a way so as to reduce the overall strain energy that is to cancel some of the strain in the lattice surrounding dislocations. The resistance to slip is greater when carbon atoms are present at the dislocation site, because overall lattice strain must increase if a dislocation is torn away from them [42]. Thus, a greater-applied stress is necessary to initiate the crack. That is why there is such a big increase of Critical stress of initiation. In case of tempered martensite, the size of cementite particles influences the mechanical behavior. Increasing the particle size decreases the ferrite-cementite phase boundary area and consequently results in a softer and weaker material. Carbon diffusion is involved in the martensite – tempered martensite transformation, increasing the

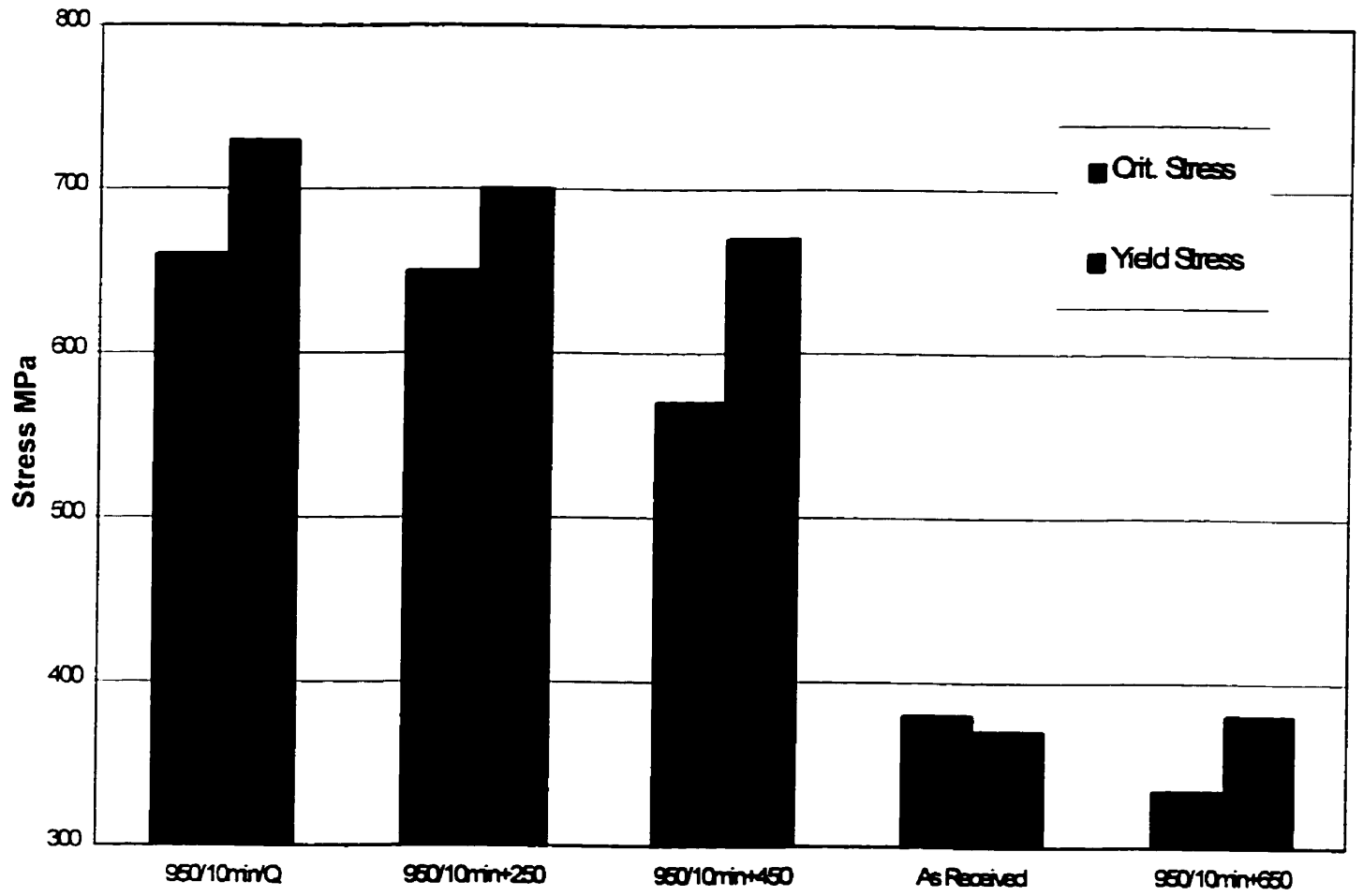


Fig 5.1.26 Critical Stress of Different Microstructure

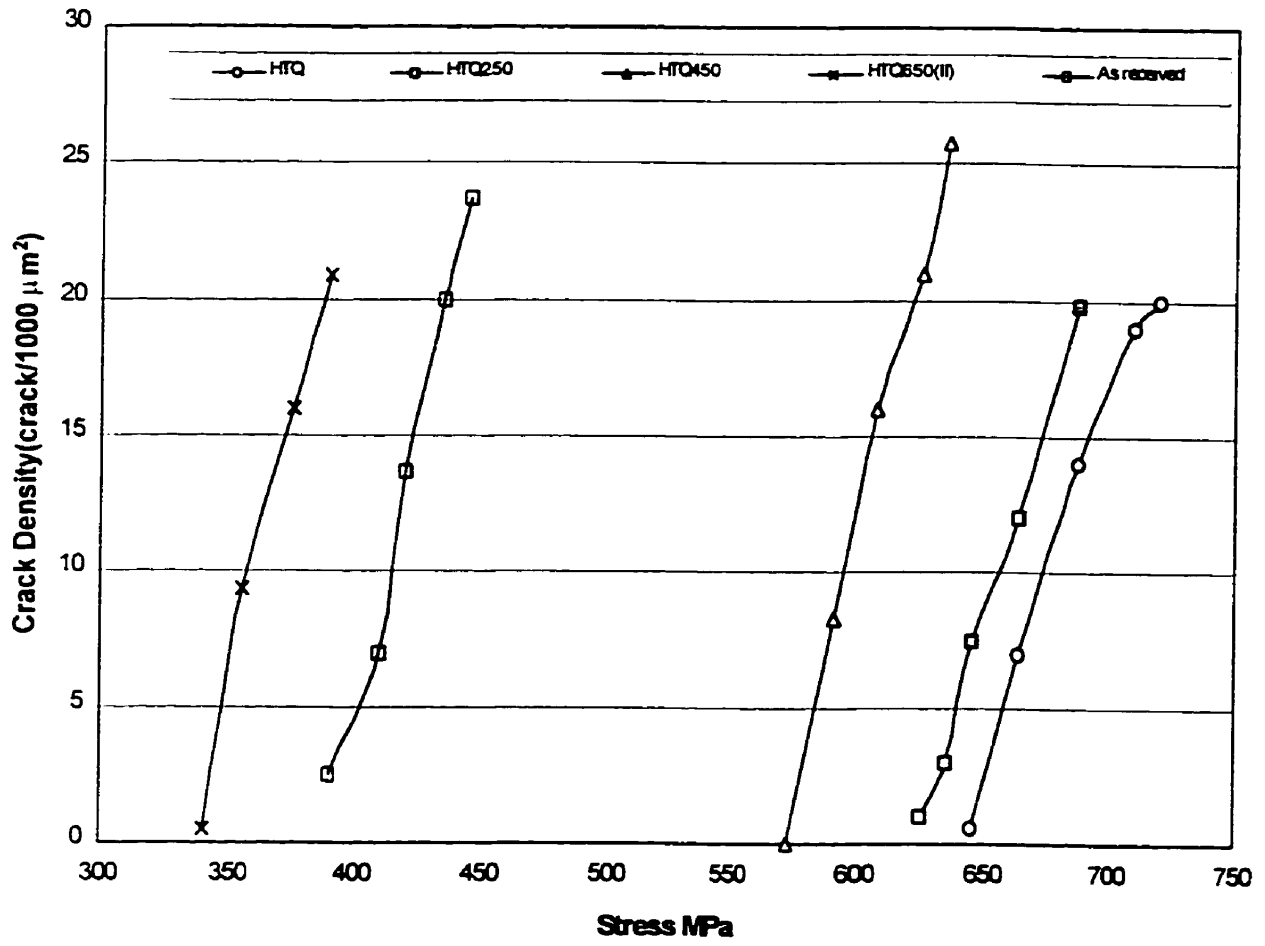


Fig 5.1.27 Crack Density vs Stress

temperature will accelerate diffusion, the rate of cementite particle growth and subsequently the rate of softening, since the amount of barriers (ferrite-cementite boundaries) for dislocation motion decreases. As a result the Critical stress decreases with increase of tempering temperature.

The Yield Stress is not the only factor from mechanical properties, which influences the susceptibility of the material. It should be noted that if we look on the pictures of different samples presented above, we can see that on some of them the cracking is very obvious (quenched, tempered at 650°C), but on others (tempered at 450°C), cracks are not as obvious. In other words the morphology of cracking for different heat-treatment is different and we can draw a conclusion that although the Yield Stress and Hardness of the sample are two major factors, there exists something else what influences the cracking. Fig 5.1.2.7 shows the dependence of crack density on stress level.

Based on observations of samples after tests we can suggest that if there is no irregularities on the surface (pits, inclusions, polishing lines, etc.) the cracks initiate at the dislocation bands. In tempered martensite, the dislocation motions are restricted by ferrite – cementite boundaries. Also atomic hydrogen tends to be trapped at the dislocation sites, leaving a slip band within a grain as the only place for crack initiation. Fig 5.2.6(a,b).

The chart on Fig 5.1.2.7 supports an idea, which was expressed above on initiation and propagation of Near-Neutral-pH SCC in the microstructure of the steel. It also shows that after critical stress was reached and cracks were initiated, the evolution of SCC (the increases of cracks in colonies as well as number of colonies) is about the same, except that for different microstructure it happens at different stress levels. And these

stress levels strongly depends on the mechanical property of each particular microstructure. In other words, for the fixed stress level the higher the Yield Stress of the microstructure, the less SCC density can be observed.

5.1.3 Influence of Microstructure Differences on SCC Growth Rate

Using the same procedure as on as-received samples for different potential in Chapter 4, the growth rate for various microstructures was calculated. On Fig 5.1.3.1 the levels of growth rates are shown. As it is seen on this chart, the higher the Yield Stress and Hardness of the material the higher the growth rate of the cracks with the exception of the sample, which was tempered at 450°C . This sample has the lowest growth rate, which suggest the slowest rate of propagation of cracks in this particular type of microstructure. It should be also recalled that cracks, found on this sample, are the least obvious compared to the cracks on the surface of samples with other types of microstructure. This is quite a remarkable result, because it suggests the steel that was heated to 950°C for 10 minutes, quenched and tempered at 450°C for 2 hours, has one of the highest resistance to SCC initiation stress wise and the highest resistance to SCC propagation, among heat treated samples. It might also suggest that the mechanisms of initiation and propagation of Stress Corrosion Cracks are different.

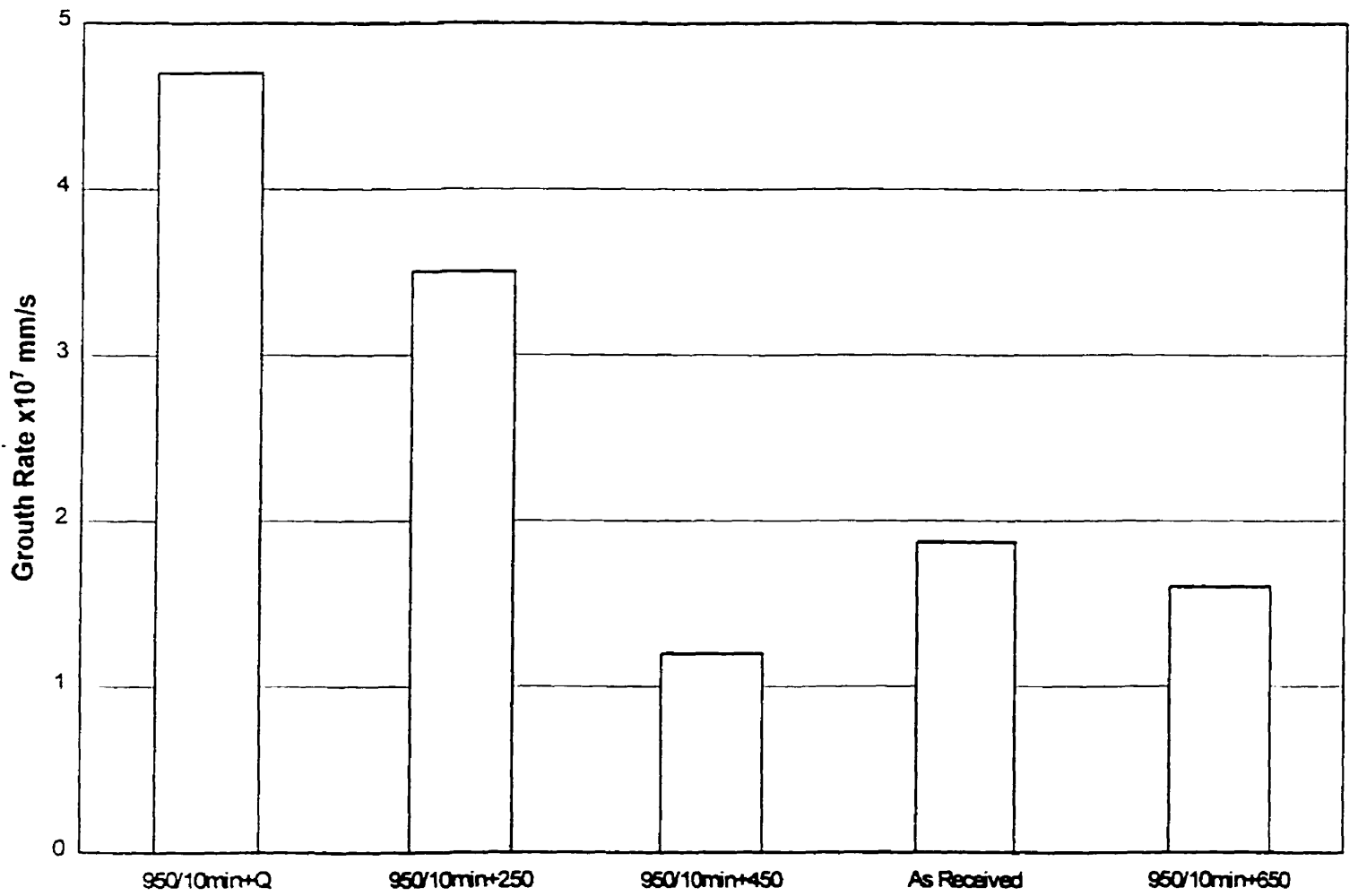


Fig 5.1.3.1 Crack Growth Rate for Different Heat-Treatment

5.2 Residual Stresses and Their Influence on Near-Neutral-pH SCC Initiation and Propagation

During fabrication of pipeline a lot of residual stresses are introduced into body of the pipe due to rolling, bending and welding procedures. All of the residual stresses, which are built up in the pipe, can be classified in three major categories. The first one is macro stresses, they are elastic and exist between different elements of the pipe. The second type is first micro-residual stresses and exists among the grains and subgrains. The last (third) type is second micro-residual stresses, which exists within the grain and appears at the slip planes and dislocation lines. Since the nature and origin of all of these three types of residual stresses different, X-rays diffract differently, when used for examination. Macro-residual stresses make the diffraction lines displace, the first micro-stresses make the diffraction lines widen, and the second micro-stresses make the intensity of the diffraction weaken. During our investigation X-ray diffraction was used to measure the magnitude and distribution of residual stresses. Measurement was done by NRC in Ottawa. Unfortunately they could only measure macro residual stresses.

The samples (30x30x12) were cut from the pipe in the welded and heat affected zone and annealed at 450°C for 2 hours and then furnace cooled. The outer surface of all samples was ground to 320 grit paper to remove the mill scale, then electrolytic polishing was used to remove residual stress layer (0.2-0.3mm), introduced by grinding. In the following table (Table 5.2.1) the results of macro-residual stress measurements are presented for X-52 pipeline steel. Minus “-“ in the table means the residual stresses are compressive. It should be noticed that X-ray diffraction method, used for residual stress

measurement is a destructive method, so some of the residual stresses in the pipe were relieved when the pipe was cut (for example, the circumferential stresses). It should be mentioned that this result might not stand for the residual stresses in the real pipe. Also technique, which was used only measure macro-residual stresses.

Table 5.2.1 Macro-Residual Stresses Measured by X-ray Diffraction Method

	Circumferential Direction	Longitudinal Direction
As-received sample	-10±20MPa , -30±20MPa	-20±20MPa , - 30±0MPa
Stress released sample	-10±10MPa , 0±20MPa	-10±10MPa , - 20±10MPa

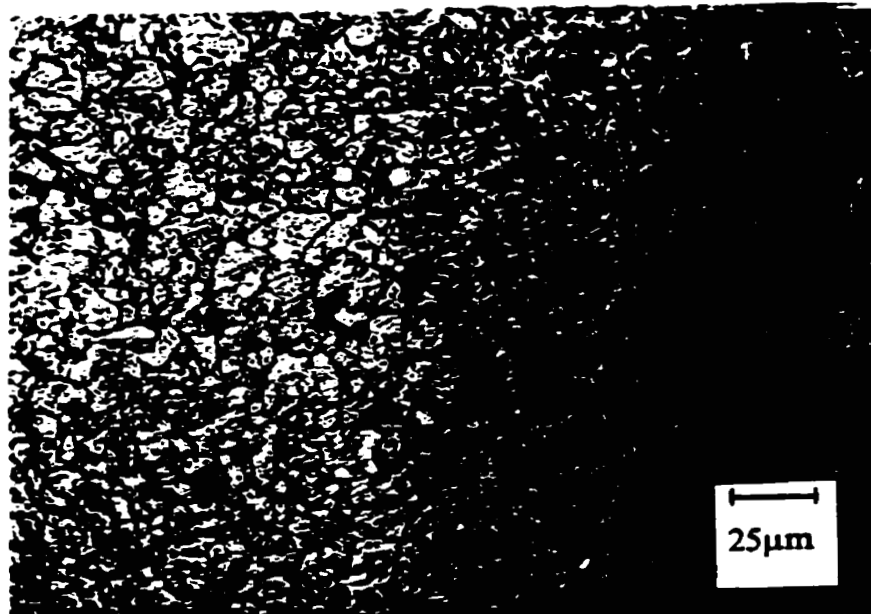
Several samples were stress relieved at different temperature. Table 5.2.2 shows mechanical properties of the stress relieved samples.

Table 5.2.2 Material Properties of Stress Relieved Samples

Conditions	Yield Stress (0.2%) (MPa)	Hardness (HRB)
As-received	370	83
250°C/2hrs/FC	390	83
450°C/2hrs/FC	395	83
550°C/2hrs/FC	400	83

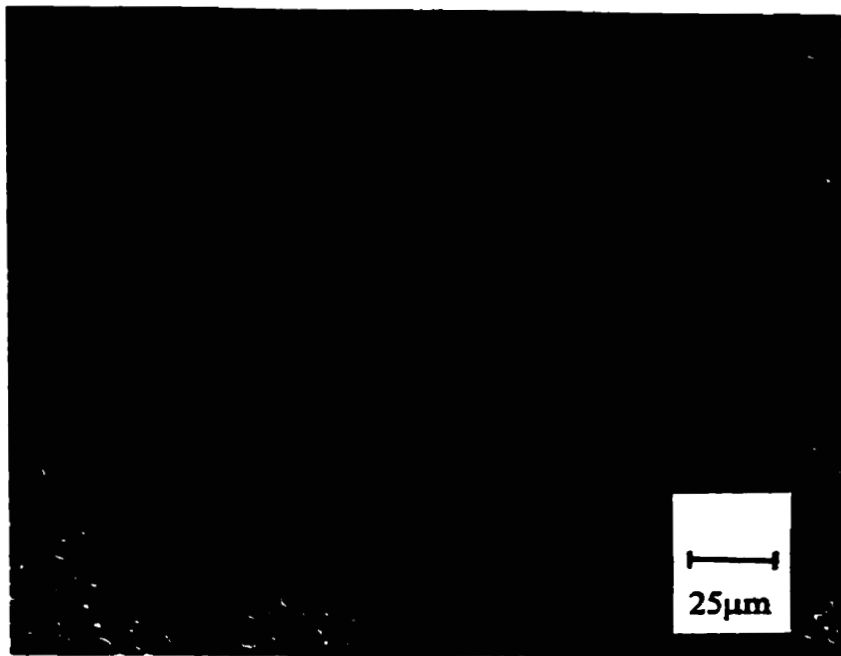


(a) Stress Relieved Sample at 250°C/2hrs

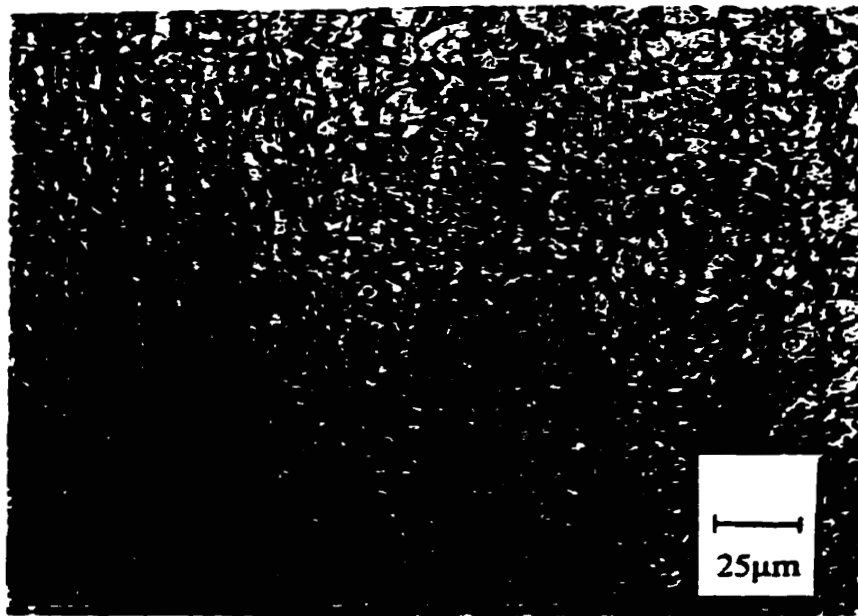


(b) Stress Relieved Sample at 450°C/2hrs

Fig 5.2.1



(c) Stress Relieved Sample at 550°C/2hrs



(d) Stress Relieved Sample at 650°C/2hrs

Fig 5.2.1

The above pictures (Fig 5.2.1) show microstructure of stress relieved samples at 250°C/2hrs (a), 450°C/2hrs (b), 550°C/2hrs (c) and 650°C/2hrs (d). As it can be seen the microstructure for stress relieved samples remain the same as for as-received sample up to 550°C. From the table above we also see that hardness is also the same. After the sample was soaked for two hours at the temperature 650°C, a partial recrystallisation occurred and the sample became softer (HRB79).

The total effective stress in pipeline is the sum of residual stresses and operational stresses. If a proper stress relief heat-treatment done, the magnitude of residual stresses can be minimized. This can cause the delay in Stress Corrosion Cracking initiation. This is exactly what we see from Fig 5.2.2, which shows stress levels of SCC initiation for different stress relieving conditions.

It is known that when the steel is heated to the temperature below recrystallization level, reduction of internal residual stresses take place. At lower temperature of treatment, like 250°C, it is called early stage recovery, elastic stresses in lattice planes are relieved and vacancies, which exist due to plastic deformation, disappear. At medium recovery temperature, like 450°C, some dislocations disappear. One of the best results gives the stress relieving temperature of 550°C. At this recovery stage temperature both macro residual and the first micro-residual stresses are relieved, some of the dislocations rearranged and subgrain forms minimized without the mechanical properties sufficient change. At higher temperature, like 650°C, recrystallization within the sample begins and mechanical properties change sufficiently (the sample become softer), effecting growth rate of cracks due to increase of ductility.

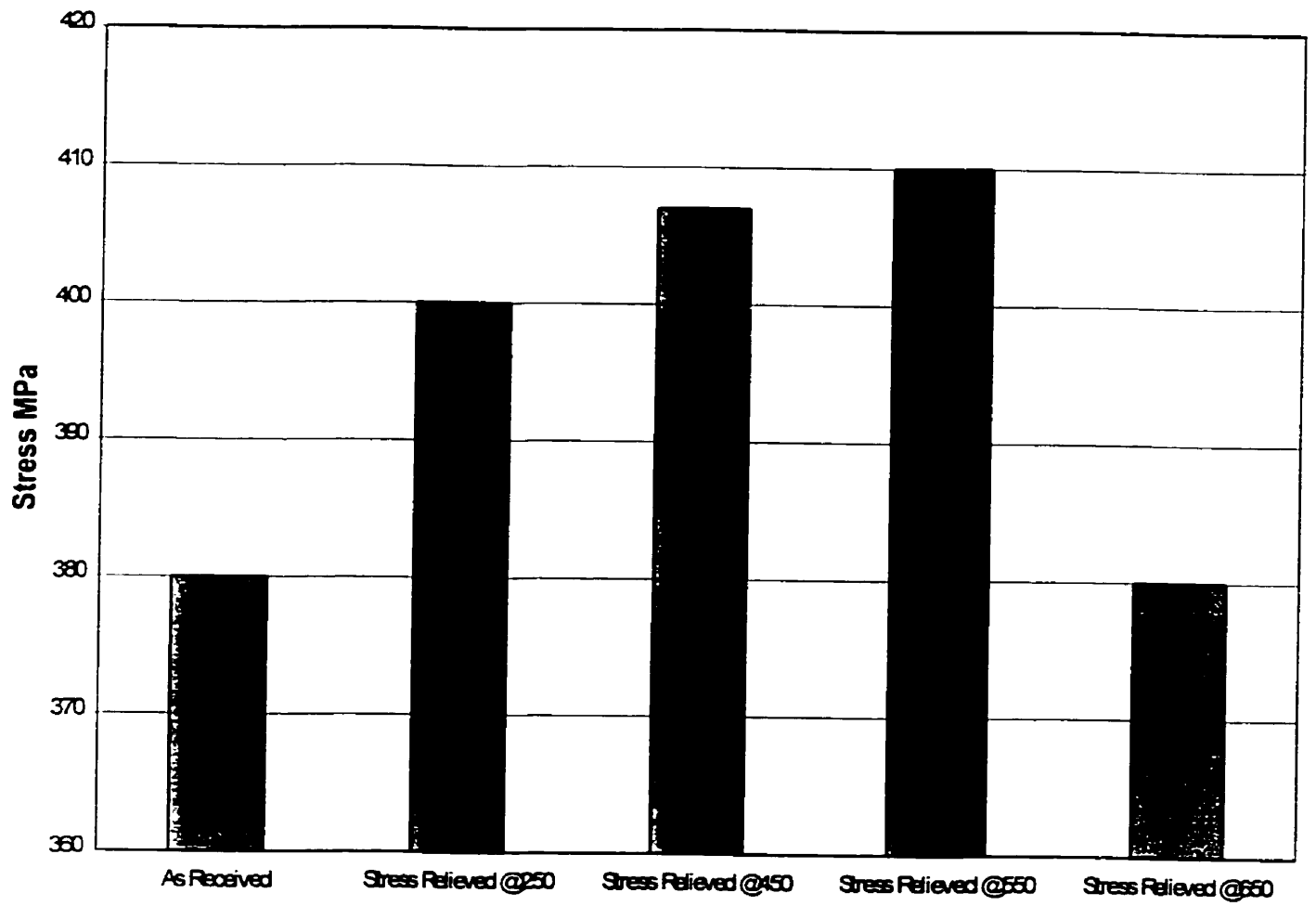


Fig 5.2.2 Critical Stress of SCC Initiation for Stress Relieved Steel

(c) $\sigma = 452 \text{ MPa}$

(d) $\sigma = 423 \text{ MPa}$

**Fig 5.2.3 Sample Surface at Different Stress Levels
(Stress Relieved at 250°C for 2 Hours)**



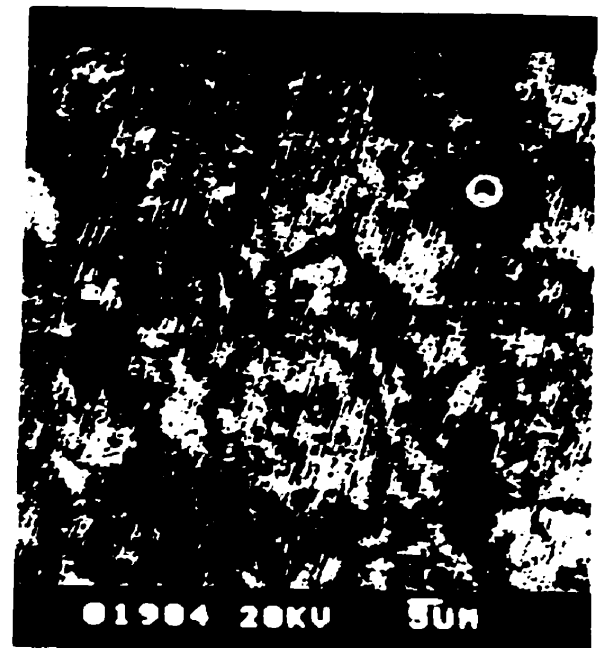
(a) $\sigma = 480$ MPa



(b) $\sigma = 464$ MPa



(c) $\sigma = 430$ MPa



(d) $\sigma = 417$ MPa

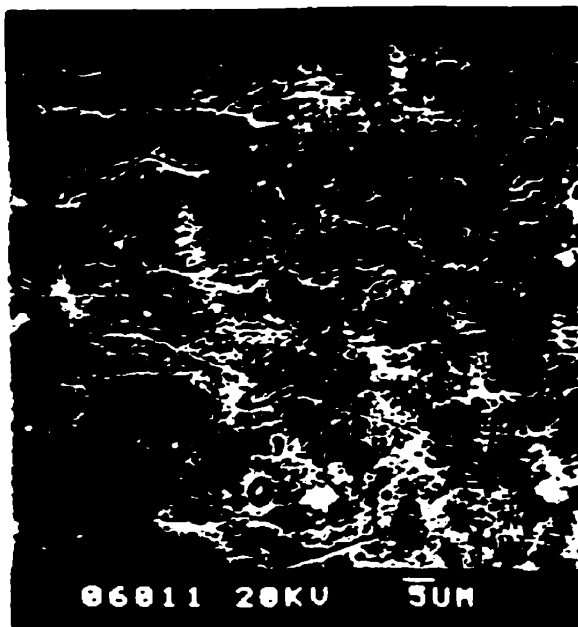
Fig 5.2.4 Sample Surface at Different Stress Levels, Stress Relieved at 450°C for 2 Hours



(a) $\sigma = 465$ MPa



(b) $\sigma = 460$ MPa



(c) $\sigma = 427$ MPa



(d) $\sigma = 408$ MPa

Fig 5.2.5 Sample Surface at Different Stress Levels, Stress Relieved at 550°C for 2 Hours

As we can see higher stress relieving temperature, more residual stresses are relieved, higher the critical stress of initiation of Stress Corrosion Cracking. So the conclusion can be made that susceptibility is increasing with decrease of residual stresses in the pipeline steel.

On the following set of pictures there are crack developments at different stress levels for different stress relieved samples (Fig 5.2.3; 5.2.4; 5.2.5).

From the pictures above it can be seen that morphology of cracks changing as stress relieving temperature increases. At lower temperatures of stress relief, two major locations such as surface irregularities (inclusions, corrosion pits, etc.) and specific crystallographical planes, which are not defined by any irregularities, are seen. When temperature of stress relief reaches 550°C the major difference can be noticed – there is only one site of crack initiation: surface irregularities. This points out to the fact that the second type of crack initiation site is the locations of residual stresses in the specific crystallographical planes (possibly slip bands). These sites were eliminated as residual stresses disappeared from the steel due to stress relieving procedure.

Several samples were etched after the experiment in order to observed crack development with respect of grains layout. For this purpose samples with following heat treatment were chosen: 950°C/1hr/WC+650°C/2hrs. This choice was made due to fairly large size of grains, which makes it easy to observe slip bands. Other heat treated samples as well as as-received sample were also etched after the experiment, but the size of the grain was too fine for the clear observation of crack initiation on dislocation bands. A number of slip bands within a grain were found at lower stress levels (Fig 5.2.6).



Fig 5.2.6(a) SEM Image of Slip Bands within Grains on Etched Surface of the Sample



Fig 5.2.6(b) SEM Image of Slip Bands within Grains on Etched Surface of the Sample
under Higher Magnification



Fig 5.2.7 (a) SEM Image of Cracks within the Grain on Etched Surface of the Sample

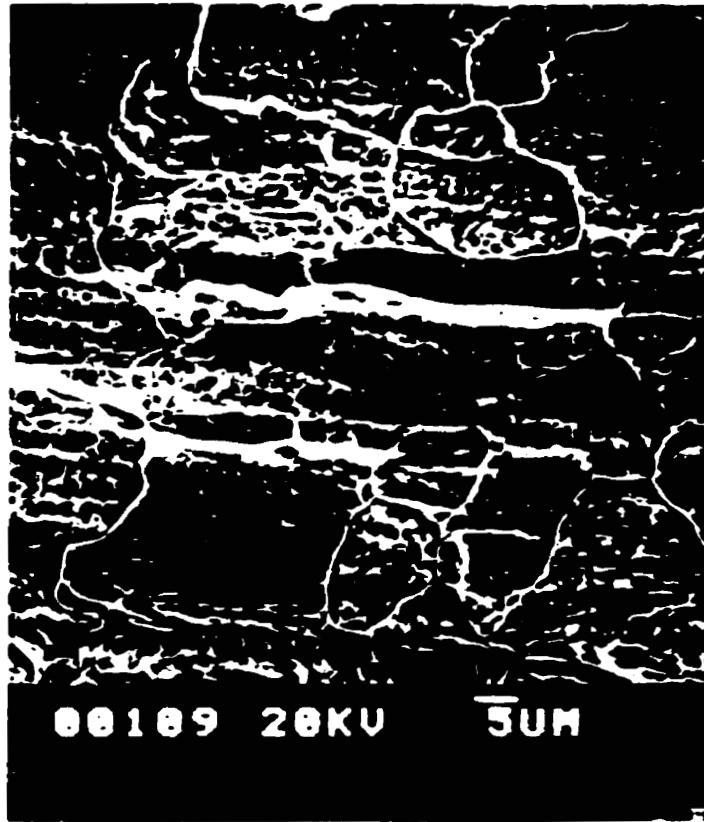


Fig 5.2.7 (b) SEM Image of Cracks Propagating Through Several Grains on Etched Surface of the Sample

When observation was made at higher stress levels mature cracks were found within grains (5.2.7(a)). Some of the cracks propagated through several grains (5.2.7(b)).

In chapter 4 the influence of highly localized dissolution and atomic hydrogen was mentioned in connection with Near-Neutral-pH SCC initiation. It should be mentioned that atomic hydrogen, tends to diffuse into the steel and get trapped by stress concentrations such as irregularities (inclusions, pits, etc.), dislocations in other words all kind of elements which give a raise the localized stresses. On the other hand, this type of areas tend to be preferential sites for highly localized dissolution, since electrons from applied cathodic current may not be able to reach this sites due to difference in the chemistry of these sites and bulk areas. Electro-chemical reactions have to take them from iron causing its dissolution. After stress relief of the sample, there are less stress concentration and residual stresses in the steel. As a result, less hydrogen builds up in the steel and there are fewer sites for highly localized dissolution, which causes the delay in Stress Corrosion Cracking initiation and propagation.

In the next presented chart (Fig 5.2.8) dependence of crack density vs. stress is shown. It is clearly seen that prior to recrystallization temperature (650°C) there is a delay in initiation and propagation stress for Near-Neutral-pH SCC. At the same time once the recrystallisation occurs, material properties of the sample change and initiation and propagation stresses decreases, although ratio of critical stress and yield stress is still high.

Near Neutral pH SCC growth rate was calculated the same way for stress relieved samples, as it was done for the samples tested at other conditions (the mechanism of calculation was explained above). They basically have almost the same magnitude as as-

received samples. Although the lower number of dislocations in the samples, which were stress relieved at higher temperatures, decreased slightly the growth rate. This happens because less atomic hydrogen can be trapped in the dislocations (dislocation bands, since there are fewer number of them) causing decrease in the influence of hydrogen embrittlement. There is no change in mechanical properties prior to recrystalisations temperature so this decrease does not have high magnitude. At the same time we can see considerable difference at the stress relief temperature of 650°C, due to recrystalization processes (Fig 5.2.9).

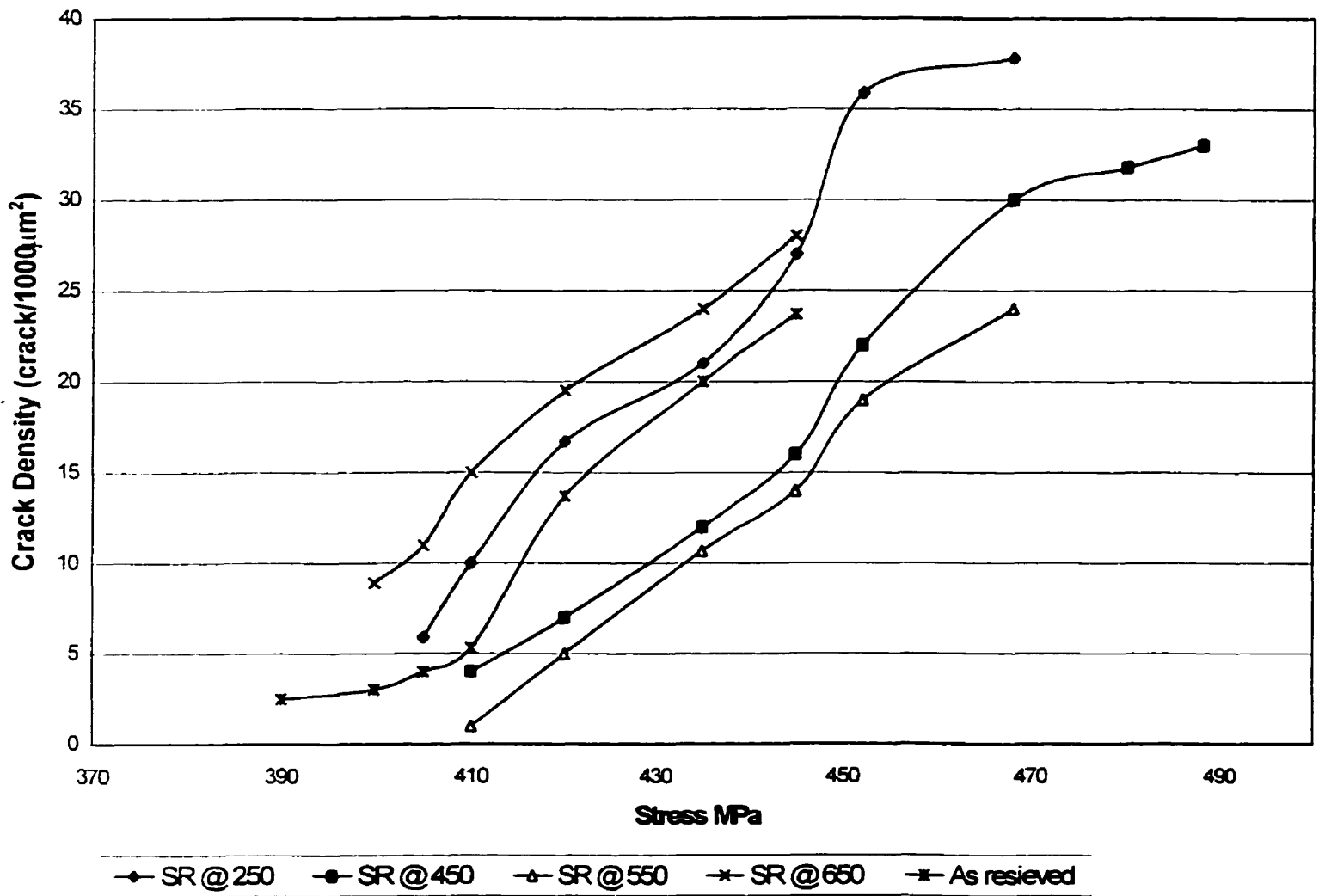


Fig 5.28 Crack Density VS Stress

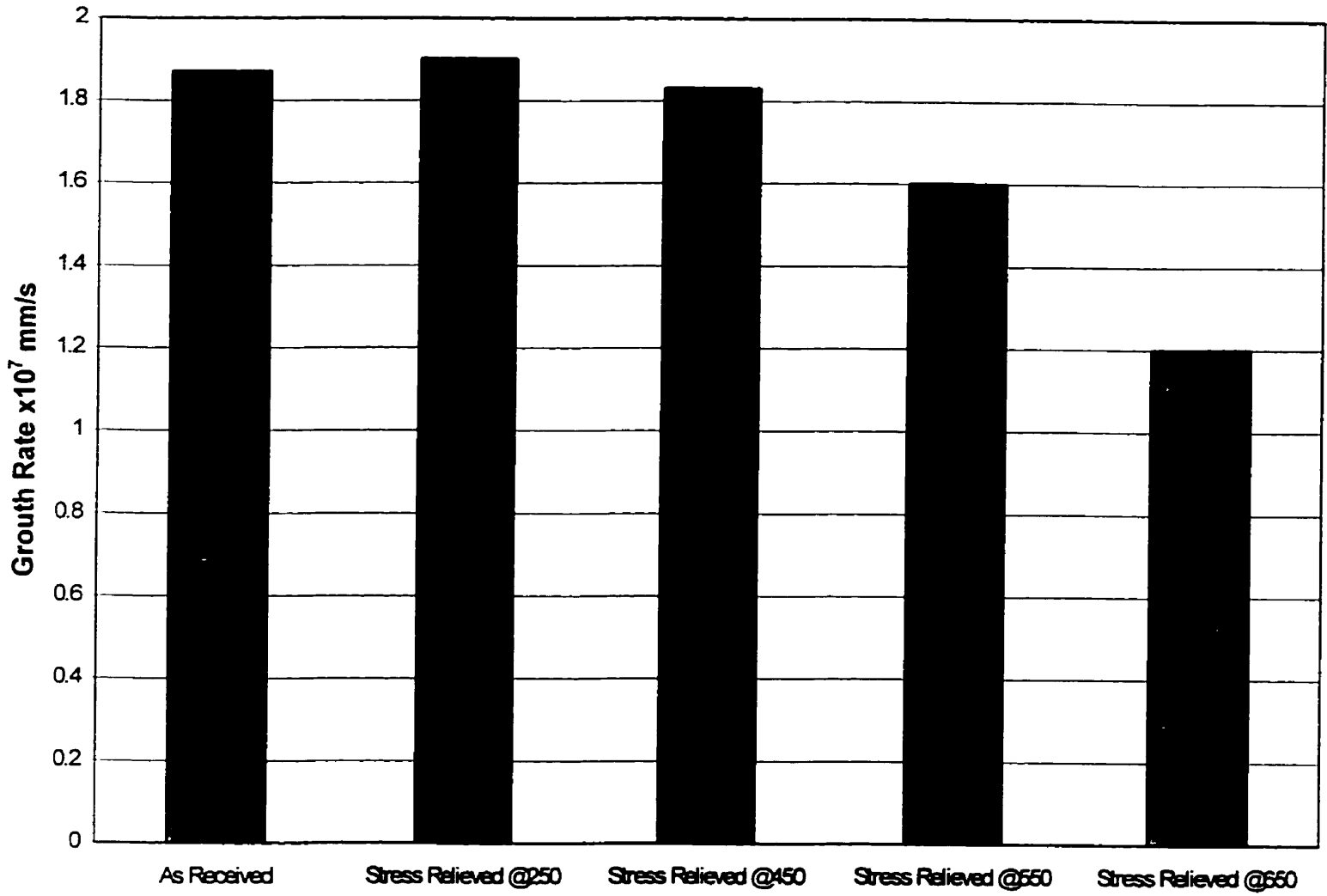


Fig 5.29 Crack Growth Rate for Stress Relieved Samples

Chapter 6

Observations and Conclusions

Slow Strain Rate Testing (SSRT) results shows that susceptibility of X-52 pipeline steel highly depends on Electro-chemical environments of experimental setting. Based on number of experiments performed during the investigation, the following conclusions can be drawn:

1. Multiple type of cracking was observed in the range of potential from $-800\text{mV}_{\text{SCE}}$ to $-1100\text{mV}_{\text{SCE}}$; strain rate from 1×10^{-7} to 1×10^{-6} 1/s.
2. The most susceptible potential for Near-Neutral-pH SCC initiation was found to be around $-900\text{mV}_{\text{SCE}}$.
3. The most susceptible strain rate for Near-Neutral-pH SCC initiation was found to be 2.5×10^{-7} 1/s. Above and below this strain rate the critical stress of initiation increased, this reflects the fact that susceptibility decreases at other strain rates. This observation lead us to a conclusion that not only evolution of hydrogen on the steel surface contributes to the initiation of Near-Neutral-pH SCC, but also highly localized dissolution at surface irregularities (inclusions, corrosion pits, etc) or/and slip bands, causes the initiation of cracks on the surface of the steel.
4. Crack density and crack length increases as the stress increases. All of the observed cracks came in colonies and as the applied stress increased they started overlapping and coalescing with each other.
5. The critical stress of Near-Neutral-pH SCC initiation for as received steel was calculated based on the experiment results. It increases as various applied potential

decreases from 102% of Yield Stress for $-800\text{mV}_{\text{SCE}}$ to 111% of Yield Stress for $-1100\text{mV}_{\text{SCE}}$ (strain rate = 5×10^{-7})

6. It was also found that critical stress also depends on strain rate of experiment, but this dependence is not as simple as on potential. If strain rate equals 0 (static load), no initiation was found. After strain rate was increased to 1×10^{-7} 1/s critical stress of initiation was found to be around 109% of Yield Stress. Further increase to 2.5×10^{-7} 1/s gave us the most susceptible conditions, when critical stress dropped to 97% of Yield Stress, then increase of strain rate to 5×10^{-7} and 1×10^{-6} 1/s gave us critical stress of 105% and 108% of Yield Stress accordingly.
7. Last two observations strongly support the idea that highly localized dissolution in the slip bands and surface irregularities is one of the major contribution of Near-Neutral-pH SCC initiation. When potential decreases, there is less and less opportunity for localized dissolution to happen and as a result critical stress is getting higher. Strain rate effect also supports this idea, when cracks initiate only with in a certain range of strain and almost inhibit outside of this range. In contrary, if hydrogen was the only cause of initiation, the critical stress would decrease with a decrease of the strain rate with minimum critical stress (maximum susceptibility) at the static load, but this did not happened, there were no cracks found during static load experiment.
8. Effect of pH value was also considered during the investigation. From observation of cracks initiation at different pH it was found that amount of hydrogen ions in the solution contribute to the level of critical stress. A number of tests were performed at Free Corrosion Potential but no cracks were found. When the pH was deliberately decreased from 6.8 to 3.8 and test was conducted at the same potential (FCP),

multiple cracks were found and the critical stress was equal to the Yield Stress. On the other hand, when solution was purged with pure nitrogen (N_2), and pH of solution had grown from 6.8 to 8.5 (applied potential = $-900mV_{SCE}$), multiple crack could be found again, but the critical stress jumped to the level of 112% of Yield Stress.

9. The influence of applied potential on growth rate was investigated. It was found that growth rate increases as potential decreases. This can be related to higher amount of hydrogen accumulated on the surface of the steel at lower potentials.
10. All of the mentioned above strongly support the idea of hydrogen induced anodic dissolution mechanism of Near-Neutral-pH SCC initiation. Which is related to both hydrogen accumulation and some electro-chemical reactions on the surface of the steel. At the same time the mechanism of crack propagation is dominated by the hydrogen induced cracking. So there exists the range of potential within which initiation and propagation of Near-Neutral-pH SCC is possible. At higher potential, more general corrosion and less hydrogen evolution can not generate SCC initiation. Whereas at more negative cathodic potential, preferential dissolution or Electro-chemical reactions necessary for SCC initiation are impossible, which results in SCC initiation susceptibility decrease.
11. Residual stress effect on initiation was investigated. Four basic temperatures of Stress Relief were considered $250^{\circ}C$, $450^{\circ}C$, $550^{\circ}C$ and $650^{\circ}C$. At the last temperature the beginning of recrystallization occurs. It was found that as the stress relieving temperature increased, the susceptibility of steel to SCC decreased (critical stress increased). At temperature of $650^{\circ}C$, recrystallization occurs and mechanical property changes (Yield Stress and Hardness decreases) so decrease the critical stress. It was

observed that as the temperature of stress relief increases fewer cracks initiate at the surface, which does not have any visible irregularities such as pits or inclusions. At the temperature of 550°C of stress relief most of the cracks initiated only from inclusions and pits. This point out to the fact that residual stress causes the initiation at the second type of initiation site – when cracks appear on visually smooth surface.

12. The investigation of residual stress effect on the growth rate of SCC was done. It was found that the growth rate decreases as the temperature of stress relief increase (more residual stresses get relieved).
13. The susceptibility of X-52 pipeline steel with various microstructures was investigated. All investigated microstructures were found to be susceptible to Near-Neutral-pH SCC. Colonies of cracks were found on all of the samples. The cracks grow and coalesced as applied stress increased. It was found that critical stress was related to the yield stress of particular microstructure. Although the tendency for critical stress to decrease as the yield stress decrease is obvious, there exists something else in the mechanism of crack initiation and propagation in various microstructure since the cracks do not look the same for the different tempering temperature.
14. From the microstructure investigation it was also found that big grains are more susceptible to Near Neutral pH SCC than fine ones.
15. And the last what was examined in this investigation is the growth rate of cracks in various types of microstructure. It was found that as the hardness of steel increased so increased and the growth rate. This is quite obvious since cracks propagate at the higher rate in the more brittle material.

References

1. ASTM G 15 - 87
2. Andrew J.H., Trans. Faraday Soc. 9(1913): p.316
3. Parr S.W., Straub F.G., Univ. Illinois Bull. (1928): p.177
4. Wolff E.B., Iron J. Steel Inst. 96 (1917): p.137
5. McAdam D.J., Proc. ASTM (Philadelphia, PA, 1931) p.259
6. Fletcher J.E., Discuss.Faraday Soc. 17 (1921): p. 158.
7. National Energy Board. Report of The Inquiry, SCC on Canadian Oil and Gas Pipelines.. Nov. 1996
8. Pilkey A.K., Lambert S.B. and Plumtree A., Corrosion 51 (1995): p.91.
9. Sutcliffe, J.M., Fessler, R.R., Boyd, W.K. and Parkins, R.N. 1972 "Stress Corrosion Cracking of Carbon Steel in Carbonate Solutions", Corrosion, Vol 28. p.313.
10. Wenk R.L.. "Field Investigation of Stress Corrosion Cracking" 5th Symp. Line Pipe Research. Catalog # L30174, (Arlington, VA: American Gas Association. 1974), p.T1
11. Parkins, R.N. 1974, "The Controlling Parameters In Stress Corrosion Cracking". 5thSymposium on Line Pipe Research. American Gas Association, Inc., Catalog No. L30174, p. U-1.
12. Koch, G.H. Beavers, J.A. and Berry, W.E. 1985"Effect of Temperature on Stress-Corrosion Cracking of Precracked Pipeline Steels" NG-18 Report #148, American Gas Association, Inc., Catalog # L51491
13. Beavers, J.A., Parkins, R.N., 1987. "Some Effects of Surface Conditions on the Dstress Corrosion Cracking on Line Pipe Steel", Corrosion/87, Paper #178

14. Beavers, J.A., Parkins, R.N., Berry, W.E. 1985. "Test Method for Defining Susceptibility of Pipeline Steels to Stress Corrosion Cracking", NG-18 Report Number 146 Catalog No. L-51484, June 1985.
15. Beavers, J.A., Parkins, R.N., 1986, "Recent Advances in Understanding The Factors Affecting SCC of Pipe Steel". 7th Symposium on Line Pipe Research. American Gas Association. Inc., Catalog # L51595, p.25-1
16. Justice, J.T. and Mackenzie, J.D., 1988, "Progress in the Control of Stress Corrosion Cracking in a 914mm O.D. Gas Transmission Pipeline", Proceedings of the NG-18/EPRG 7th Biennial Joint Technical Meeting on Line Pipe Research, Pipeline Research Committee of the American Gas Association Paper No.28.
17. Beavers, J.A. and Thompson, N.G. 1988. Unpublished Research Performed at CC Technologies for TransCanada Pipelines Limited.
18. Parkins, R.N., 1994, "Transgranular Stress Corrosion Cracking of High-Pressure Pipeline in Contact with Solutions of Near Neutral pH", Corrosion, Vol.50, No. 5, p.384.
19. Harle, B.A., Beavers, J.A. and Jaske, C.E., 1994. "Low-pH Stress Corrosion Cracking of Natural Gas Pipelines."Corrosion/94, Paper No.242.
20. Harle, B.A., Beavers, J.A. and Jaske, C.E., 1995 "Mechanical and Metallurgical Effects on Low-pH SCC of Natural Gas Pipelines."Corrosion/95, Paper646
21. Harle, B.A., Beavers, J.A. and Jaske, C.E., 1995 "Mechanical and Metallurgical Effects on Low-pH SCC of Natural Gas Pipelines,"Corrosion/95, Paper646
22. Jones, R. H. and Ricker, R. E., 1992. "Mechanisms of Stress Corrosion Cracking", Stress Corrosion Cracking, Ed.R.H. Jones, ASM International.

23. NACE, 1977, "Stress Corrosion Cracking and Hydrogen Embrittlement of Iron Base Alloys", Proceedings of a Conference Held in Firminy, France, June 1973, NACE-5, 1977
24. Schmidt, G., 1983, "Fundamental Aspects of CO₂ Corrosion", Corrosion/83, Paper No.43.
25. Netic, J., Postlethwaite, J., Olsen, S., "An Electro-Chemical Model for Prediction of Corrosion of Mild Steel in Aqueous Carbon Dioxide Solution", Corrosion, 52 (1996), 280-294.
26. CAN/CSA – Z245.1 – M90 Steel Line Pipe, May 1990
27. Schmidt, G., 1983, "Fundamental Aspects of CO₂ Corrosion", Corrosion/83, Paper No.43.
28. Netic, J., Postlethwaite, J., Olsen, S., "An Electro-Chemical Model for Prediction of Corrosion of Mild Steel in Aqueous Carbon Dioxide Solution", Corrosion, 52 (1996), 280-294.
29. Parkins R.N., " Further Cyclic Loading Tests Relating to Environment-Sensitive Fracture in the TransCanada Pipeline System", report to Trans Canada Pipe Lines (1991)
30. Lambert S.B., Plumtree A., Ahmed T.M., Pilkey A.K.L., "Stress Corrosion Cracking Crack Growth Rates", Report to Nova Gas Transmission Ltd., Alberta (1992).
31. Harle B.A., Beavers J.A., Jaske C.E. "Low-pH Stress Corrosion Cracking of Natural Gas Pipeline". Proc. NACE Canadian Region Western Conference, Calgary, Alberta (Houston, TX: NACE, 1994), p. 473.

32. Revie R.W., Zheng W., Roy G., Shchata M.T., Vosikovsky O., Kilt D.,
“Methodology for Realistic Full Scale SCC Testing of Linepipe”, Proc. NACE Conf.
Calgary, Canada (Houston, TX: NACE, 1994)
33. Parkins R.N., Blanchard Jr W.K., Delanty B.S., Corrosion 50 (1994): p.394.
34. Szklarska-Smialowska Z., Xia Z., Rebak R.B., Corrosion 50 (1994):p.334
35. Beavers J.A., “On the Mechanism of Stress Corrosion Cracking of Natural Gas
Pipelines”, 8th Symposium on Line Pipe Research, American Gas Association, Inc.,
Catalog No.L51680, p. 17-1, 1993.
36. Parkins R.N. and Delanty B.S.. “ The Initiation and Early Stages of Growth of Stress
Corrosion Cracks Exposed to a Dilute, Near-Neutral-pH Solution”, 9th Symposium on
Pipeline Research, American Gas Association, Arlington, VA, LISA, Catalog
No.L51746, 1996, 19-1/19-14.
37. Jack T.R., Van Boven G., Wilmott M. and Sutherby R.L., “Parameters Affecting the
Growth of Low pH Stress Corrosion Cracking of Pipeline Steels”. NACE
International Canadian Western region Conference. Calgary, 1994, 504-526.
38. Harle B.A., Beavers J.A. and Jaske C.E., “Low pH Stress Corrosion Crack Growth in
Pipeline Steels”, loc. cit., 473-503.
39. Beavers J.A. and Hagerdorn E.L., “Near-Neutral-pH SCC: Mechanical Effects on
Crack Propagation”, 9th Symposium on Pipeline Research, American Gas
Association, Arlington, VA, USA. Catalog No.L51746, 1996, 24-1/24-19.
40. Zheng W., Revie R.W., Dinardo O., Macleod F.A., Tyson W.R. and Kiff D.,
“Pipeline SCC in Near-Neutral-pH Environment: Effects of Environmental and
Metallurgical Variables”, loc. cit. 22-1/22-18.

41. Chen W., Wilmott M., Jack T. "Effect of Cathodic Protection of Neutral pH SCC Crack Initiation of X-70 Pipeline Steel", NACE Northern Area Western Conference, Conference Proceedings, 1999.
42. Callister W. D., "Material Science and Engineering", John Wiley & Sons, Inc., 1997.